Biosynthetic study of miuraenamide A, an antifungal antibiotic of a slightly halophilic myxobacterium

亜好塩性粘液細菌の抗真菌抗生物質 miuraenamide A の生合成に関する研究

LIU Ying

Nagoya University

Graduate School of Bioagricultural Sciences

Department of Applied Biosciences

Laboratory of Bioactive Molecules

March 2023

Contents

Chapter 1. Introduction **1**

1.1. Microbial secondary metabolites for the treatment of diseases 1

1.2. Myxobacteria, a microbial drug factory 2

1.3. Genome mining for secondary metabolite discovery 6

1.4. Heterologous expression of secondary metabolite BGCs 7

1.5. *Paraliomyxa miuraensis* and miuraenamide A 8

1.6. Outline of this work 10

References 12

Chapter 2. Genomic analysis of *P. miuraensis* SMH-27-4 ..... **16**

2.1. Introduction 16

2.2. Results and discussion 18

2.3. Materials and methods 32

2.4. Summary 38

References 40

Chapter 3. Heterologous biosynthesis of miuraenamide A **44**

3.1. Introduction 44

3.2. Results and discussion 45

3.3. Materials and methods 65

3.4. Summary 73

References 76

Chapter 4. Conclusion **79**

4.1. Genomic analysis of *P. miuraensis* SMH-27-4 79

4.2. Heterologous biosynthesis of miuraenamide A 80

Acknowledgements **82**

Chapter 1. Introduction

1.1. Microbial secondary metabolites for the treatment of diseases

Humans have a long history of using medicinal plants for healing. The secondary metabolites are sources of medicines from plants. Unlike primary metabolites (such as organic acids, amino acids, vitamins, and nucleotides), which are directly involved in the normal growth, development, or reproduction of the organisms, secondary metabolites are produced to confer a selective advantage, for example, by functioning as defense compounds or signaling molecules. Although all organisms produce secondary metabolites, microbes have become an essential source in drug discovery since 1928, the discovery of penicillin from *Penicillium notatum* [1]. Compared with traditional drug discovery from the plant source, the microbial source has unique advantages due to its biodiversity and availability. To date, many commercially available pharmaceuticals are originated from microbes. Different drugs obtained from microbial sources have been found to possess anticancer (Ixabepilone (**1**), derived from the myxobacterium *Sorangium cellulosum* [2]), antibacterial (Tigecycline (**2**), derived from the actinobacterium *Streptomyces aureofaciens* [3]), hypocholesterolemic (Lovastatin (**3**), derived from the fungus *Aspergillus terreus* [4]), immunosuppressant (Everolimus (**4**), derived from actinobacterium *Streptomyces hygroscopicus* [5]), antifungal (Caspofungin (**5**), derived from the fungus *Glarea lozoyensis* [6]), and antiparasitic activities (Ivermectin (**6**), derived from the actinobacterium *Streptomyces avermitilis* [7]) (Figure 1-1).

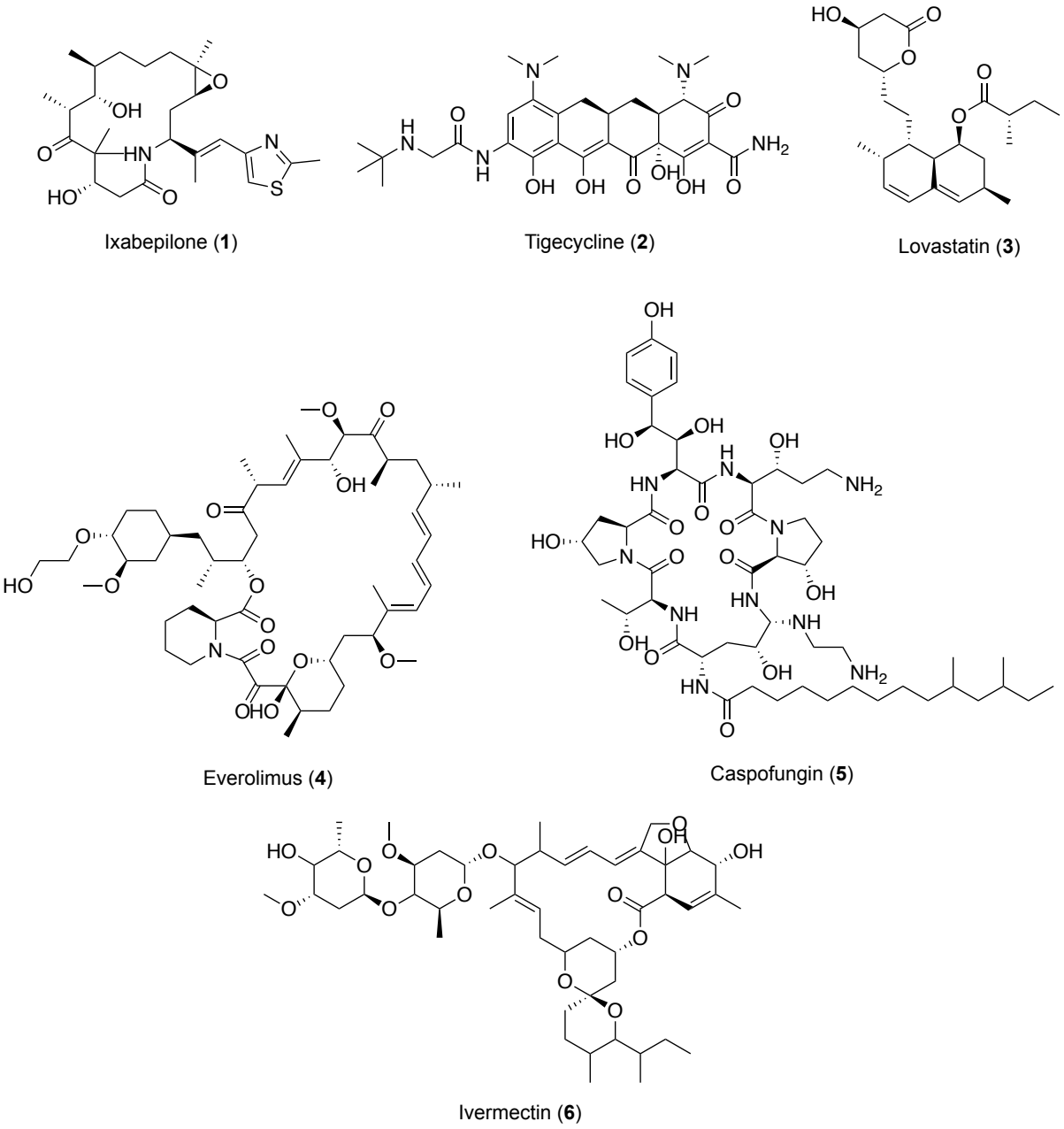

Figure 1-1. Chemical structures of some FDA-approved drugs derived from microbes.

1.2. Myxobacteria, a microbial drug factory

Myxobacteria are famous for their complex life cycle of multicellular fruiting body formation and cooperative preying behavior (Figure 1-2) [8]. On solid surfaces, rod-shaped vegetative cells move in a coordinated manner in search of prey, forming dynamic multicellular swarms. When swarms reach the prey, the cells penetrate the prey colony and lyse its cells. While starving, the cells move collectively, first forming aggregates and later constructing

millimeter-long upright fruiting bodies filled with myxospores, the metabolically quiescent cells that can disperse to other environments and germinate when nutritional conditions improve.

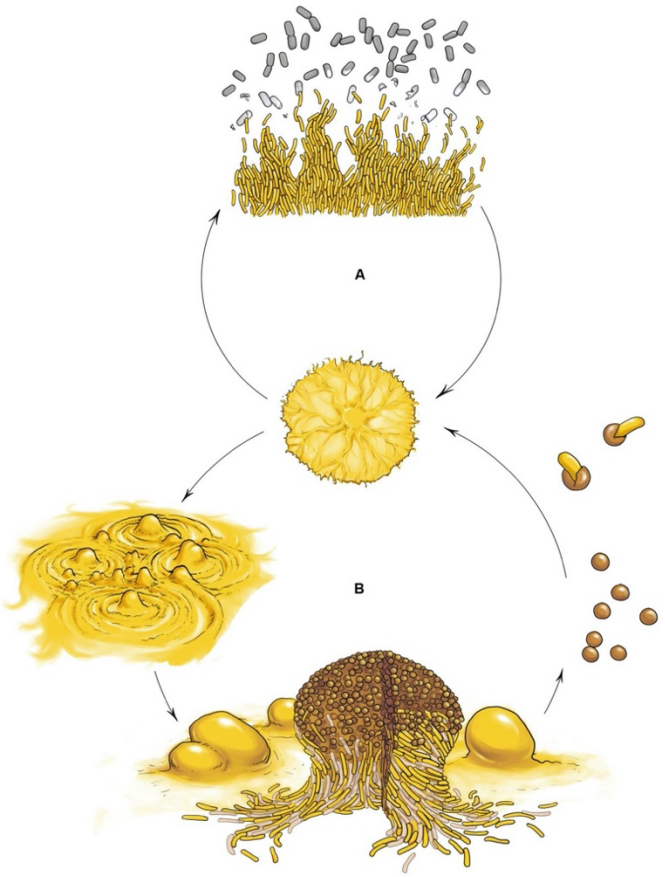

Figure 1-2. *Myxococcus xanthus* multicellular cell cycle [8].

Aside from behavior's complexity, their potential for immense secondary metabolites production also makes them candidates for a next-generation microbial drug factory [9-11]. Over the last decades, Myxobacteria are a critical source of diverse secondary metabolites that exhibit unique modes-of-action across a broad range of biological activities. Till 2021, over 80 novel myxobacterial secondary metabolite compound families were isolated with their biological activity and mode-of-action had been clarified [12].

Myxobacteria are phylogenetically united in the order Myxococcales belonging to the class δ-proteobacteria. The order Myxococcales comprises three suborders, namely Cystobacterineae, Sorangineae, and Nannocystineae [11]. Since their first description as a

novel taxon in 1892 [13], myxobacteria were considered terrestrial bacteria until 1998, when the first isolation of obligate halophilic marine myxobacteria was reported by Iizuka et al [14]. Although the difficulty with isolation and cultivation obstructs the discovery of halophiles, the limited number of strains already shows great potential for producing novel bioactive leads with unique molecular scaffolds and activities (Figure 1-3) [15-16].

To date, all discovered and cultivable halophilic myxobacteria, are grouped into the suborder Nannocystineae, including *Haliangium ochraceum*, *Haliangium tepidum, Enhygromyxa salina*, *Plesiocystis pacifica*, *Pseudenhygromyxa salsuginis*, *"Enhygromyxa niigataensis"* and *Paraliomyxa miuraensis*. Their bioactive secondary metabolites including haliangicins (**7**-**10**), haliamide (**11**), salimabromide (**12**), salimyxins (**13**-**14**), enhygromic acid (**15**), enhygrolides (**16**-**19**), miuraenamides (**20**-**25**), and so on [17-25].

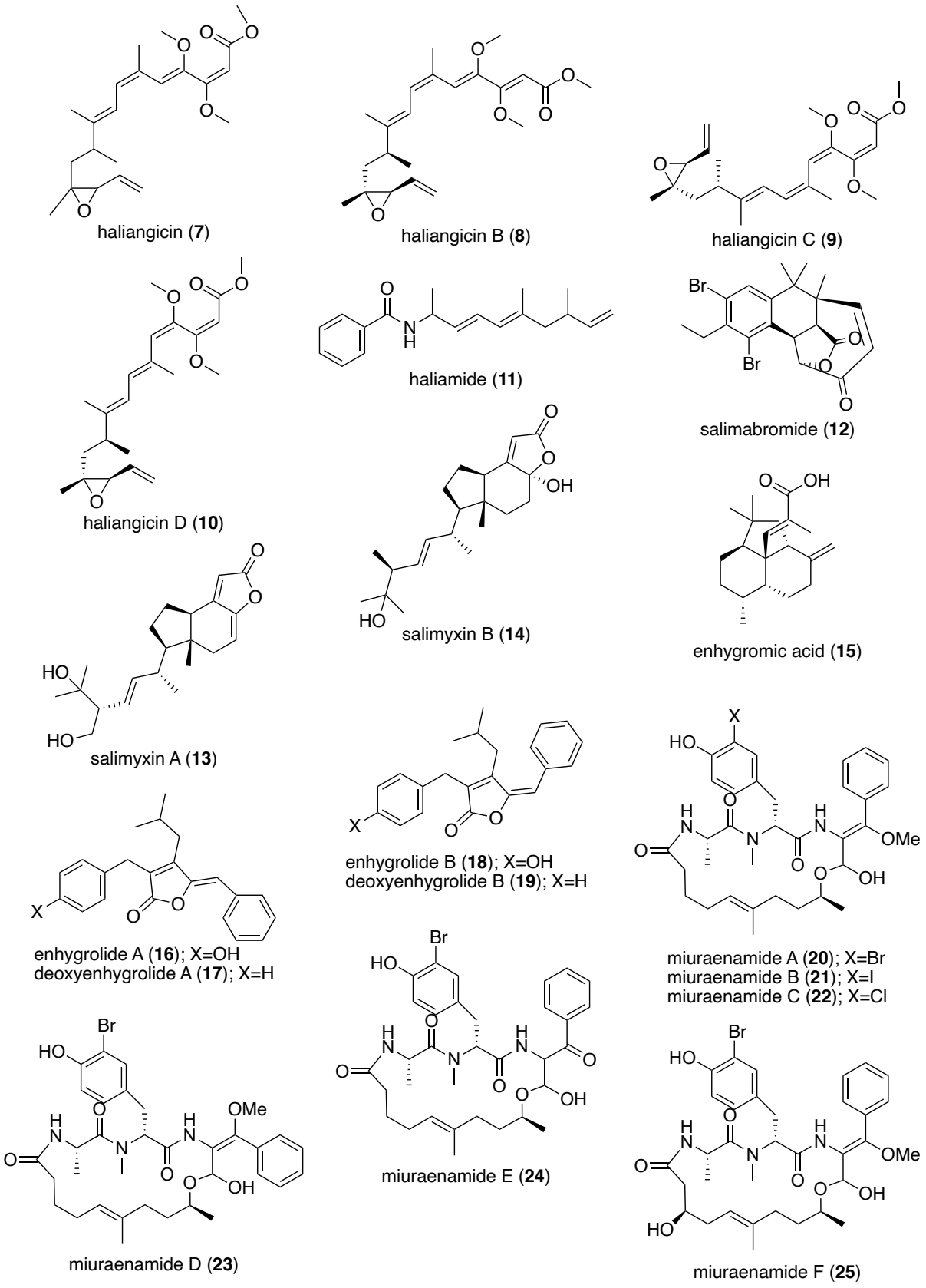

Figure 1-3. Some secondary metabolites from halophilic myxobacteria.

1.3. Genome mining for secondary metabolite discovery

The classical approach to discovering bioactive secondary metabolites is by combining isolation techniques and bioactive screening (e.g., the discovery of penicillin). This strategy had a prime time during the 1950s-1960s. Since then, the application of this strategy has been hampered by high rediscovery rates [26]. When the time approached the 21st century, breakthroughs in sequencing technology brought biological research into a new era. Genome mining provided a faster and cheaper way to obtain novel secondary metabolites [27-28].

The microbial secondary metabolites include several chemical classes, such as terpenoids, polyketides, alkaloids, peptides, and saccharides. The genes co-encoding biosynthetic pathway to produce a secondary metabolite are usually arranged contiguously in the genome, called the biosynthetic gene cluster (BGC). Since the biosynthetic pathway encoded by BGCs follows a highly conserved biosynthetic logic, novel BGCs can be detected by the genome mining strategy based on the sequence similarity of enzymes/genes.

The antibiotics & Secondary Metabolite Analysis SHell (antiSMASH) [29] and PRediction Informatics for Secondary Metabolomes (PRISM) [30] are the most noteworthy software for genome mining. Both can provide predictions of BGCs for a wide range of secondary metabolite classes and are closely linked to other databases or bioinformatics to link the BGCs to their molecular products.

The antiSMASH is closely connected to the minimum information on biosynthetic gene cluster (MiBIG) database [31], which provides a repository of BGCs that have been experimentally connected to their molecular products and annotated according to the MiBIG data standard. The establishment of MiBIG provides references for interpreting the function and novelty of predicted BGCs. Two software tools, biosynthetic gene similarity clustering and prospecting engine (BiG-SCAPE) and core analysis of syntenic orthologues to prioritize

natural product gene clusters (CORASON) enable comparisons between antiSMASH-predicted BGCs and MIBIG's empirical biosynthesis data [32]. BiG-SCAPE constructs BGC sequence similarity networks and groups BGCs into gene cluster families (GCFs). CORASON facilitates in exploration of gene cluster diversity linked to enzyme phylogenies within and across GCFs.

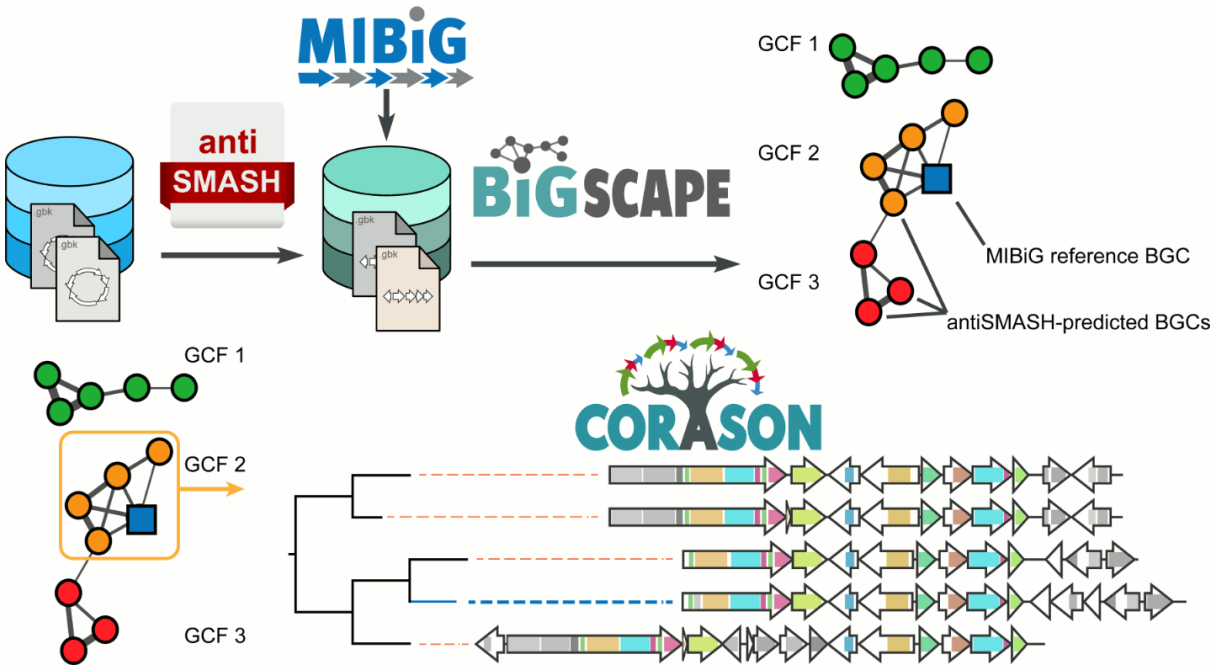

Figure 1-4. The BiG-SCAPE/CORASON workflow [32].

PRISM provides genome mining focused on predicting the chemical structure of biosynthetic pathways. Based on a retro-biosynthesis tool (generalized retro-biosynthetic assembly prediction engine, GRAPE) [33], the polyketide and non-ribosome peptide BGCs predicted by PRISM are linked to known natural products or are defined as clusters encoding new compounds. PRISM-predicted BGCs can also be matched to LC-MS/MS data via genomes-to-natural products platform (GNP) [34].

1.4. Heterologous expression of secondary metabolite BGCs

Genome mining revealed the abundance of uncharacterized BGCs, exceeding the known BGCs over 10-fold [35]. The discovery of the molecular products of these uncharacterized BGCs is extremely difficult since most of them are transcriptionally silent under laboratory

culture conditions. On the other hand, the characterizations of the biosynthetic pathways of some known secondary metabolites are sometimes hampered by the difficulty of culturing and genetically manipulating the host. In the above-mentioned cases, heterologous expression of the BGCs in an easy-to-culture and genetically amenable host can address those obstacles [11, 36].

The myxobacterial model strain *Myxococcus xanthus* has been used as a heterologous host for the expression of myxobacterial secondary metabolites due to its close phylogenetic relationship to the native producers plus additional advantageous features. These include established genetic tools, growth in suspension, short doubling time (~ 5 h) compared to other myxobacteria, as well as available fermentation know-how [37]. The strain is also characterized as a promising producer of natural products, indicating the availability of common biosynthetic precursors and two broad-spectrum phosphopantetheinyl transferases, which are required for posttranslational activation of PKS/NRPS megasynthetases were identified in 2008 [39]. *M. xanthus* has been successfully applied into the heterologous biosynthesis of the cyclodepsipeptide epothilone [39], siderophore pseudochelin [40], polyketide haliangicin [41] and so on.

1.5. *Paraliomyxa miuraensis* and miuraenamide A

The slightly halophilic myxobacterium *P. miuraensis* SMH-27-4 is the type strain and to date the only member of the fifth isolated halophilic myxobacterial genus [42]. In 2006, the strain was isolated from a near-seashore soil in Japan [24]. The phylogenetic analysis based on a partial 16S rRNA gene sequence suggested that it represents a new genus of the family Nannocystaceae [24, 42]. Nannocystaceae is the most ecologically diverse myxobacterial family and, besides *Paraliomyxa*, contains four genera: two marine-derived genera *Plesiocystis* and *Enhygromyxa*, a brackish water genus *Pseudenhygromyxa*, and a terrestrial genus *Nannocystis* [43]. In 2016, Iizuka reported the chemotaxonomic and

physiological characteristics of the strain SMH-27-4 and provided the descriptions of *Paraliomyxa* gen. nov. and *Paraliomyxa miuraensis* sp. nov. [42]. The optimal salt concentrations for the growth of *P. miuraensis* SMH-27-4 were determined as 0.5-1.0% (w/v) NaCl, and it requires Mg^{2+} and Ca^{2+} for the growth. On the agar plate, the strain swarms in a radial pattern and sometimes cleaves the agar gel matrix. The major cellular fatty acids are iso-$C_{15:0}$ and iso-$C_{17:0}$. It does not degrade filter papers or grow in a yeast medium VY/2 agar generally used for terrestrial myxobacteria. The above characteristics were shared with the slightly halophilic myxobacteria *Pseudenhygromyxa* [42, 44]. However, its major cellular quinone is MK-8, and long-chain polyunsaturated fatty acids were not detected. These two properties are the same as the terrestrial strain *Nannocystis exedens* DSM 71 [42, 45]. No distinct fruiting body was observed for this strain, which made it more enigmatic [24, 42].

The major secondary metabolite of *P. miuraensis* SMH-27-4, miuraenamide A (**20**) (Figure 1-3), exhibited potent antifungal activity, especially against the phytopathogenic oomycete *Phytophthora capsici* at a minimum inhibition dose of 25 ng/disk by inhibiting the mitochondrial respiratory chain [24]. It also stabilizes actin filaments to change tumor cell morphology [46]. The cellular studies of **20** demonstrated the effects on cell migration and transcriptional activity [47, 48]. It is reported that **20** has a unique actin binding mode different from jasplakinolide, a commonly used pharmacological tool to study actin organization and dynamics in living cells [49]. More recently, **20** has been shown to induce actin filaments elongation and to shift the nucleus toward the cell center [50]. **20** is considered as a new tool to facilitate understanding the role of actin in living cells.

Besides miuraenamide A, there are six other congeners have been isolated from the *P. miuraensis* SMH-27-4, miuraenamide B-F (**21**-**25**, Figure 1-3) [24,25]. The productivity of **21**-**25** (0.02 mg/L, 0.003 mg/L, 0.01 mg/L, 0.10 mg/L, 0.02 mg/L) are much lower than miuraenamide A (0.98 mg/L). The strong antifungal activity of three halogenated tyrosine containing miuraenamides (**20**-**22)** and the low activity of the **23**-**25**, indicated the

halogenation, geometry of the β-methoxyacrylate group, and the lipophilicity of the polyketide moiety affected activity of these compounds. The total synthesis and the structure-activity studies of several derivatives have also been reported. In 2015, Kazmaier et al. reported a total synthesis scheme of **20** requiring 15 steps with a 1.9% overall yield [51]. In 2016, Ojima et al. achieved the total synthesis of **20** of 20 steps with a 3.2% overall yield [52]. In 2018, Kazmaier et al. synthetized 44 miuraenamide derivatives and performed detailed SAR studies [53]. The results indicated that the bromination of the central tyrosine is essential for high cytotoxicity, while the C-terminus of the tripeptide fragment (the phenylalanine) can be varied or can even be removed.

1.6. Outline of this work

In this thesis, the potential of the secondary metabolite production of *P. miuraensis* SMH-27-4 and the biosynthetic machinery for miuraenamide A were illustrated.

In chapter 2, a genomic analysis of *P. miuraensis* SMH-27-4 was performed using the first whole-genome sequencing data completed by our laboratory. The draft genome of *P. miuraensis* SMH-27-4 was sequenced and de novo assembled into 11.8 Mbp consisting of 164 contigs. The analysis suggested a high degree of completeness of the genome assembly (93% coverage of the complete genome). The result of genome sequence-based phylogenetic analysis supported the taxonomy of the strain as representing a novel genus, *Paraliomyxa*, in the family Nannocystaceae. Seventeen biosynthetic gene clusters (BGCs) were found in the genome. One of them, type I polyketide synthase/nonribosomal peptide synthase hybrid type (PKS/NRPS), was estimated to be the BGC for miuraenamide A based on gene functional analyses. The 16 other BGCs contained two PKS/NRPS hybrids, four terpenoid biosynthetic gene clusters, etc., which showed low or no similarity with the BGCs for the previously reported products, revealing the great potential of the strain to produce novel secondary metabolites. The similar distribution of the COG functional categories through the strains from five genera

within the family Nannocystaceae indicated conserved genomic functions of this family. On the other hand, the average distribution of COG functional categories by the core, accessory, and strain-specific genes suggests that the five genera have diverse signal transduction and gene transcription mechanisms.

In chapter 3, the BGC for miuraenamide A (*miu* cluster) was successfully cloned and heterologously expressed in the well-known terrestrial myxobacterium *Myxococcus xanthus*. The biosynthetic machinery was verified by gene-disruption in the heterologous host and a multi-gene region that significantly affected the production was demonstrated. The constructed transformant which contains the complete *miu* cluster produced miuraenamide A in 6% of that of SMH-27-4. Two PKSs, one NRPS, one *O*-methyltransferase and one halogenase were confirmed two be responsible for the miuraenamide A biosynthesis. The removal of a gene region resulted in a substantial increase of the yield of miuraenamide A, and feeding the mutant on 3-bromo-L-tyrosine promoted its production five times as effective as that of SMH-27-4 (considering the cultivation time).

References

1. Fleming, A. On the antibacterial action of cultures of Penicillium, with special reference to their use in the isolation of B. influenzae. *Br. J. Exp. Pathol.* **1929**, *10*, 226–236.
2. Peterson, J.K.; Tucker, C.; Favours, E.; Cheshire, P.J.; Creech, J.; Billups, C.A.; Smykla, R.; Lee, F.Y.F.; Houghton, P.J. In vivo evaluation of Ixabepilone (BMS247550), A novel epothilone B derivative, against pediatric cancer models. *Clin. Cancer Res.* **2005**, *11*, 6950–6958.
3. Zhanel, G.G.; Homenuik, K.; Nichol, K.; Noreddin, A.; Vercaigne, L.; Embil, J.; Gin, A.; Karlowsky, J.A.; Hoban, D.J. The glycylcyclines. *Drugs* **2004**, *64*, 63–88.
4. López, J.L.C.; Pérez, J.A.S.; Sevilla, J.M.F.; Fernández, F.G.A.; Grima, E.M.; Chisti, Y. Production of lovastatin by Aspergillus terreus: Effects of the C: N ratio and the principal nutrients on growth and metabolite production. *Enzyme Microb. Technol.* **2003**, *33*, 270–277.
5. Chapman, T.M.; Perry, C.M. Everolimus. *Drugs* **2004**, *64*, 861–872.
6. Carmichael, W.W. Cyanobacteria secondary metabolites-The cyanotoxins. *J. Appl. Bacteriol.* **1992**, *72*, 445–459.
7. Shikiya, K.; Kinjo, N.; Uehara, T.; Uechi, H.; Ohshiro, J.; Arakaki, T.; Kinjo, F.; Saito, A.; Iju, M.; Kobari, K.; et al. Efficacy of ivermectin against Strongyloides stercoralis in humans. *Intern. Med.* **1992**, *31*, 310–312.
8. Muñoz-dorado, J.; Marcos-torres, F.J.; García-bravo, E.; Moraleda-muñoz, A.; Pérez, J. Myxobacteria: moving , killing , feeding , and surviving together. *Front. Microbiol.* **2016**, *7*, 781.
9. Wenzel, S.C.; Müller, R. Myxobacteria —‘ microbial factories ’ for the production of bioactive secondary metabolites. *Mol. BioSyst.* **2009**, *5*, 567–574.
10. Diez, J.; Martinez, J.P.; Mestres, J.; Sasse, F.; Frank, R.; Meyerhans, A. Myxobacteria: natural pharmaceutical factories. *Microb. Cell Fact.* **2012**, *11*, 2–4.
11. Hug, J.J.; Müller, R. Host development for heterologous expression and biosynthetic studies of myxobacterial natural products. In *Comprehensive Natural Products III*, 3rd ed.; Liu, H., Begley, T.P., Eds.; Elsevier: San Diego, California, USA, 2020; Vol. 6, pp. 149–216.
12. Bhat, M.A.; Mishra, A.K.; Bhat, M.A.; Banday, M.I.; Bashir, O.; Rather, I.A.; Rahman, S.; Shah, A.A.; Jan, A.T. Myxobacteria as a Source of New Bioactive Compounds: A Perspective Study. *Pharmaceutics* **2021**, *13*, 1265.
13. Thaxter, R. Contributions from the cryptogamic laboratory of Harvard University. XVIII. On the Myxobacteriaceae, a new order of Schizomycetes. *Bot. Gaz.* **1892**, *12*, 389–406.
14. Iizuka, T.; Jojima, Y.; Fudou, R.; Yamanaka, S. Isolation of myxobacteria from the marine environment. *FEMS Microbiol. Lett.* **1998**, *169*, 317–322.
15. Albataineh, H. & Stevens, D. C. Marine Myxobacteria : A Few Good Halophiles. *Mar.*

Drugs **2018**, *16*, 209.
16. Gemperlein, K.; Zaburannyi, N.; Garcia, R.; Clair, J.L.; Müller, R. Metabolic and Biosynthetic Diversity in Marine Myxobacteria. *Mar. Drugs* **2018**, *16*, 314.
17. Fudou, R.; Iizuka, T.; Yamanaka, S. Haliangicin, a novel antifungal metabolite produced by a marine myxobacterium. 1. Fermentation and biological characteristics. *J. Antibiot.* **2001**, *54*, 149–152.
18. Fudou, R.; Iizuka, T.; Sato, S.; Ando, T.; Shimba, N.; Yamanaka, S. Haliangicin, a novel antifungal metabolite produced by a marine myxobacterium. 2. Isolation and structural elucidation. J. Antibiot. **2001**, *54*, 153–156.
19. Kundim, B.A.; Itou, Y.; Sakagami, Y.; Fudou, R.; Iizuka, T.; Yamanaka, S.; Ojika, M. New haliangicin isomers, potent antifungal metabolites produced by a marine myxobacterium. *J. Antibiot.* **2003**, *56*, 630–638.
20. Sun, Y.; Feng, Z.; Tomura, T.; Suzuki, A.; Miyano, S.; Tsuge, T.; Mori, H.; Suh, J.-W.; Iizuka, T.; Fudou, R.; et al. Isolation and Biosynthetic Analysis of Haliamide, a New PKS-NRPS Hybrid Metabolite from the Marine Myxobacterium *Haliangium ochraceum*. *Molecules* **2016**, *21*, 59
21. Felder, S.; Felder, S.; Dreisigacker, S.; Kehraus, S.; Neu, E.; Bierbaum, G.; Wright, P.R.; Menche, D.; Schäberle, T.F.; König, G.M. Salimabromide: Unexpected chemistry from the obligate marine myxobacterium *Enhygromyxa salina*. *Chemistry* **2013**, *19*, 9319–9324.
22. Felder, S.; Kehraus, S.; Neu, E.; Bierbaum, G.; Schäberle, T.F.; König, G.M. Salimyxins and enhygrolides: Antibiotic, sponge-related metabolites from the obligate marine myxobacterium *Enhygromyxa salina*. *ChemBioChem* **2013**, *14*, 1363–1371.
23. Tomura, T.; Nagashima, S.; Yamazaki, S.; Iizuka, T.; Fudou, R.; Ojika, M. An Unusual Diterpene—Enhygromic Acid and Deoxyenhygrolides from a Marine Myxobacterium, *Enhygromyxa sp. Mar. Drugs* **2017**, *15*, 109.
24. Iizuka, T.; Fudou, R.; Jojima, Y.; Ogawa, S.; Yamanaka, S.; Inukai, Y.; Ojika, M. Miuraenamides A and B, novel antimicrobial cyclic depsipeptides from a new slightly halophilic myxobacterium: taxonomy, production, and biological properties. *J. Antibiot.* **2006**, *59*, 385–391.
25. Ojika, M.; Inukai, Y.; Kito, Y.; Hirata, M.; Iizuka, T.; Fudou, R. Miuraenamides: antimicrobial cyclic depsipeptides isolated from a rare and slightly halophilic myxobacterium, *Chem. Asian J.* **2008**, *3*, 126–133.
26. Li, J.W.; Vederas, C. Drug discovery and natural products: End of an era or an endless frontier? *Science* **2009**, *325*, 161–165.
27. Ziemert, N.; Alanjary, M.; Weber, T. The evolution of genome mining in microbes-a review. *Nat. Prod. Rep*. **2016**, *33*, 988–1005.
28. Albarano, L.; Esposito, R.; Ruocco, N.; Costantini, M. Genome mining as new challenge in natural products discovery. *Mar. drugs Rev.* **2020**, *18*, 199.

29. Blin, K.; Shaw, S.; Kloosterman, A.M.; Charlop-Powers, Z.; van Wezel, G.P.; Medema, M.H.; Weber, T. AntiSMASH 6.0: improving cluster detection and comparison capabilities. *Nucleic Acids Res.* **2021**, *49*, W29–W35.
30. Skinnider, M.A.; Johnston, C.W.; Gunabalasingam, M.; Merwin, N.J.; Kieliszek, A.M.; MacLellan, R.J.; Li, H.; Ranieri, M.R.M.; Webster, A.L.H.; Cao, M.P.T.; et al. Comprehensive prediction of secondary metabolite structure and biological activity from microbial genome sequences. *Nat. Commun.* **2020**, *11*, 1–9,
31. Kautsar, S.A.; Blin, K.; Shaw, S.; Navarro-Muñoz, J.C.; Terlouw, B.R.; van der Hooft, J.J.J.; van Santen, J.A.; Tracanna, V.; Suarez Duran, H.G.; Pascal Andreu, V.; et al. MIBiG 2.0: a repository for biosynthetic gene clusters of known function. *Nucleic Acids Res.* **2020**, *48*, D454–D458.
32. Navarro-Muñoz, J.C.; Selem-Mojica, N.; Mullowney, M.W.; Kautsar, S.A.; Tryon, J.H.; Parkinson, E.I.; De Los Santos, E.L.C.; Yeong, M.; Cruz-Morales, P.; Abubucker, S.; et al. A computational framework to explore large-scale biosynthetic diversity. *Nat. Chem. Biol.* **2020**, *16*, 60–68.
33. Dejong, C.A.; Chen, G.M.; Li, H.; Johnston, C.W.; Edwards, M.R.; Rees, P.N.; Skinnider, M.A.; Webster, A.L.H.; Magarvey, N.A. Polyketide and nonribosomal peptide retro-biosynthesis and global gene cluster matching. *Nat. Chem. Biol.* **2016**, *12*, 1007–1014,
34. Johnston, C.W.; Skinnider, M.A.; Wyatt, M.A.; Li, X.; Ranieri, M.R.M.; Yang, L.; Zechel, D.L.; Ma, B.; Magarvey, N.A. An automated Genomes-to-Natural Products platform (GNP) for the discovery of modular natural products. *Nat Commun* **2015**, *6*, 8421.
35. Baltz RH. Genome mining for drug discovery: progress at the front end. *J Ind Microbiol Biotechnol.* **2021,** *48*, 9-10.
36. Ongley, S.E.; Bian, X.; Neilan, B.A.; Müller, R. Recent advances in the heterologous expression of microbial natural product biosynthetic pathways. *Nat. Prod. Rep.* **2013**, *30*, 1121-1138.
37. Wenzel, S.C.; Müller, R. Host Organisms: Myxobacterium. In *Industrial Biotechnology: Microorganisms.*; Wittmann, C., Liao, J.C.; Wiley-VCH: Weinheim, Germany, 2016; Vol. 2, pp. 453–485.
38. Meiser, P.; Müller, R. Two functionally redundant Sfp-type 4′-phosphopantetheinyl transferases differentially activate biosynthetic pathways in *Myxococcus xanthus*. *ChemBioChem* **2008**, *9*, 1549 – 1553.
39. Julien B.; Shah S. Heterologous Expression of Epothilone Biosynthetic Genes in *Myxococcus xanthus*. *Antimicrob Agents Chemother* **2002**, *46*, 2772-2778.
40. Korp J.; Winand L.; Sester A.; Nett M. Engineering pseudochelin production in *Myxococcus xanthus*. *Appl Environ Microbio* **2018,** *84*. e01789-1.
41. Sun, Y.; Feng, Z.; Tomura, T.; Suzuki, A.; Miyano, S.; Tsuge, T.; Mori, H.; Suh, J.W.; Iizuka, T.; Fudou, R.; et al. Heterologous production of the marine myxobacterial antibiotic

haliangicin and its unnatural analogues generated by engineering of the biochemical pathway. *Sci. Rep.* **2016**, *6*, 220911.

42. Iizuka, T. Isolation and characterization of novel myxobacteria and their significance as biomedical resources. Ph. D. thesis, Toyohashi University of Technology, Toyohashi, Aichi, Japan, 2016-01.
43. Garcia, R.; Müller, R. The family Nannocystaceae. In *The prokaryotes - deltaproteobacteria and epsilonproteobacteria*, 4t ed.; Rosenberg, E., Delong, E.F., Loy, S., Stackebrandt, E., Thompson, F., Eds.; Springer-Verlag: Berlin Heidelberg, Germany, 2014; Vol. 10, pp 213-229.
44. Iizuka, T.; Jojima, Y.; Hayakawa, A.; Fujii, T.; Yamanaka, S.; Fudou, R. *Pseudenhygromyxa salsuginis* gen. nov., sp. nov., a myxobacterium isolated from an estuarine marsh. *Int. J. Syst. Evol. Microbiol.* **2013**, *63*, 1360–1369.
45. Reichenbach, H. Nannocystis exedens gen. nov., spec. nov., a new myxobacterium of the family Sorangiaceae. *Arch. Mikrobiol.* **1970**, *70*, 119–138.
46. Sumiya, E.; Shimogawa, H.; Sasaki, H.; Tsutsumi, M.; Yoshita, K.; Ojika, M.; Suenaga, K.; Uesugi, M. Cell-morphology profiling of a natural product library identifies bisebromoamide and miuraenamide A as actin filament stabilizers. *ACS Chem. Biol*. **2011**, *6*, 425–431.
47. Moser, C.; Rüdiger, D.; Förster, F.; Blume, J. Von; Yu, P.; Kazmaier, U.; Vollmar, A.M.; Zahler, S. Persistent inhibition of pore-based cell migration by sub-toxic doses of miuraenamide, an actin filament stabilizer. *Sci. Rep.* **2017**, *7*, 16407.
48. Gegenfurtner, F.A.; Zisis, T.; Al Danaf, N.; Schrimpf, W.; Kliesmete, Z.; Ziegenhain, C.; Enard, W.; Kazmaier, U.; Lamb, D.C.; Vollmar, A.M.; et al. Transcriptional effects of actin-binding compounds: the cytoplasm sets the tone. *Cell. Mol. Life Sci.* **2018**, *75*, 4539–4555.
49. Wang, S.; Crevenna, A.H.; Ugur, I.; Marion, A.; Antes, I.; Kazmaier, U.; Hoyer, M.; Lamb, D.C.; Gegenfurtner, F.; Kliesmete, Z.; et al. Actin stabilizing compounds show specific biological effects due to their binding mode. *Sci. Rep.* **2019**, *9*, 9731.
50. Baltes, C.; Thalla, D.G.; Kazmaier, U.; Lautenschläger, F. Actin stabilization in cell migration. *Front. Cell Dev. Biol.* **2022**, *10*, 931880.
51. Karmann, L.; Schultz, K.; Herrmann, J.; Müller, R.; Kazmaier, U. Total syntheses and biological evaluation of miuraenamides. *Angew.Chem. Int. Ed.* **2015**, *54*, 4502–4507.
52. Ojima, D.; Yasui, A.; Tohyama, K.; Tokuzumi, K.; Toriihara, E.; Ito, K.; Iwasaki, A.; Tomura, T.; Ojika, M.; Suenaga, K. Total synthesis of miuraenamides A and D. *J. Org. Chem.* **2016**, *81*, 9886–9894.
53. Kappler, S.; Karmann, L.; Prudel, C.; Herrmann, J.; Caddeu, G.; Müller, R.; Vollmar, A.M.; Zahler, S.; Kazmaier, U. Synthesis and biological evaluation of modified miuraenamides. *Eur. J. Org. Chem.* **2018**, 6952–6965.

Chapter 2. Genomic analysis of *P. miuraensis* SMH-27-4

2.1. Introduction

Myxobacteria are famous for their complex life cycle of multicellular fruiting body formation and cooperative preying behavior. They are considered as a template for the study of bacterial social behavior [1-3]. Aside from this, their potential for immense secondary metabolite production also makes them candidates for a next-generation microbial drug factory [4-6]. Since their first description as a novel taxon in 1892 [7], myxobacteria were considered terrestrial bacteria until 1998, when the first isolation of obligate halophilic marine myxobacteria was reported by Iizuka et al. [8]. Although the difficulty with isolation and cultivation obstructs the discovery of halophiles, the limited number of strains already shows great potential for producing novel bioactive leads with unique molecular scaffolds and activities [9-12]. To date, all discovered and cultivable halophilic myxobacteria are grouped into the suborder Nannocystineae, which consists of two families, Kofleriaceae and Nannocystaceae [10].

In 2006, the myxobacterium strain SMH-27-4 was isolated from a near-seashore soil in Japan and tentatively named *Paraliomyxa miuraensis* [13]. The phylogenetic analysis based on a partial 16S rRNA gene sequence suggested that it represents a new genus of the family Nannocystaceae [13,14]. Nannocystaceae is the most ecologically diverse myxobacterial family and, besides *Paraliomyxa*, contains four genera: two marine-derived genera *Plesiocystis* and *Enhygromyxa*, a brackish water genus *Pseudenhygromyxa*, and a terrestrial genus *Nannocystis* [15].

In 2016, Iizuka reported the chemotaxonomic and physiological characteristics of the strain SMH-27-4 and provided the descriptions of *Paraliomyxa* gen. nov. and *Paraliomyxa miuraensis* sp. nov. (Reference S1) [14]. The optimal salt concentrations for the growth of *P. miuraensis* SMH-27-4 were determined as 0.5–1.0% (w/v) NaCl, and requires Mg^{2+} and Ca^{2+}

for its growth [13]. On the agar plate, the strain swarms in a radial pattern and sometimes cleaves the agar gel matrix (Figure 2-1A) [14]. The major cellular fatty acids are iso-$C_{15:0}$ and iso-$C_{17:0}$. They do not degrade filter papers or grow in a yeast medium, such as VY/2 agar, generally used for terrestrial myxobacteria. The above characteristics were shared with the slightly halophilic myxobacteria *Pseudenhygromyxa* [14,16]. However, its major cellular quinone is MK-8, and long-chain polyunsaturated fatty acids were not detected. These two properties are the same as the terrestrial strain *Nannocystis exedens* DSM 71 [14,17]. No distinct fruiting body was observed for this strain, which made it more enigmatic [13,14]. The major secondary metabolite of *P. miuraensis* SMH-27-4, miuraenamide A (Figure 2-1B), exhibited potent antifungal activity, especially against the phytopathogenic oomycete *Phytophthora capsici* at a minimum inhibition dose of 25 ng/disk by inhibiting the mitochondrial respiratory chain [13]. It was also shown to significantly change the morphology of the cytoplasm and nucleus of a tumor cell line by stabilizing actin filaments [18]. Over the last decade, its total synthesis and biological activity as an actin filament stabilizer have been broadly explored [19–26]. The potential of miuraenamide A for medical applications makes this strain more worthy of investigation.

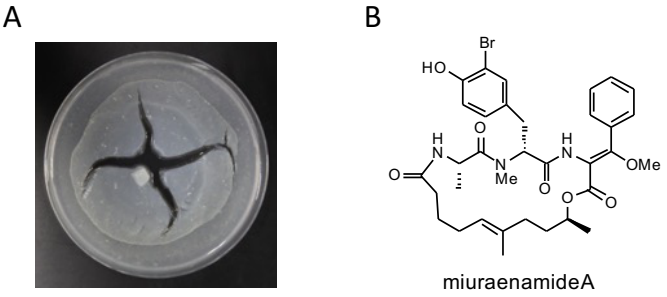

Figure 2-1. miuraenamide A and its producer. (A) *P. miuraensis* SMH-27-4 cleaves the agar gel matrix. (B) Chemical structure of miuraenamide A.

To confirm the taxonomy of *P. miuraensis* SMH-27-4 as well as the productivity of other secondary metabolites and the distribution of gene functions. In this chapter, the draft genome sequence of the strain was comprehensively analyzed.

2.2. Results and discussion

2.2.1. Draft genome sequencing, assembly, and annotation

A total of 2313 Mbp was obtained from Illumina HiSeq paired-end sequencing. The results are summarized in Table 2-1. The assembled *P. miuraensis* SMH-27-4 draft genome size is 11,849,290 bp, equal to 100.1% of the estimated genome size based on Kmer analysis. The overall GC content is 69.7%. The draft genome consists of 164 contigs, with the N50 and L50 values of 398,768 bp and 11, respectively. The completeness of the draft genome assembly was evaluated by calculating coverage for a set of single-copy orthologous genes in deltaproteobacteria using BUSCO. The results showed that the genome coverage rate was 93.0 %. PGAP annotation predicted 9280 genes in the genome, including 31 pseudogenes, 84 RNAs, and 9156 protein-coding genes that account for 90.7% coding density. The 9156 protein sequences were aligned to the BUSCO database to evaluate the annotation quality, and the coverage rate of 92.6% suggested a high degree of completeness of the gene prediction. A total of 38.3% (3508) of the protein-coding genes were annotated as hypothetical proteins.

Table 2-1. Assembly and annotation statistics for the draft genome sequence of *P. miuraensis* SMH-27-4.

Number of contigs	164
GC Content (%)	69.7
Estimated genome size based on Kmer analysis	11,832,550 bp
Assembled genome size	11,849,290 bp (100.1%)
N50 (bp)	398,768
L50	11
Genes (total)	9280
Pseudogenes (total)	40
Genes (RNA)	84
tRNAs	77
rRNAs	1, 1, 1 (5S, 16S, 23S)
ncRNAs	4
Genes (coding)	9156
Coding density	90.7%
Hypothetic proteins	3508 (38.3%)
Percentage (%) of complete BUSCOs in the genome assembly	93.0%
Percentage (%) of complete BUSCOs among the annotated genes	92.6%

2.2.2. Phylogenetic analysis

Both the 16S rRNA gene sequence-based and genome sequence-based phylogenetic analyses of the order Myxococcales were performed. The complete 16S rRNA gene sequence of *P. miuraensis* SMH-27-4 consisted of 1544 bp (locus_tag = OEB96_36580), which is identical to the reported partial 16S rRNA gene sequence (1504 bp) [13]. In the 16S rRNA gene sequence-based phylogenetic tree (Figure 2-2A), the strains in the family Nannocystaceae were divided into two subclades with a support value of 100%. Although *P. miuraensis* SMH-27-4 shared a subclade with the terrestrial genus *Nannocystis*, it branched out of the strains of the genus *Nannocystis* with a support value of 76%. The strains of (slightly) halophilic genera (*E. salina* DSM 15217, *P. salsuginis* DSM 21377, and *P. pacifica* DSM 14875) formed the other subclade.

To perform genome-based taxonomic classification, the average nucleotide identity (ANI) was compared between *P. miuraensis* SMH-27-4 and 51 other sequenced myxobacterial strains. The resulting genome-based phylogenetic tree (ANI tree, Figure 2-2B) indicated that *P. miuraensis* SMH-27-4 was grouped into the family Nannocystaceae but did not form any subclade with other strains of this family. This result is similar to the 16S rRNA gene sequence-based tree (Figure 2-2A), supporting the novelty of the genus *Paraliomyxa*.

A

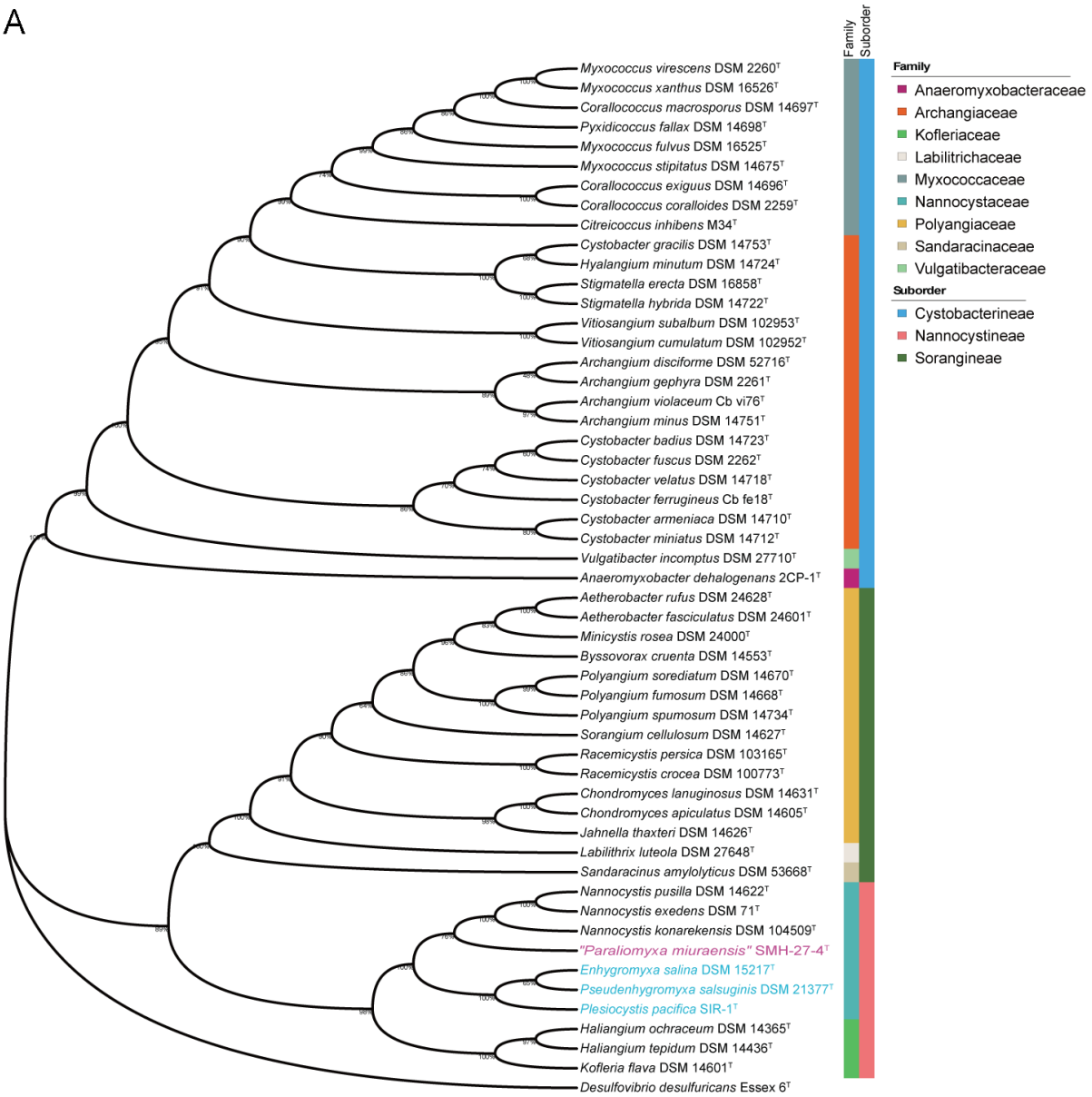
Family
Suborder
Family
Anaeromyxobacteraceae
Archangiaceae
Kofleriaceae
Labilitrichaceae
Myxococcaceae
Nannocystaceae
Polyangiaceae
Sandaracinaceae
Vulgatibacteraceae
Suborder
Cystobacterineae
Nannocystineae
Sorangineae
Myxococcus virescens DSM 2260T
Myxococcus xanthus DSM 16526T
Corallococcus macrosporus DSM 14697T
Pyxidicoccus fallax DSM 14698T
Myxococcus fulvus DSM 16525T
Myxococcus stipitatus DSM 14675T
Corallococcus exiguus DSM 14696T
Corallococcus coralloides DSM 2259T
Citreicoccus inhibens M34T
Cystobacter gracilis DSM 14753T
Hyalangium minutum DSM 14724T
Stigmatella erecta DSM 16858T
Stigmatella hybrida DSM 14722T
Vitiosangium subalbum DSM 102953T
Vitiosangium cumulatum DSM 102952T
Archangium disciforme DSM 52716T
Archangium gephyra DSM 2261T
Archangium violaceum Cb vi76T
Archangium minus DSM 14751T
Cystobacter badius DSM 14723T
Cystobacter fuscus DSM 2262T
Cystobacter velatus DSM 14718T
Cystobacter ferrugineus Cb fe18T
Cystobacter armeniaca DSM 14710T
Cystobacter miniatus DSM 14712T
Vulgatibacter incomptus DSM 27710T
Anaeromyxobacter dehalogenans 2CP-1T
Aetherobacter rufus DSM 24628T
Aetherobacter fasciculatus DSM 24601T
Minicystis rosea DSM 24000T
Byssovorax cruenta DSM 14553T
Polyangium sorediatum DSM 14670T
Polyangium fumosum DSM 14668T
Polyangium spumosum DSM 14734T
Sorangium cellulosum DSM 14627T
Racemicystis persica DSM 103165T
Racemicystis crocea DSM 100773T
Chondromyces lanuginosus DSM 14631T
Chondromyces apiculatus DSM 14605T
Jahnella thaxteri DSM 14626T
Labilithrix luteola DSM 27648T
Sandaracinus amylolyticus DSM 53668T
Nannocystis pusilla DSM 14622T
Nannocystis exedens DSM 71T
Nannocystis konarekensis DSM 104509T
"Paraliomyxa miuraensis" SMH-27-4T
Enhygromyxa salina DSM 15217T
Pseudenhygromyxa salsuginis DSM 21377T
Plesiocystis pacifica SIR-1T
Haliangium ochraceum DSM 14365T
Haliangium tepidum DSM 14436T
Kofleria flava DSM 14601T
Desulfovibrio desulfuricans Essex 6T

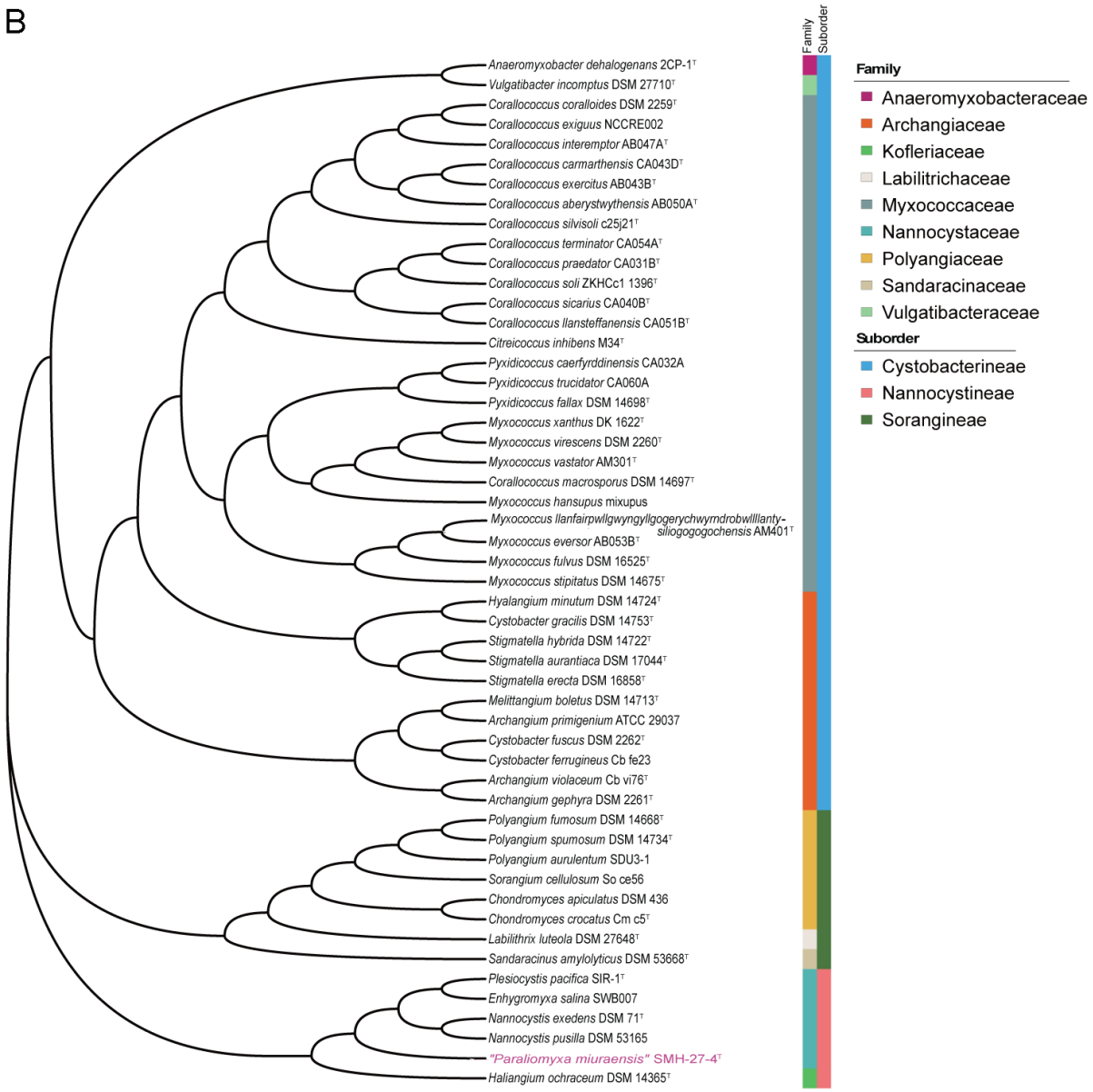

Figure 2-2. Phylogenetic trees of myxobacteria in comparison with *P. miuraensis* SMH-27-4. (A) 16S rRNA gene sequence-based tree. The numbers at the nodes indicate branch support values. The (slightly) halophilic strains of the family Nannocystaceae are in light blue. (B) Genome sequence-based tree.

2.2.3. Biosynthetic gene clusters (BGCs)

The antiSMASH detected 30 protoclusters, which, due to the presence of some hybrid types, were partially compiled to obtain 24 candidate BGC regions for secondary metabolite biosynthesis (Table 2-2). The RiPPMiner retrieved five ribosomally synthesized and post-translationally modified peptide (RiPP) protoclusters (Table 2-3). After the removal of protoclusters of unspecific BGC type and combination of close protoclusters based on the

rules described in Section 2.3.4, 17 BGCs in total were annotated from the genome of P. miuraensis SMH-27-4 (Figures 2-3), their locations in the genome were shown in Figure 2-4. The BGCs include three hybrids of non-ribosomal peptide synthetases/type I polyketide synthase (NRPS/T1PKS), one siderophore, four terpenes, three thioamitides, one NRPS, one linear azol(in)e-containing peptide/aryl polyene hybrid (LAP/APE, probably hybrid), two class-I lanthipeptides, one glycocin and one head-to-tail cyclized bacteriocin.

Table 2-2. Candidate secondary metabolite BGC regions identified with antiSMASH.

Region	Locus (contigs)	Type	From	To
Region 1	JAOVZF010000162.1	T1PKS, NRPS	272536	360088
Region 2	JAOVZF010000163.1	NRPS, T1PKS	507693	593915
Region 3	JAOVZF010000152.1	NRPS, T1PKS	276778	336871
Region 4	JAOVZF010000134.1	siderophore	46935	61490
Region 5	JAOVZF010000149.1	terpene	186818	209109
Region 6	JAOVZF010000161.1	terpene	243759	261662
Region 7	JAOVZF010000157.1	terpene	74778	96691
Region 8	JAOVZF010000161.1	terpene	376547	398295
Region 9	JAOVZF010000163.1	RiPP-like	304798	312818
Region 10	JAOVZF010000163.1	RiPP-like	470102	481025
Region 11	JAOVZF010000162.1	RiPP-like	203558	223128
Region 12	JAOVZF010000157.1	RiPP-like	162301	173182
Region 13	JAOVZF010000133.1	RiPP-like	94703	104650
Region 14	JAOVZF010000160.1	RiPP-like	84202	96013
Region 15	JAOVZF010000139.1	RiPP-like	7088	18050
Region 16	JAOVZF010000158.1	RiPP-like	403850	414788
Region 17	JAOVZF010000145.1	thioamitides	21637	44219
Region 18	JAOVZF010000139.1	thioamitides	85971	108523
Region 19	JAOVZF010000155.1	thioamitides	363283	385917
Region 20	JAOVZF010000159.1	other	55245	97845
Region 21	JAOVZF010000163.1	RiPP-like, NRPS	269655	313831
Region 22	JAOVZF010000163.1	LAP, APE	113265	184966
Region 23	JAOVZF010000151.1	Class-I lanthipeptide, RiPP-like	105469	134267
Region 24	JAOVZF010000164.1	Class-I lanthipeptide	312593	342102

Table 2-3. RiPP protoclusters revealed by RiPPMiner.

Protocluster	Locus (contigs)	RiPP class	From	To
Protocluster 1	JAOVZF010000146.1	Glycocin	115465	174581
Protocluster 2	JAOVZF010000146.1	Head-to-tail cyclized	178690	235768
Protocluster 3	JAOVZF010000151.1	Class-I lanthipeptide	85529	149744
Protocluster 4	JAOVZF010000163.1	LAP	86181	174179
Protocluster 5	JAOVZF010000164.1	Class-I lanthipeptide	309536	377957

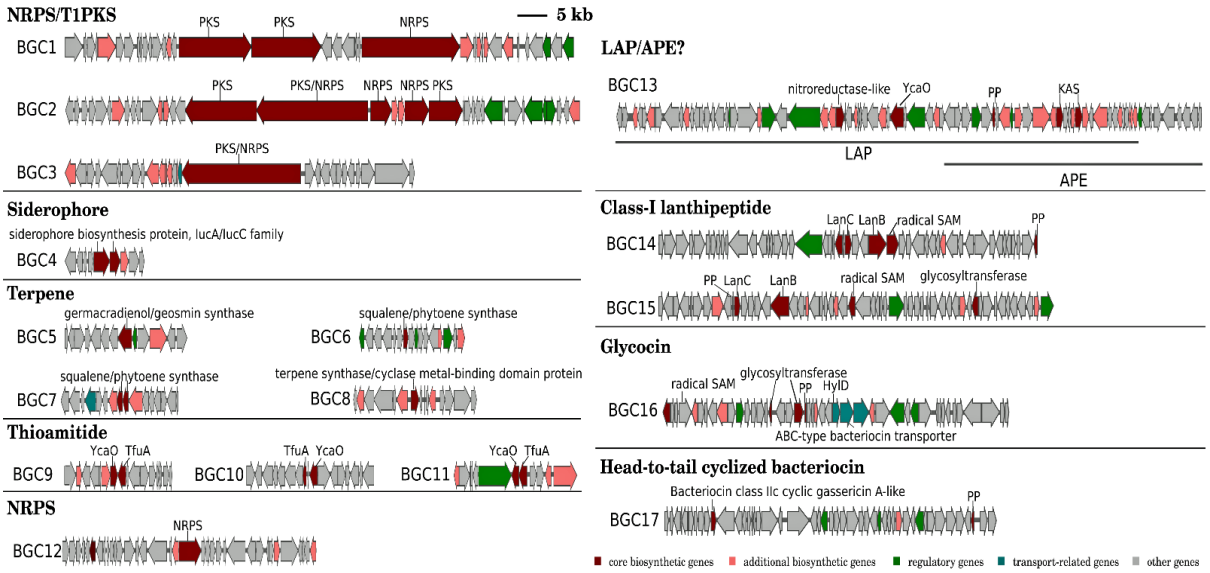

Figure 2-3. Organizations of putative BGCs in the genome of *P. miuraensis* SMH-27-4.

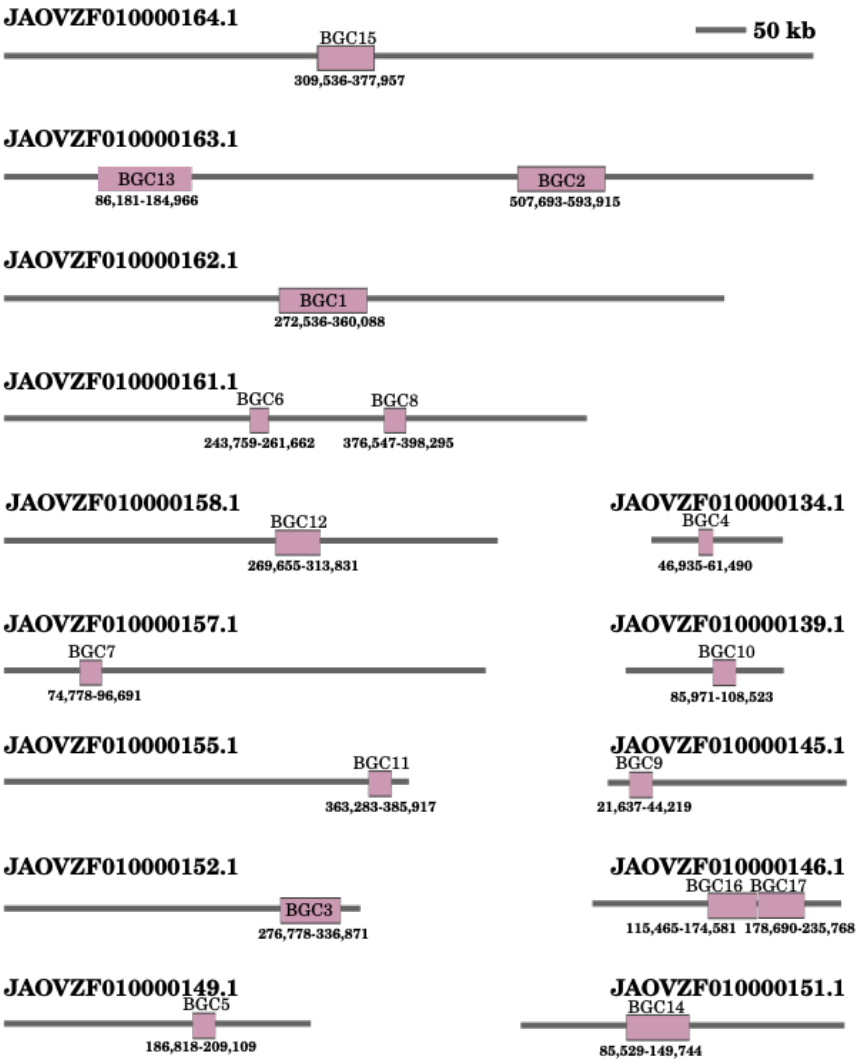

Figure 2-4. Locations of BGCs.

BGC1 (NRPS/T1PKS) was regarded as the BGC for miuraenamide A because the predicted substrate selectivity of its eight modules and their assembly order matched the backbone of miuraenamide A, consisting of five polyketide units and a tripeptide composed of alanine, tyrosine, and phenylalanine.

The BGC sequence similarity network obtained by Big-SCAPE suggested the great potential of this strain to produce novel secondary metabolites. Each of the five BGCs (BGC1–BGC5) formed a cluster with the known BGCs from the minimum information about a biosynthetic gene cluster (MIBiG) database (Figure 2-5), while the other 12 BGCs showed no similarity with the BGCs for known products. The chemical structures of the products encoded by them were listed with the same numbers in Figure 2-6.

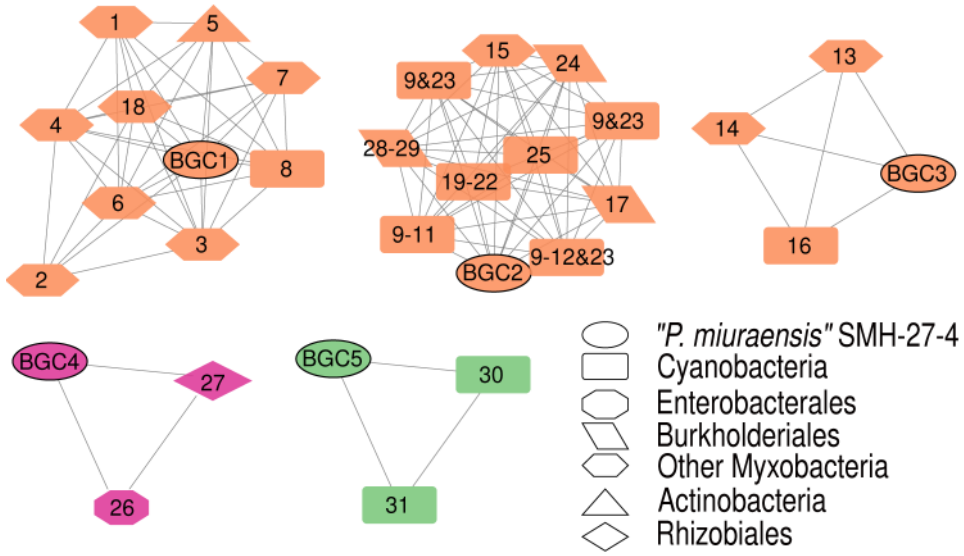

Figure 2-5. BGC sequence similarity networks of *P. miuraensis* SMH-27-4 and related sequences from the MIBiG database. Nodes are color-coded according to BGC types and shape-coded according to biosynthesis origins (legend). Numbered nodes represent the BGCs from the MIBiG database.

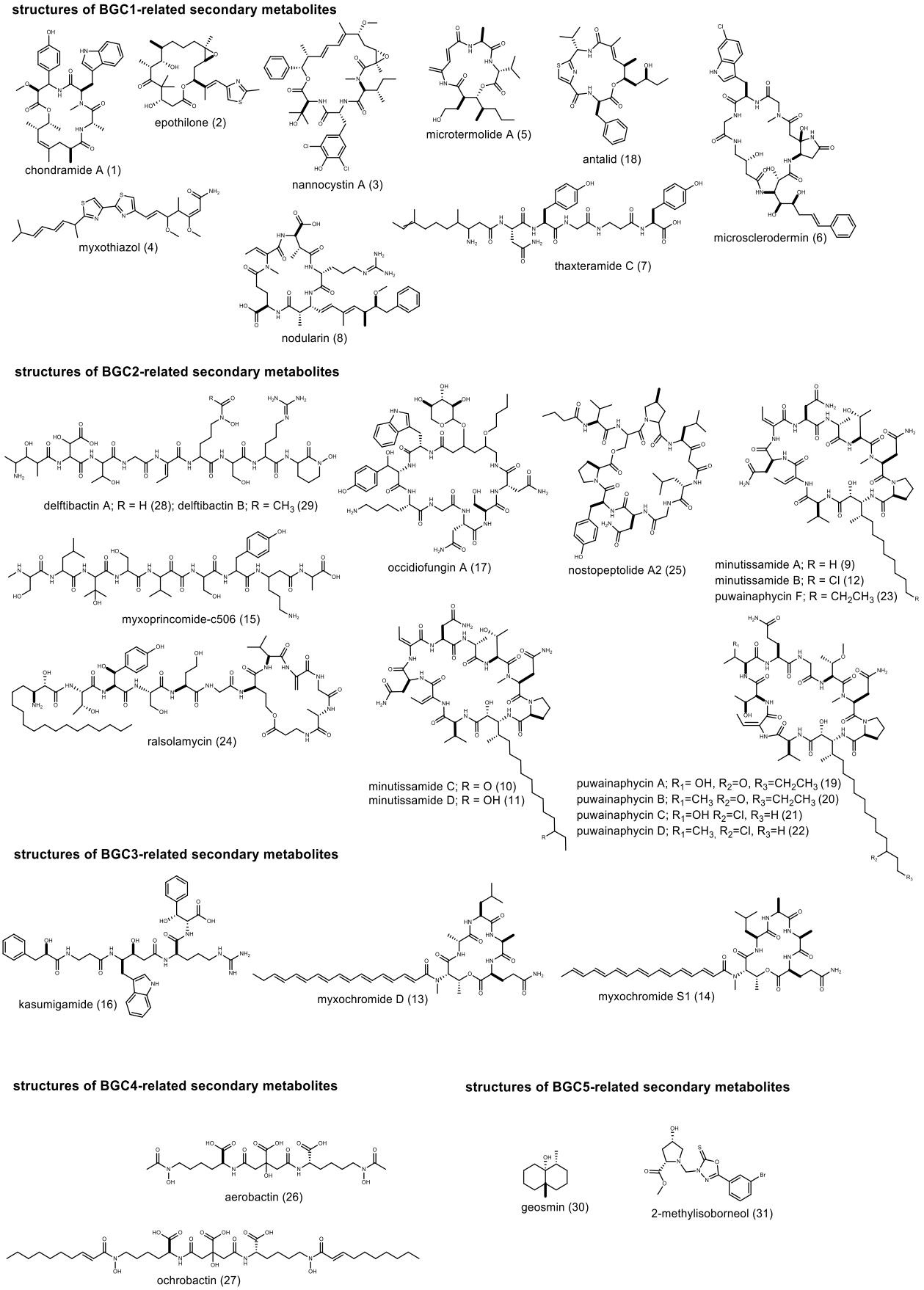

Figure 2-6. Chemical structures of the secondary metabolites described in Figure 2-5.

BGC1 was clustered with the BGCs encoding the biosynthesis of nine myxobacterial depsipeptides: chondramide A (**1**), epothilone (**2**), nannocystin A (**3**), myxothiazol (**4**), microsclerodermin (**6**), thaxteramide C (**7**), antalid (**18**), and two cyclic depsipeptides from actinobacteria and cyanobacteria, microtermolide A (**5**) and nodularin (**8**). The organizations of BGC1 and its related BGCs of other species were shown in Figure 2-7.

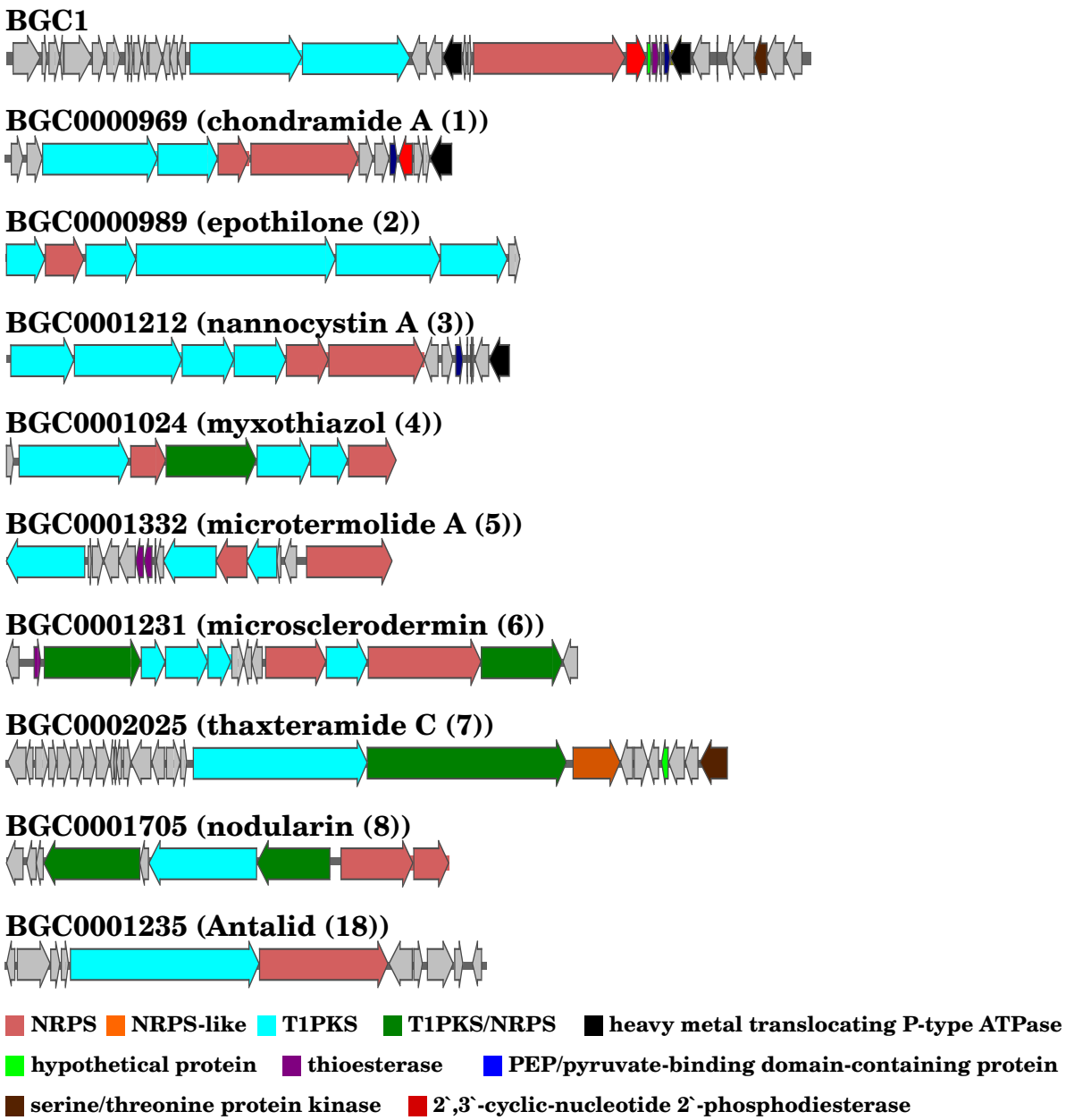

Figure 2-7. Organizations of BGC1 and its related BGCs of other species. The BGC numbers were obtained by BiG-SCAPE. PKS and NRPS related genes (NRPS, NRPS-like, T1PKS, and T1PKS/NRPS) are colored by their types. The other colored genes (except grey) are based on blastp results (e-value ≤10-10, identity ≥30%).

The BGC2 was clustered with the BGCs encoding the following metabolites' biosynthesis: two groups of cyanobacterial cyclic lipopeptides minutissamides (**9**–**12**) and puwainaphycins (**19**–**23**), a cyanobacterial non-ribosomal peptide nostopeptolide A2 (**25**) [44], the membrane morphology-disrupting fungicide occidiofungin A (**17**) [45], the fungal chlamydospore formation-inducer ralsolamycin (**24**) [46], the delftibactins that are able to detoxify toxic soluble gold (**28**, **29**) [47], and the myxobacterial linear peptide myxoprincomide-c506 (**15**). The organizations of BGC2 and its related BGCs of other species were shown in Figure 2-8.

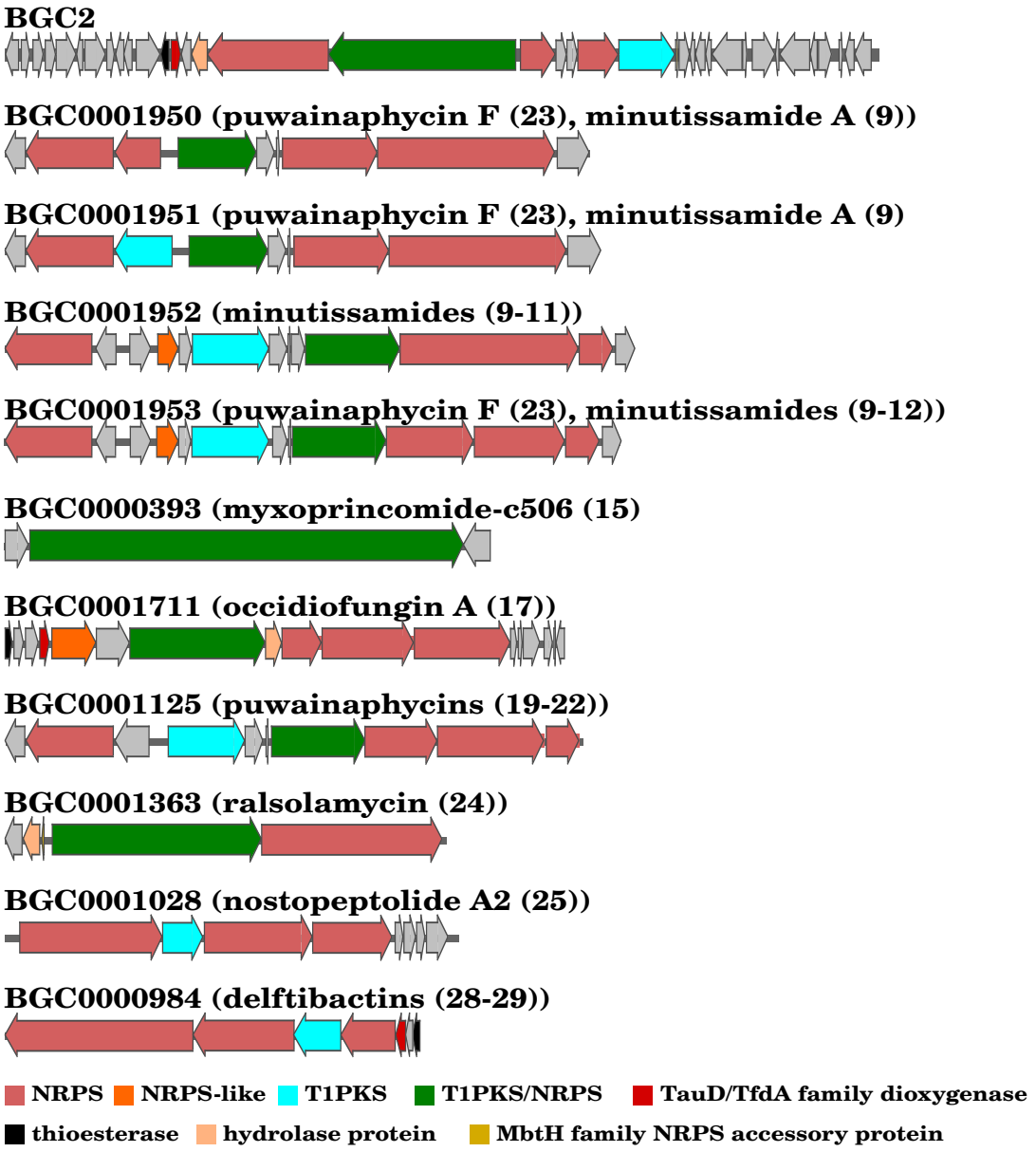

Figure 2-8. Organizations of BGC2 and its related BGCs of other species.

BGC3 was clustered with the BGCs encoding the biosynthesis of the myxobacterial cyclic depsipeptides myxochromides (**13**, **14**) and the antialgal cyanobacterial peptide kasumigamide (**16**) [48]. BGC4 was clustered with the BGCs encoding the biosynthesis of the bacterial siderophores aerobactin (**26**) and ochrobactin (**27**). BGC5 was clustered with the BGCs encoding the biosynthesis of geosmin (**30**) and 2-methylisoborneol (**31**), both of which are responsible for the earthy–musty odor in water. The organizations of BGC3-5 and its related BGCs of other species were shown in Figure 2-9, 2-10, 2-11, respectively.

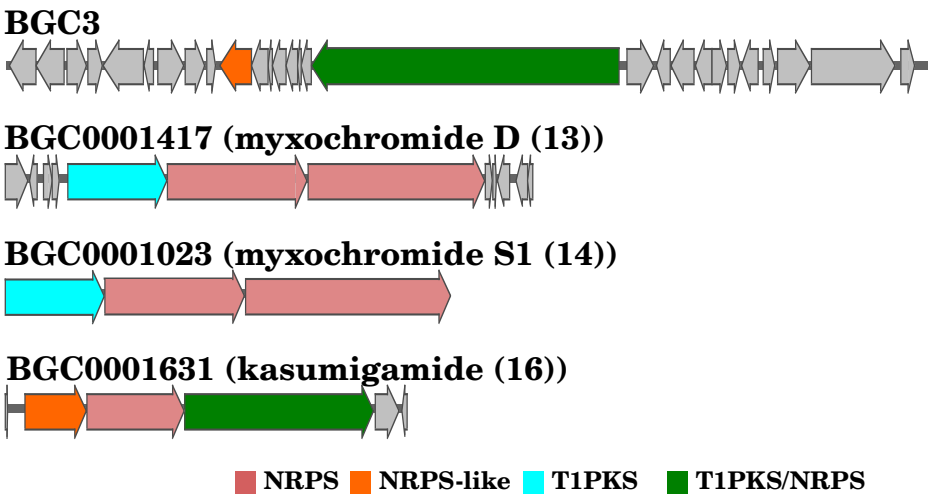

Figure 2-9. Organizations of BGC3 and its related BGCs of other species.

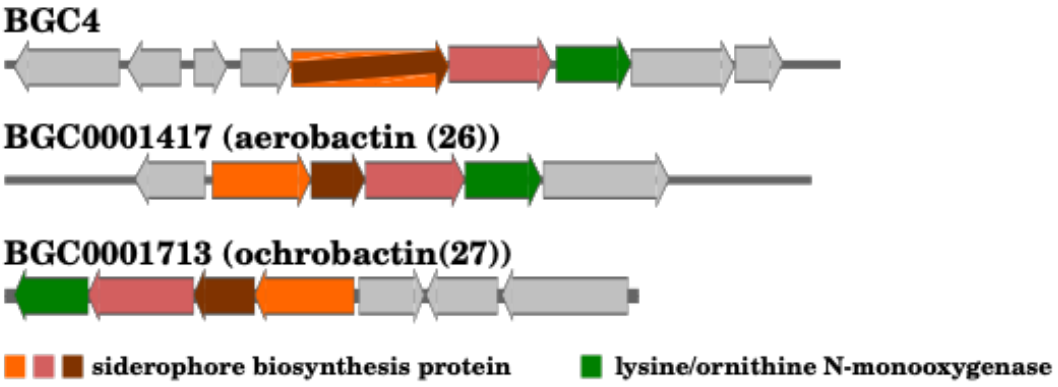

Figure 2-10. Organizations of BGC4 and its related BGCs of other species.

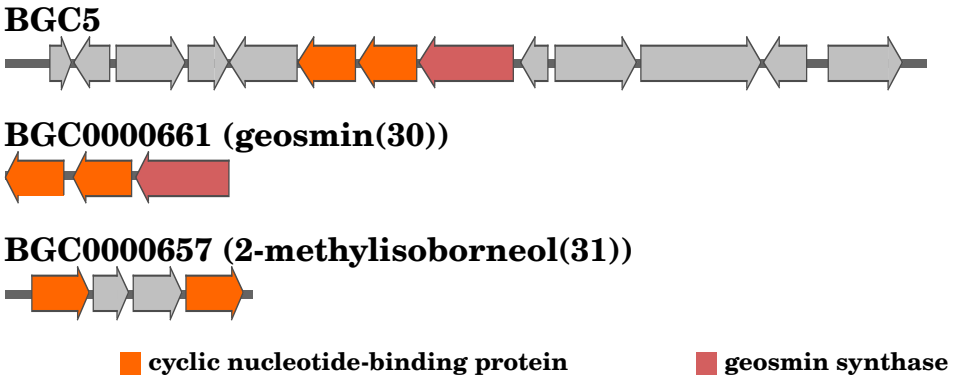

Figure 2-11. Organizations of BGC5 and its related BGCs of other species.

2.2.4. Distribution of gene functions of the strains of the family nannocystaceae

The family Nannocystaceae that contains *P. miuraensis* SMH-27-4 is known to be ecologically diverse. To explore the distribution of the gene functions of this family, a comparative genomic analysis was performed for the genomes of representative strains from five different genera in the family Nannocystaceae: *P. miuraensis* SMH-27-4, *N. exedens* DSM 71, *P.* sp. WMMC2535, *P. pacifica* DSM 14875, and *E. salina* DSM 15201. The orthologous protein-coding genes were identified, and the genomic functional annotation was performed by the clusters of orthologous groups (COG) approach. Here, the protein-coding genes were divided into core, accessory, and strain-specific genes based on the distribution of orthologous genes through the examined strains (Table 2-4). The core genes, common genes in the five strains, accounted for 16–19% of each genome, while the strain-specific genes accounted for 44–59%. The others were classified into the accessory genes that occupied 25–37% of the genomes. The COG approach performs microbial genome-wide functional annotation against the COG database, which consists of COGs with manually curated annotation and classifies the COGs into 26 functional categories. The distribution of COG functional categories can reveal to some extent the metabolic or physiological features of the bacteria. Approximately 43% of the protein-coding genes of each strain were classified in COG superfamilies, while more than half were not, suggesting

that the genomic resources of myxobacteria are underexplored. The numbers of genes of each COG functional category are listed in Table 2-5.

Table 2-4. Comparative genomic analysis of five strains of the family Nannocystaceae.

Strains	Protein-Coding Genes	Orthologous Genes			COG Annotated Genes
		Core Genes	Accessory Genes	Strain-Specific Genes	
Pm	9145 (100%)	1460 (16%)	2500 (27%)	5185 (57%)	3891 (43%)
Ne	9295 (100%)	1469 (16%)	2347 (25%)	5479 (59%)	4020 (43%)
Ps	7726 (100%)	1475 (19%)	2847 (37%)	3404 (44%)	3389 (44%)
Pp	8182 (100%)	1448 (18%)	2859 (35%)	3875 (47%)	3516 (43%)
Es	8079 (100%)	1448 (18%)	2788 (35%)	3843 (48%)	3390 (42%)

The strains included in this analysis are the following: Pm *P. miuraensis* SMH-27-4, Ne *N. exedens* DSM 71, Ps *P.* sp. WMMC2535, Pp *P. pacifica* SIR-1, Es *E. salina* DSM 1520.

Table 2-5. COG classification of the protein-coding genes of five strains in the family Nannocystaceae.

COG functional categories	Number of genes*				
	***N. exedens* DSM 71**	***P.* sp. WMMC 2535**	***P. miuraensis* SMH-27-4**	***E. salina* DSM 1520**	***P. pacifica* SIR-1**
A: RNA processing and modification	3	0	3	1	2
C: Energy production and conversion	200	17	186	169	165
D: Cell cycle control, cell division, chromosome partitioning	59	82	85	79	72
E: Amino acid transport and metabolism	166	156	174	162	185
F: Nucleotide transport and metabolism	64	61	63	53	65
G: Carbohydrate transport and metabolism	102	73	98	79	90
H: Coenzyme transport and metabolism	158	154	151	141	164
I: Lipid transport and metabolism	266	252	244	260	256
J: Translation, ribosomal structure and biogenesis	238	237	231	222	215
K: Transcription	442	278	338	257	381
L: Replication, recombination and repair	147	137	137	138	118
M: Cell wall/membrane/envelope biogenesis	246	207	275	224	215

N: Cell motility	20	21	21	22	18
O: Posttranslational modification, protein turnover, chaperones	255	229	263	237	243
P: Inorganic ion transport and metabolism	139	125	121	122	117
Q: Secondary metabolites biosynthesis, transport and catabolism	90	60	63	81	74
T: Signal transduction mechanisms	599	489	635	474	490
U: Intracellular trafficking, secretion, and vesicular transport	54	60	68	56	45
V: Defense mechanisms	175	117	143	135	112
W: Extracellular structures	14	13	21	15	13
X: Mobilome: prophages, transposons	105	35	31	24	35
Z: Cytoskeleton	7	17	11	16	8
R: General function prediction only	387	354	461	362	374
S: Function unknown	84	61	71	63	61

*The numbers of genes were counted using in-house Python script and rounded to intigers.

The distribution of functional categories of all COGs was similar between the five strains (Figure 2-12A), indicating a possibility of conservation in the genomic functions within this family. Except for the poorly characterized categories [R] and [S], the most abundant categories were related to signal transduction mechanisms [T], transcription [K], and lipid transport and metabolism [I]. The abundance of these categories suggests that these myxobacterial strains evolved particular environmental response mechanisms of extra- and intracellular signals that include diverse proteins and metabolites. The average population of functional categories in this family quite varied by the number of core, accessory, and strain-specific genes (Figure 2-12B). In the accessory genes, signal transduction mechanisms [T] showed the significantly high distribution (16.6%) compared to the other categories (lower than 11.2%). In the strain-specific genes, both signal transduction mechanisms [T] and transcription [K] categories accounted for high distributions (14.4–17.2%). On the other

hand, the distribution of the core genes was more homogeneous. This trend was evidenced by the standard deviations of the distribution of 4.3%, 3.9%, and 3.4% for the strain-specific, accessory, and core genes, respectively. The variation of the gene functions and the percentage of the gene number (Table 2-4) in the strain-specific genes give an account of the diversity of these genera in the family Nannocystaceae.

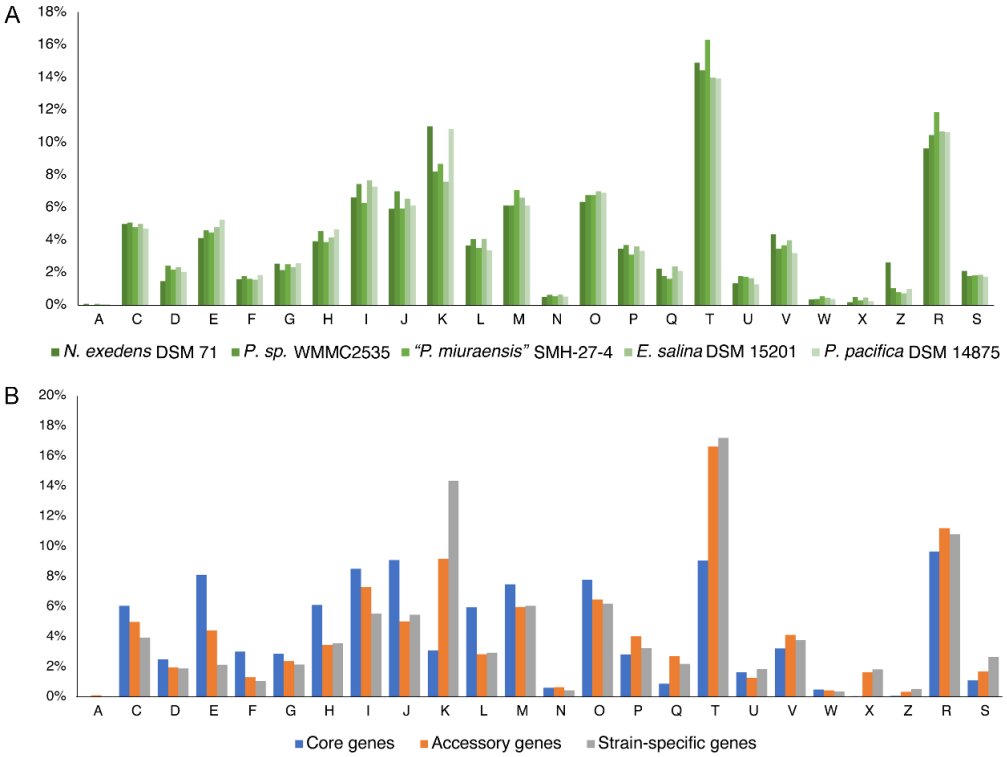

Figure 2-12. Distribution of COG functional categories in five strains of the family Nannocystaceae. (A) Distribution of functional categories in COGs by strains; (B) Average distribution of functional categories of all strains by the core, accessory, and strain-specific genes.

2.3. Materials and methods

2.3.1. Cultivation and genomic DNA isolation

Isolation of *P. miuraensis* SMH-27-4 was previously described [13]. The strain is registered in DBRP as STAJ0000000110262 and deposited in NBRC (Kisarazu, Chiba, Japan) as NBRC 111985. On the VY/2-1/5SWS agar plate [13], the strain swarms in a radial pattern and burrows into the agar. The outer edge of the swarm was cut out of the agar strip and frozen as glycerol stock in 12% (*w*/*v*) glycerol solution at −80 °C [14]. After thawing, the

glycerol stock was washed with autoclaved Milli-Q water and planted on the $Vy_5.S_{75.15}$ agar plate (see below). The plates were cultured for 14 days at 27 °C. Ten 0.5 cm square agar strips were cut out of the swarm edge and added to 750 mL of $N_{2.0}$-$S_{75.10}$ broth (see below) in a 2 L Erlenmeyer flask, which was shaken at 180 rpm. The cells tended to aggregate together, forming cell masses in the liquid broth. After 14 days of cultivation, the broth was filtrated by suction, and the orange or yellow cell mass on the filter paper was collected. Approximately 50 mg (wet weight) of the cells was used for the isolation of genomic DNA by a QIAGEN Genomic-tip 100/G (QIAGEN, Venlo, Nederland) and Genomic DNA Buffer Set (QIAGEN) according to standard protocols.

$Vy_5.S_{75.15}$ medium: 0.5% (*w*/*v*) yeast cake, 0.01% (*w*/*v*) Bacto™ yeast extract (Thermo Fisher Scientific, Waltham, MA, USA) and 1.5% (*w*/*v*) NaCl were suspended in 75% Sea Water Solution (SWS) [8], and pH was adjusted to 7.2–7.4 with 1 M NaOH before autoclaving. Vitamin B_{12} (0.5 mg/1 mL water) was sterilized by filtration and added to the autoclaved solution (1 L). Yeast cake: Dried yeast (Mitsubishi Tanabe Pharma, Osaka, Japan) was suspended in Milli-Q water (10% (*w*/*v*)). The supernatant was discarded after centrifugation (10,000× *g* rpm, 5 min), and the yeast cake was washed three times with water by suspending, vortexing, and centrifugation. The cake was stored at –30 °C until use. $N_{2.0}$-$S_{75.10}$ medium: 2% (*w*/*v*) casein sodium (FUJIFILM Wako Pure Chemical Corporation, Osaka, Japan) and 1% (*w*/*v*) NaCl were suspended in 75% Sea Water Solution (SWS), and the pH was adjusted to 7.2–7.4 with 1 M NaOH before autoclaving. Vitamin B_{12} (0.5 mg/1 mL water) was sterilized by filtration and added to the autoclaved solution (1 L).

2.3.2. Draft genome sequencing, assembly, and annotation

The whole genome was sequenced using the Illumina HiSeq platform, paired-end, 101 bp X 2 sequencing. The adapter sequence and low-quality bases were trimmed from raw reads files using Cutadapt (version 1.1) [27] and Trimmomatic (version 0.32) [28]. After trimming, sequence reads were assembled into contigs using the de novo genome assembler Velvet

(version 1.2.08) [29]. The gapclose module of Platanus (version 1.2.1) [30] was then applied to reduce the N content introduced into the genome during scaffolding. The contigs shorter than 200 bp were removed. Automated annotation of the draft genome sequence was performed with the prokaryotic genome annotation pipeline (PGAP) of NCBI (version 6.3) [31]. The estimated genome size was calculated by KmerGenie (version 1.7051) based on Kmer analysis. The completeness of genome assembly and annotation were assessed using benchmarking universal single-copy orthologs (BUSCO) scores (version 5.3.2) [32].

2.3.3. Phylogenetic analysis

The complete 16S rRNA gene sequence was identified by PGAP genome annotation. A dataset of 16S rRNA gene sequences of 52 Myxococcales strains and *Desulfovibrio desulfuricans* Essex 6 were retrieved from GenBank (Table 2-5). *D. desulfuricans* Essex 6 was used as an outgroup to root the tree. The 16S rRNA gene sequences were aligned by MAFFT (version 7.487) [33]. Maximum likelihood analyses were constructed in IQ-TREE (version 2.1.4-beta) [34] using the best-fit model TN + F + R4, selected by the software according to the Bayesian information criterion (BIC) scores. Bootstrap values were based on 1000 replicates, and the obtained tree was visualized using iTOL [35].

The genome sequences of 51 strains of the order Myxococcales were retrieved from the NCBI reference sequence (RefSeq) database (Table 2-6). The average nucleotide identity (ANI)-based distance tree was produced using the ANI-matrix genome distance calculator [36]. The ANI tree was clustered using the neighbor-joining method.

Table 2-6. Information of 16S rRNA genes used in Figure 2-2A.

Strains	Accession number of 16S rRNA gene	Length
Haliangium tepidum DSM 14436 ^{T}	NR_024781.1	1508
Plesiocystis pacifica SIR-1 ^{T}	NR_024795.1	1484
Enhygromyxa salina DSM 15217 ^{T}	NR_024807.1	1480
Cystobacter ferrugineus Cb fe18 ^{T}	NR_025343.1	1517
Chondromyces apiculatus DSM 14605 ^{T}	NR_025344.1	1534
Chondromyces lanuginosus DSM 14631 ^{T}	NR_025345.1	1535

Anaeromyxobacter dehalogenans 2CP-1 ^{T}	NR_027547.1	1545
Nannocystis exedens DSM 71 ^{T}	NR_040928.1	1480
Kofleria flava DSM 14601 ^{T}	NR_041981.1	1498
Corallococcus exiguus DSM 14696 ^{T}	NR_042330.1	1517
Byssovorax cruenta DSM 14553 ^{T}	NR_042341.1	1529
Stigmatella erecta DSM 16858 ^{T}	NR_042398.1	1534
Cystobacter armeniaca DSM 14710 ^{T}	NR_043939.1	1491
Cystobacter badius DSM 14723 ^{T}	NR_043940.1	1491
Cystobacter fuscus DSM 2262 ^{T}	NR_043941.1	1491
Cystobacter miniatus DSM 14712 ^{T}	NR_043942.1	1491
Archangium violaceum Cb vi76 ^{T}	NR_043943.1	1489
Cystobacter velatus DSM 14718 ^{T}	NR_043944.1	1491
Pyxidicoccus fallax DSM 14698 ^{T}	NR_043948.1	1493
Hyalangium minutum DSM 14724 ^{T}	NR_043949.1	1491
Stigmatella hybrida DSM 14722 ^{T}	NR_043952.1	1502
Corallococcus coralloides DSM 2259 ^{T}	NR_074852.2	1536
Haliangium ochraceum DSM 14365 ^{T}	NR_074917.1	1544
Myxococcus stipitatus DSM 14675 ^{T}	NR_102512.2	1535
Nannocystis pusilla DSM 14622 ^{T}	NR_104789.1	1518
Desulfovibrio desulfuricans Essex 6 ^{T}	NR_104990.1	1542
Myxococcus xanthus DSM 16526 ^{T}	NR_112544.1	1463
Myxococcus fulvus DSM 16525 ^{T}	NR_112545.1	1463
Myxococcus virescens DSM 2260 ^{T}	NR_112546.1	1463
Pseudenhygromyxa salsuginis DSM 21377 ^{T}	NR_113269.1	1494
Cystobacter gracilis DSM 14753 ^{T}	NR_115862.1	1491
Corallococcus macrosporus DSM 14697 ^{T}	NR_115865.1	1493
Sorangium cellulosum DSM 14627 ^{T}	NR_116678.1	1553
Archangium gephyra DSM 2261 ^{T}	NR_117459.1	1482
Jahnella thaxteri DSM 14626 ^{T}	NR_117461.1	1550
Archangium disciforme DSM 52716 ^{T}	NR_117600.1	1528
Sandaracinus amylolyticus DSM 53668 ^{T}	NR_118001.1	1506
Archangium minus DSM 14751 ^{T}	NR_125514.1	1491
Vulgatibacter incomptus DSM 27710 ^{T}	NR_126181.1	1479
Labilithrix luteola DSM 27648 ^{T}	NR_126182.1	1483
Minicystis rosea DSM 24000 ^{T}	NR_134090.1	1550
Aetherobacter fasciculatus DSM 24601 ^{T}	NR_148644.1	1548
Aetherobacter rufus DSM 24628 ^{T}	NR_148645.1	1551
Racemicystis crocea DSM 100773 ^{T}	NR_149306.1	1549
Racemicystis persica DSM 103165 ^{T}	NR_156102.1	1505
Vitiosangium cumulatum DSM 102952 ^{T}	NR_156939.1	1526
Vitiosangium subalbum DSM 102953 ^{T}	NR_156940.1	1528
Nannocystis konarekensis DSM 104509 ^{T}	NR_159914.1	1499
Polyangium fumosum DSM 14668 ^{T}	NR_160522.1	1550
Polyangium sorediatum DSM 14670 ^{T}	NR_160536.1	1552
Polyangium spumosum DSM 14734 ^{T}	NR_160537.1	1553
Citreicoccus inhibens M34 ^{T}	NR_173636.1	1536

Table 2-7. Information of genome sequences used in Figure 2-2B.

Strain	Assembly accession
Anaeromyxobacter dehalogenans 2CP-1^T	GCF_000022145.1
Archangium gephyra DSM 2261^T	GCF_001027285.1
Archangium primigenium ATCC 29037	GCF_016904885.1
Archangium violaceum Cb vi76^T	GCF_000733295.1
Chondromyces apiculatus DSM 436	GCF_000601485.1
Chondromyces crocatus Cm c5^T	GCF_001189295.1
Citreicoccus inhibens M34^T	GCF_019039035.1
Corallococcus aberystwythensis AB050A^T	GCF_003612165.1
Corallococcus carmarthensis CA043D^T	GCF_003611695.1
Corallococcus coralloides DSM 2259^T	GCF_000255295.1
Corallococcus exercitus AB043B^T	GCF_013116705.1
Corallococcus exiguous NCCRE002	GCF_017302975.1
Corallococcus interemptor AB047A^T	GCF_003668875.1
Corallococcus llansteffanensis CA051B^T	GCF_003612055.1
Corallococcus macrosporus DSM 14697^T	GCF_002305895.1
Corallococcus praedator CA031B^T	GCF_003612125.1
Corallococcus sicarius CA040B^T	GCF_003611735.1
Corallococcus silvisoli c25j21^T	GCF_009909145.1
Corallococcus soli ZKHCc1 1396^T	GCF_014930455.1
Corallococcus terminator CA054A^T	GCF_003611635.1
Cystobacter ferrugineus Cbfe23	GCF_001887355.1
Cystobacter fuscus DSM 2262^T	GCF_000335475.2
Cystobacter gracilis DSM 14753^T	GCF_020103725.1
Enhygromyxa salina SWB007	GCF_002994635.1
Haliangium ochraceum DSM 14365^T	GCF_000024805.1
Hyalangium minutum DSM 14724^T	GCF_000737315.1
Labilithrix luteola DSM 27648^T	GCF_001263205.1
Melittangium boletus DSM 14713^T	GCF_002305855.1
*Myxococcus eversor*AB053B^T	GCF_010894455.1
*Myxococcus fulvus*DSM 16525^T	GCF_900111765.1
Myxococcus hansupus mixupus	GCF_000280925.3
Myxococcus llanfairpwllgwyngyllgogerychwyrndrobwllllantysiliogogogochensis AM401^T	GCF_006636215.1
Myxococcus stipitatus DSM 14675^T	GCF_000331735.1
Myxococcus vastator AM301^T	GCF_010894475.1
Myxococcus virescens DSM 2260^T	GCF_900101905.1
Myxococcus xanthus DK 1622^T	GCF_000012685.1
Nannocystis exedens DSM 71^T	GCF_002343915.1
Nannocystis pusilla DSM 53165^T	GCF_020073745.1
Plesiocystis pacifica SIR-1^T	GCF_000170895.1
Polyangium aurulentum SDU3-1	GCF_005144635.2
Polyangium fumosum DSM 14668^T	GCF_005144585.1
Polyangium spumosum DSM 14734^T	GCF_009649845.1
Pyxidicoccus caerfyrddinensis CA032A	GCF_010894405.1

Pyxidicoccus fallax DSM 14698^T	GCF_012933655.1
Pyxidicoccus trucidator CA060A	GCF_010894435.1
Sandaracinus amylolyticus DSM 53668^T	GCF_000737325.1
Sorangium cellulosum So ce56	GCF_000067165.1
Stigmatella aurantiaca DSM 17044^T	GCF_900109545.1
Stigmatella erecta DSM 16858^T	GCF_900111745.1
Stigmatella hybrida DSM 14722^T	GCF_020103775.1
Vulgatibacter incomptus DSM 27710^T	GCF_001263175.1

2.3.4. BGCs prediction and generation of similarity networks

The draft genome sequence of *P. miuraensis* SMH-27-4 was mined using the antibiotics and secondary metabolite analysis shell (antiSMASH) (version 6.1.1) [37] to identify the secondary metabolite protoclusters using the “strict” setting. A machine learning-based ribosomally synthesized and post-translationally modified peptide (RiPPs)-mining tool, RiPPMiner [38] was also used to retrieve the RiPP protoclusters. The protoclusters were regarded as BGCs under the following criteria: (1) in the case that the overlapping area of two close protoclusters contains core biosynthetic genes, those with different cluster types are united to one “hybrid” BGC, whereas those with same cluster types are united to one BGC; (2) the following protoclusters predicted by antiSMASH were not considered as BGCs: “RiPP-like”, non-specific RiPP-containing post-translational modification proteins such as DUF 692 family, a function-unknown protein family, and “other” protoclusters that cannot be classified into the known categories. All the predicted BGCs were then analyzed using the biosynthetic gene similarity clustering and prospecting engine (BiG-SCAPE) software package (version 1.1.2) [39], with the MiBIG database (version 2.1) [40] as a reference. BiG-SCAPE was conducted on auto mode with a distance cut-off score of 0.75 and the parameters of “-clans-off”, “-no_classify”, and “-mix”. The *P. miuraensis* SMH-27-4 BGCs-related records were extracted, and the generated networks were visualized with Cytoscape (version 3.8.2) [41].

2.3.5. Identification of orthologous proteins and functional categorization

The genome sequences of four strains of the family Nannocystaceae (*Nannocystis exedens* DSM 71, *Pseudenhygromyxa* sp. WMMC2535 (GCA_011083025.2), *Plesiocystis pacifica* SIR-1, and *Enhygromyxa salina* DSM 15201 (GCA_000737335.3)) were retrieved from the NCBI genome and RefSeq database. Their genomes, including that of P. miuraensis SMH-27-4, were re-annotated by the stand-alone PGAP (version 2021-07-01. build5508) with the same parameters. The orthologous proteins were identified by Proteinortho [42]. The protein functional annotation was conducted using the domain-based annotation tool reCOGnizer (version 1.7.2) [43]. The results derived from the clusters of orthologous groups of proteins (COGs) database were used for functional categorization, which consists of 26 categories. Some proteins were classified into more than one functional category. In this case, each protein was assigned as an equal portion of weight for each functional category.

2.3.6. Availability of nucleotide sequence data

The whole genome shotgun project of *P. miuraensis* SMH-27-4 has been deposited at DDBJ/ENA/GenBank under the accession number JAOVZF000000000. The version described in this paper is version JAOVZF010000000. The raw sequencing data were submitted to the Sequence Read Archive database under the accession number SRR21887204.

2.4. Summary

The draft genome of *P. miuraensis* SMH-27-4 was sequenced, and de novo assembled into 11.8 Mbp of 164 contigs. Both Kmer and BUSCO analyses suggested a high degree of completeness of the genome assembly. The results of the 16S rRNA gene-sequence-based phylogenetic analysis and the genome-based taxonomic classification by ANI values were consistent with each other and indicated that this difficult-to-culture myxobacterium represents a novel genus in the family Nannocystaceae. Aside from the BGC for

miuraenamide A, the strain has 16 other BGCs that showed low or no similarity with the BGCs for known products, revealing a great potential of the strain to produce novel secondary metabolites. The similar distribution of the COG functional categories through the strains from five genera within the family Nannocystaceae indicated conserved genomic functions of this family. On the other hand, the average distribution of COG functional categories by the core, accessory, and strain-specific genes suggests that the five genera have diverse signal transduction and gene transcription mechanisms. Regardless of the taxonomic and physiological novelty of this rare slightly halophilic myxobacterium, the potential of great secondary metabolites production makes it worthy of studying.

References

1. Velicer, G.J.; Vos, M. Sociobiology of the myxobacteria. *Annu. Rev. Microbiol.* **2009**, *63*, 599–623.
2. Kaiser, D.; Robinson, M.; Kroos, L. Myxobacteria, polarity, and multicellular morphogenesis. *Cold Spring Harb. Perspect. Biol.* **2010**, *2*, a000380.
3. Muñoz-dorado, J.; Marcos-torres, F.J.; García-bravo, E.; Moraleda-muñoz, A.; Pérez, J. Myxobacteria: Moving, killing, feeding, and surviving together. *Front. Microbiol.* **2016**, *7*, 781.
4. Wenzel, S.C.; Müller, R. Myxobacteria—'Microbial factories' for the production of bioactive secondary metabolites. *Mol. BioSyst.* **2009**, *5*, 567–574.
5. Diez, J.; Martinez, J.P.; Mestres, J.; Sasse, F.; Frank, R.; Meyerhans, A. Myxobacteria: Natural pharmaceutical factories. *Microb. Cell Fact.* **2012**, *11*, 2–4.
6. Hug, J.J.; Müller, R. Host development for heterologous expression and biosynthetic studies of myxobacterial natural products. In *Comprehensive Natural Products III*, 3rd ed.; Liu, H., Begley, T.P., Eds.; Elsevier: San Diego, CA, USA, 2020; Volume 6, pp. 149–216.
7. Thaxter, R. Contributions from the cryptogamic laboratory of Harvard University. XVIII. On the Myxobacteriaceae, a new order of Schizomycetes. *Bot. Gaz.* **1892**, *12*, 389–406.
8. Iizuka, T.; Jojima, Y.; Fudou, R.; Yamanaka, S. Isolation of myxobacteria from the marine environment. *FEMS Microbiol. Lett.* **1998**, *169*, 317–322.
9. Dávila-Céspedes, A.; Hufendiek, P.; Crüsemann, M.; Schäberle, T.F.; König, G.M. Marine-derived myxobacteria of the suborder Nannocystineae: An underexplored source of structurally intriguing and biologically active metabolites. *Beilstein J. Org. Chem.* **2016**, *12*, 969–984.
10. Albataineh, H.; Stevens, D.C. Marine myxobacteria: A few good halophiles. *Mar. Drugs* **2018**, *16*, 209.
11. Gemperlein, K.; Zaburannyi, N.; Garcia, R.; La Clair, J.J.; Müller, R. Metabolic and biosynthetic diversity in marine myxobacteria. *Mar. Drugs* **2018**, *16*, 314.
12. Moghaddam, J.A.; Crüsemann, M.; Alanjary, M.; Harms, H.; Dávila-Céspedes, A.; Blom, J.; Poehlein, A.; Ziemert, N.; König, G.M.; Schäberle, T.F. Analysis of the genome and metabolome of marine myxobacteria reveals high potential for biosynthesis of novel specialized metabolites. *Sci. Rep.* **2018**, *8*, 16600.
13. Iizuka, T.; Fudou, R.; Jojima, Y.; Ogawa, S.; Yamanaka, S.; Inukai, Y.; Ojika, M. Miuraenamides A and B, novel antimicrobial cyclic depsipeptides from a new slightly halophilic myxobacterium: Taxonomy, production, and biological properties. *J. Antibiot.* **2006**, *59*, 385–391.
14. Iizuka, T. Isolation and Characterization of Novel Myxobacteria and Their Significance as Biomedical Resources. Ph.D. Thesis, Toyohashi University of Technology, Toyohashi, Japan, January 2016.

15. Garcia, R.; Müller, R. The family Nannocystaceae. In *The prokaryotes—Deltaproteobacteria and Epsilonproteobacteria*, 4th ed.; Rosenberg, E., Delong, E.F., Loy, S., Stackebrandt, E., Thompson, F., Eds.; Springer: Berlin/Heidelberg, Germany, 2014; Volume 10, pp. 213–229.
16. Iizuka, T.; Jojima, Y.; Hayakawa, A.; Fujii, T.; Yamanaka, S.; Fudou, R. *Pseudenhygromyxa salsuginis* gen. nov., sp. nov., a myxobacterium isolated from an estuarine marsh. *Int. J. Syst. Evol. Microbiol.* **2013**, *63*, 1360–1369.
17. Reichenbach, H. *Nannocystis exedens* gen. nov., spec. nov., a new myxobacterium of the family Sorangiaceae. *Arch. Mikrobiol.* **1970**, *70*, 119–138.
18. Sumiya, E.; Shimogawa, H.; Sasaki, H.; Tsutsumi, M.; Yoshita, K.; Ojika, M.; Suenaga, K.; Uesugi, M. Cell-morphology profiling of a natural product library identifies bisebromoamide and miuraenamide A as actin filament stabilizers. *ACS Chem. Biol.* **2011**, *6*, 425–431.
19. Karmann, L.; Schultz, K.; Herrmann, J.; Müller, R.; Kazmaier, U. Total syntheses and biological evaluation of miuraenamides. *Angew. Chem. Int. Ed.* **2015**, *54*, 4502–4507.
20. Ojima, D.; Yasui, A.; Tohyama, K.; Tokuzumi, K.; Toriihara, E.; Ito, K.; Iwasaki, A.; Tomura, T.; Ojika, M.; Suenaga, K. Total synthesis of miuraenamides A and D. *J. Org. Chem.* **2016**, *81*, 9886–9894.
21. Moser, C.; Rüdiger, D.; Förster, F.; von Blume, J.; Yu, P.; Kazmaier, U.; Vollmar, A.M.; Zahler, S. Persistent inhibition of pore-based cell migration by sub-toxic doses of miuraenamide, an actin filament stabilizer. *Sci. Rep.* **2017**, *7*, 16407.
22. Kappler, S.; Karmann, L.; Prudel, C.; Herrmann, J.; Caddeu, G.; Müller, R.; Vollmar, A.M.; Zahler, S.; Kazmaier, U. Synthesis and biological evaluation of modified miuraenamides. *Eur. J. Org. Chem.* **2018**, *48*, 6952–6965.
23. Gegenfurtner, F.A.; Zisis, T.; Al Danaf, N.; Schrimpf, W.; Kliesmete, Z.; Ziegenhain, C.; Enard, W.; Kazmaier, U.; Lamb, D.C.; Vollmar, A.M.; et al. Transcriptional effects of actin-binding compounds: The cytoplasm sets the tone. *Cell. Mol. Life Sci.* **2018**, *75*, 4539–4555.
24. Wang, S.; Crevenna, A.H.; Ugur, I.; Marion, A.; Antes, I.; Kazmaier, U.; Hoyer, M.; Lamb, D.C.; Gegenfurtner, F.; Kliesmete, Z.; et al. Actin stabilizing compounds show specific biological effects due to their binding mode. *Sci. Rep.* **2019**, *9*, 9731.
25. Wang, S.; Meixner, M.; Yu, L.; Zhuo, L.; Karmann, L.; Kazmaier, U.; Vollmar, A.M.; Antes, I.; Zahler, S. Turning the actin nucleating compound miuraenamide into nucleation inhibitors. *ACS Omega* **2021**, *6*, 22165–22172.
26. Baltes, C.; Thalla, D.G.; Kazmaier, U.; Lautenschläger, F. Actin stabilization in cell migration. *Front. Cell Dev. Biol.* **2022**, *10*, 931880.
27. Martin, M. Cutadapt removes adapter sequences from high-throughput sequencing reads. *EMBnet J.* **2011**, *17*, 10–12.

28. Bolger, A.M.; Lohse, M.; Usadel, B. Trimmomatic: A flexible trimmer for illumina sequence data. *Bioinformatics* **2014**, *30*, 2114–2120.
29. Zerbino, D.R.; Birney, E. Velvet: Algorithms for de novo short read assembly using de bruijn graphs. *Genome Res.* **2008**, *18*, 821–829.
30. Kajitani, R.; Toshimoto, K.; Noguchi, H.; Toyoda, A.; Ogura, Y.; Okuno, M.; Yabana, M.; Harada, M.; Nagayasu, E.; Maruyama, H.; et al. Efficient de novo assembly of highly heterozygous genomes from whole-genome shotgun short reads. *Genome Res.* **2014**, *24*, 1384–1395.
31. Tatusova, T.; Dicuccio, M.; Badretdin, A.; Chetvernin, V.; Nawrocki, E.P.; Zaslavsky, L.; Lomsadze, A.; Pruitt, K.D.; Borodovsky, M.; Ostell, J. NCBI prokaryotic genome annotation pipeline. *Nucleic Acids Res.* **2016**, *44*, 6614–6624.
32. Manni, M.; Berkeley, M.R.; Seppey, M.; Simão, F.A.; Zdobnov, E.M. BUSCO update: Novel and streamlined workflows along with broader and deeper phylogenetic coverage for scoring of eukaryotic, prokaryotic, and viral genomes. *Mol. Biol. Evol.* **2021**, *38*, 4647–4654.
33. Yamada, K.D.; Tomii, K.; Katoh, K. Application of the MAFFT sequence alignment program to large data–reexamination of the usefulness of chained guide trees. *Bioinformatics* **2016**, *32*, 3246–3251.
34. Minh, B.Q.; Schmidt, H.A.; Chernomor, O.; Schrempf, D.; Woodhams, M.D.; Von Haeseler, A.; Lanfear, R.; Teeling, E. IQ-TREE 2: New models and efficient methods for phylogenetic inference in the genomic era. *Mol. Biol. Evol.* **2020**, *37*, 1530–1534.
35. Letunic, I.; Bork, P. Interactive tree of life (ITOL) v5: An online tool for phylogenetic tree display and annotation. *Nucleic Acids Res.* **2021**, *49*, W293–W296.
36. Rodriguez-R, L.M.; Konstantinidis, K.T. The enveomics collection: A toolbox for specialized analyses of microbial genomes and metagenomes. *PeerJ Prepr*. **2016**, *4*, e1900v1.
37. Blin, K.; Shaw, S.; Kloosterman, A.M.; Charlop-Powers, Z.; van Wezel, G.P.; Medema, M.H.; Weber, T. AntiSMASH 6.0: Improving cluster detection and comparison capabilities. *Nucleic Acids Res.* **2021**, *49*, W29–W35.
38. Agrawal, P.; Khater, S.; Gupta, M.; Sain, N.; Mohanty, D. RiPPMiner: A bioinformatics resource for deciphering chemical structures of RiPPs based on prediction of cleavage and cross-links. *Nucleic Acids Res.* **2017**, *45*, W80–W88.
39. Navarro-Muñoz, J.C.; Selem-Mojica, N.; Mullowney, M.W.; Kautsar, S.A.; Tryon, J.H.; Parkinson, E.I.; De Los Santos, E.L.C.; Yeong, M.; Cruz-Morales, P.; Abubucker, S.; et al. A computational framework to explore large-scale biosynthetic diversity. *Nat. Chem. Biol.* **2020**, *16*, 60–68.
40. Kautsar, S.A.; Blin, K.; Shaw, S.; Navarro-Muñoz, J.C.; Terlouw, B.R.; van der Hooft, J.J.J.; van Santen, J.A.; Tracanna, V.; Suarez Duran, H.G.; Pascal Andreu, V.; et al. MIBiG

2.0: A repository for biosynthetic gene clusters of known function. *Nucleic Acids Res.* **2020**, *48*, D454–D458.

41. Shannon, P.; Markiel, A.; Ozier, O.; Baliga, N.S.; Wang, J.T.; Ramage, D.; Amin, N.; Schwikowski, B.; Ideker, T. Cytoscape: A software environment for integrated models of biomolecular interaction networks. *Genome Res.* **2003**, *13*, 2498–2504.
42. Lechner, M.; Findeiß, S.; Steiner, L.; Marz, M.; Stadler, P.F.; Prohaska, S.J. Proteinortho: Detection of (co-) orthologs in large-scale analysis. *BMC Bioinform.* **2011**, *12*, 124.
43. Sequeira, J.C.; Rocha, M.; Alves, M.M.; Salvador, A.F. UPIMAPI, ReCOGnizer and KEGGCharter: Bioinformatics tools for functional annotation and visualization of (meta)-omics datasets. *Comput. Struct. Biotechnol. J.* **2022**, *20*, 1798–1810.
44. Liaimera, A.; Helfrichb, E.J.N.; Hinrichsc, K.; Guljamowc, A.; Ishidab, K.; Hertweck, C.; Dittmann, E. Nostopeptolide plays a governing role during cellular differentiation of the symbiotic cyanobacterium *Nostoc punctiforme*. *Proc. Natl. Acad. Sci. USA* **2015**, *112*, 1862–1867.
45. Lu, S.E.; Novak, J.; Austin, F.W.; Gu, G.; Ellis, D.; Kirk, M.; Wilson-Stanford, S.; Tonelli, M.; Smith, L. Occidiofungin, a unique antifungal glycopeptide produced by a strain of *Burkholderia contaminans*. *Biochemistry* **2009**, *48*, 8312–8321.
46. Baldeweg, F.; Kage, H.; Schieferdecker, S.; Allen, C.; Hoffmeister, D.; Nett, M. Structure of ralsolamycin, the interkingdom morphogen from the crop plant pathogen *Ralstonia solanacearum*. *Org. Lett.* **2017**, *19*, 4868–4871.
47. Johnston, C.W.; Wyatt, M.A.; Li, X.; Ibrahim, A.; Shuster, J.; Southam, G.; Magarvey, N.A. Gold biomineralization by a metallophore from a gold-associated microbe. *Nat. Chem. Biol.* **2013**, *9*, 241–243.
48. Ishida, K.; Murakami, M. Kasumigamide, an antialgal peptide from the cyanobacterium *Microcystis aeruginosa*. *J. Org. Chem.* **2000**, *65*, 5898–5900.

Chapter 3. Heterologous biosynthesis of miuraenamide A

3.1. Introduction

Myxobacteria are gram-negative bacteria that are characterized by gliding, multicellular fruiting body formation and large genome size [1–3]. They are considered as good candidates for a next-generation microbial drug factory because of their potential for the production of structurally novel secondary metabolites [4–6]. The limited number of halophilic strains, despite the difficulty of isolation and cultivation, have been reported and showed great potential for producing novel bioactive leads [7–10]. In 2006, *Paraliomyxa miuraensis* SMH-27-4 was isolated from a near-seashore soil in Japan [11]. The strain required low salt concentrations of 0.5–1.0% for optimum growth and was regarded as a slightly halophilic myxobacterium. The major secondary metabolite miuraenamide A (**1**, Figure 3-1) exhibited potent antifungal activity, especially against the phytopathogenic oomycete *Phytophthora capsici* at a minimum inhibition dose of 25 ng/disk by inhibiting the mitochondrial respiratory chain. It also stabilizes actin filaments to change tumor cell morphology [12]. The cellular studies of **1** demonstrated the effects on cell migration and transcriptional activity [13, 14]. It is reported that **1** has a unique actin binding mode different from jasplakinolide, a commonly used pharmacological tool to study actin organization and dynamics in living cells [15]. More recently, **1** has been shown to induce actin filaments elongation and to shift the nucleus toward the cell center [16]. Miuraenamide A (1) is considered as a new tool to facilitate understanding the role of actin in living cells. The total synthesis and the structure-activity studies of several derivatives have also been reported [17–19]. We recently analyzed the genome of the strain SMH-27-4 and revealed the presence of 17 biosynthetic machineries for secondary metabolites [20], the detailed biosynthetic mechanism of **1** is still blank.

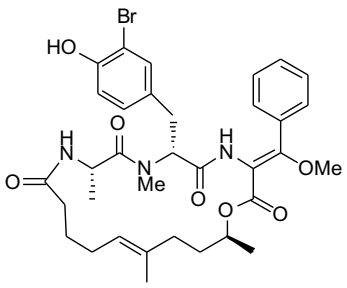

miuraenamide A (**1**)

Figure 3-1. Chemical structure of miuraenamide A (**1**).

The original producer of **1**, SMH-27-4, requires the culture period of 18 days to reach the maximal production (1 mg/L) of **1** [11] and is difficult to handle. On a sea water agar medium, the strain burrows into the agar and does not form distinct single-cell colonies. In liquid broths, the cells aggregate to form cell clusters, making obtaining a homogeneous cell suspension impossible. Therefore, the genetic manipulation of the original producer to elucidate the biosynthetic mechanism of **1** is challenging.

In this chapter, the identification and heterologous expression of the biosynthetic gene cluster (BGC) for **1** was described. The proposed biosynthetic pathway was verified by gene disruption and a multi-gene region that significantly affected the production of **1** was demonstrated.

3.2. Results and discussion

3.2.1. Identification and heterologous expression of BGC for miuraenamide A

The backbone of **1** can be divided into a five-unit polyketide and a tripeptide composed of alanine, bromotyrosine, and methoxylated phenylalanine, suggesting that it is a hybrid metabolite of the polyketide synthase-nonribosomal peptide synthase (PKS-NRPS) type. The draft genome of *P. miuraensis* SMH-27-4 [20] was analyzed by antiSMASH to find a PKS-NRPS type gene cluster that possessed the predicted substrate selectivity of the constituent modules and the assembly order matching the backbone of **1**. This cluster was, therefore, considered as the BCG for **1** (*miu* cluster), which spread over the tentative range

of 85.9 kb containing 36 open reading frames (orfs) (Figure 3-2A). It is noteworthy that antiSMASH tends to overpredict the range of the cluster, the *orf1* and *orf29* may not be the true boundaries of the BGC for **1**.

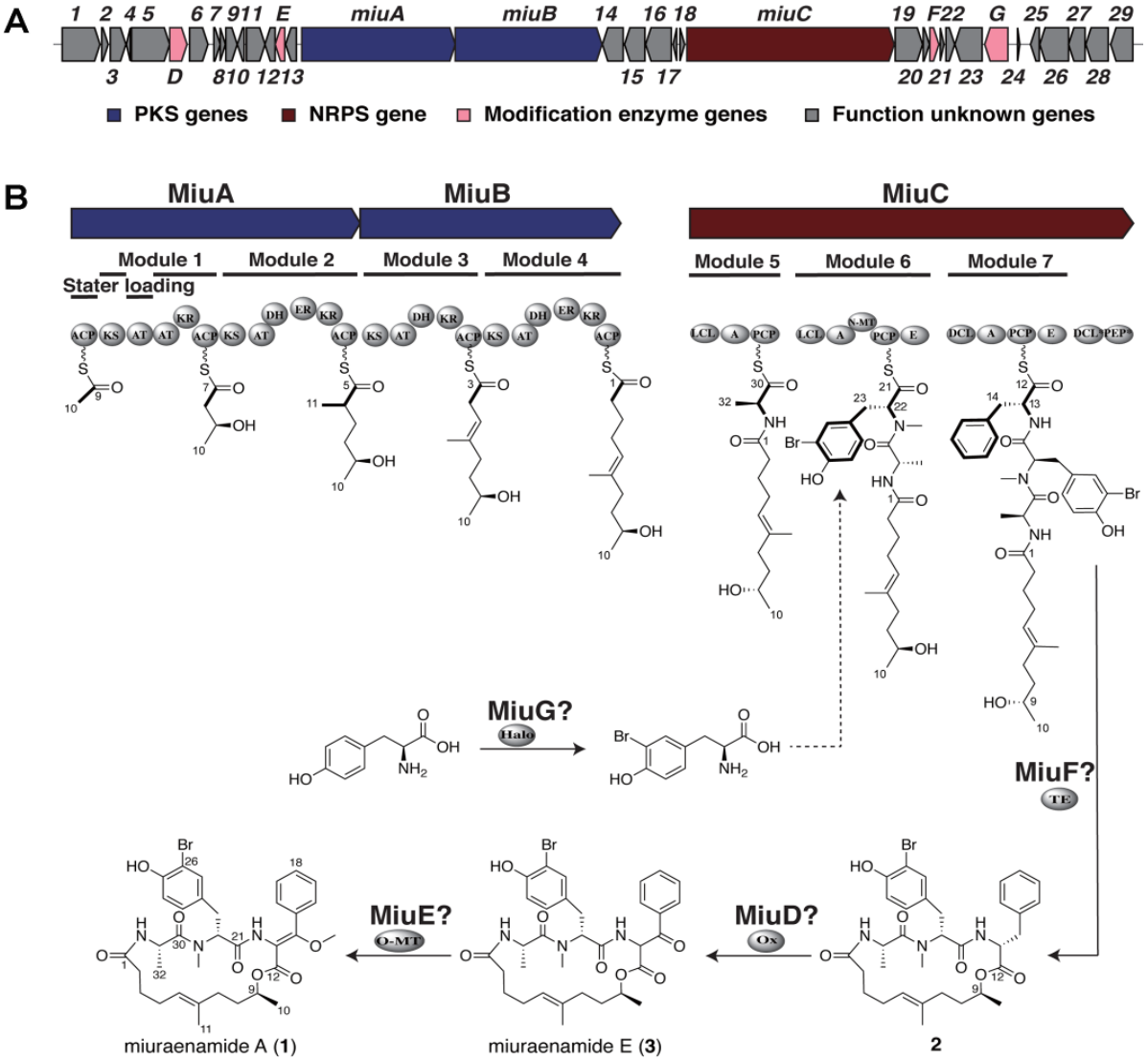

Figure 3-2. Organization of *miu* cluster and proposed biosynthetic pathway for miuraenamide A (**1**). (A) Map and gene organization of *miu* cluster. (B) Proposed biosynthetic pathway for **1**. Abbreviations: ACP, acyl carrier protein; AT, acyl transferase; DH, β-hydroxy dehydratase; ER, enoyl reductase; KR, β-ketoacyl reductase; KS, ketosynthase; A, adenylation domain; PCP, peptidyl carrier protein; E, epimerization domain; O-MT, *O*-methyltransferase domain; N-MT, *N*-methyltransferase domain; LCL, condensation domain that catalyzes the formation of a peptide bond between two L-amino acids; DCL, condensation domain that links an L-amino acid to a growing peptide ending with a D-amino acid; PEP, phosphoenolpyruvate synthase domain; TE, thioesterase; Ox, oxygenase; Halo, Halogenase. * marked domains (DCL* and PEP*) are biosynthetic function unassigned domains in this proposed biosynthetic pathway.

It was found that there were two cutting sites for the restriction enzyme BlnI outside the *miu* cluster but not inside. To clone the *miu* cluster, a genomic BAC library of *P. miuraensis* SMH-27-4 was constructed through complete digestion of the genome by BlnI. The BAC vector (p17-9A) that contained the full length of *miu* cluster was screened out by PCR. The BAC vector was modified through the Red/ET recombination technology to replace a DNA fragment (18.5 kbp) outside the *orf29* of the *miu* cluster with a "5TA-Kan", which contained kanamycin resistant gene and a 5.0 kbp DNA fragment homologous to a myxovirescin A biosynthetic gene *ta-1* [21] of the terrestrial myxobacterial model strain *Myxococcus xanthus*. The resulting recombinant BAC vector *miu* BAC was integrated into the genome of *M. xanthus* via single crossover homologous recombination (Figure 3-3). The constructed strain *M. xanthus*::*miu* was found to produce **1** successfully as demonstrated by LC-MS analysis (Figure 3-4), verifying that the *miu* cluster is responsible for the biosynthesis of **1**, although the yield was only 0.06 mg/L.

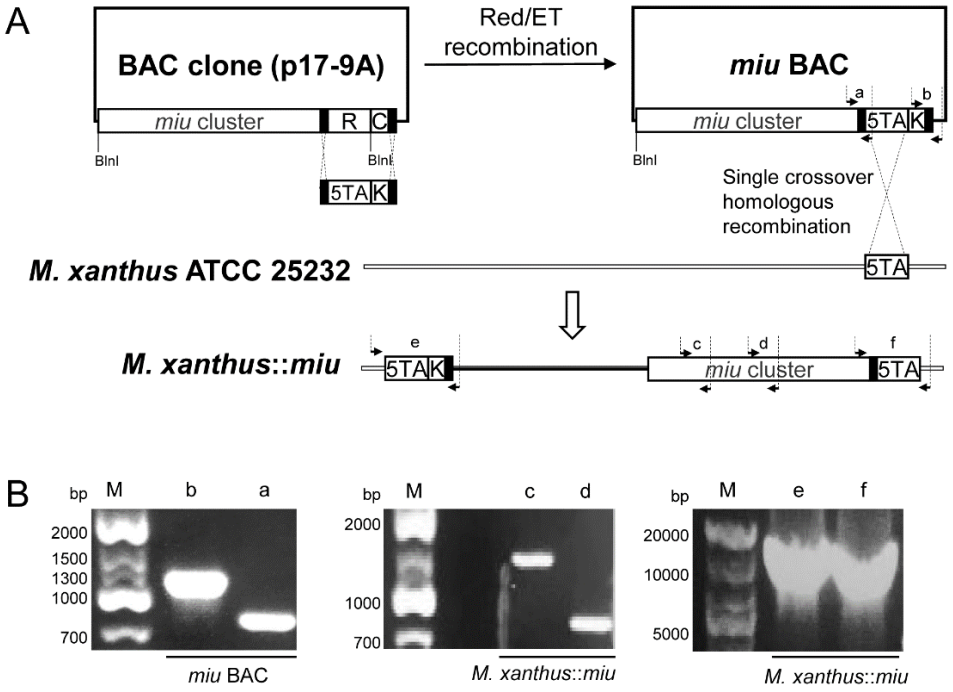

Figure 3-3. Construction of *M. xanthus*::*miu*. (A) The redundant fragment (genomic fragment outside the miu cluster) and chloramphenicol resistance gene (R|C) in the BAC clone p17-9A was replaced with the cassette 5TA-Kan^R (5TA|K, amplified from p5TA-KanR with primer pair ploTA-Kan red F/R) by Red/ET recombination. The generated miu BAC was integrated into the genome of *M. xanthus* ATCC 25232 by homologous recombination via the 5TA region. (B) PCR verification of the constructed vector and mutant by the following primer pairs: a (loTA cF/loTA cR, 886 bp), b (kanf/pCC1BAC R, 1299 bp), c (T1PKS1 cF/T1PKS1 cR, 1274 bp), d (T1PKS2 cF/T1PKS2 cR, 783 bp), e (loupF/loupR, 7957 bp), and f (0lodownF/2lodownR, 7488). M: DNA marker (Gene Ladder Wide 1, Nippon Gene).

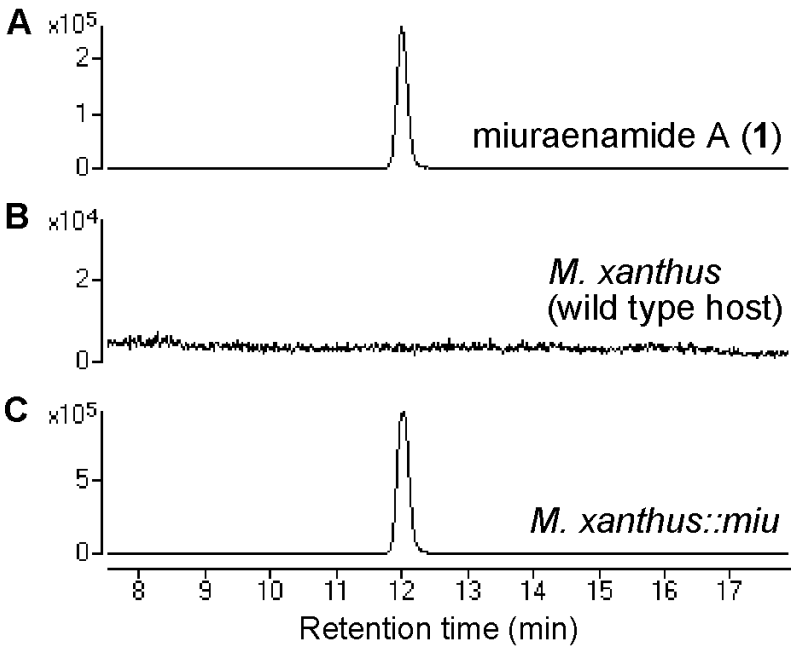

Figure 3-4. Production of miuraenamide A (**1**) by the heterologous transformant. Extracted ion chromatogram (*m/z* 684.2216) of standard **1** (A), an extract of the wild-type host *M. xanthus* (B), and an extract of the heterologous transformant harboring *miu* cluster (C).

3.2.2. Proposed mechanism for the biosynthesis of miuraenamide A

Since the *miu* cluster was confirmed to be the biosynthetic machinery for **1**, the function of 36 orfs composing the cluster was then predicted based on BLASTP results obtained from the NCBI non-redundant protein sequences (nr) database and the in the minimum information on biosynthetic gene cluster (MiBIG, version 3.1) database (Table 3-1). There are seven plausible structural genes designated as *miuA*–*miuG*. Besides the backbone-constructing PKSs (MiuA, MiuB) and NRPS (MiuC) genes, the four gene products were predicted as modification enzymes: cytochrome P450 (MiuD), *O*-methyltransferase (MiuE), thioesterase (MiuF), and FAD-dependent oxidoreductase/brominase (MiuG). Although the blast result suggested that MiuG is a brominase, chlorinated and iodinated analogues were also isolated from the original producer *P. miuraensis.* The MiuG was considered as a halogenase.

Table 3-1. Predicted functions of orfs in the *miu* cluster.

Orfs	Size(aa)	Closest homolog (BLASTP)	Origin	Accession number	Identity/ Similarity (%)
orf1	1008	Hypothetical protein	*Nannocystis pusilla*	WP_224196465.1	40/53
orf2	173	Hypothetical protein	*Nannocystis exedens*	WP_096327445.1	29/40
orf3	418	Hypothetical protein	Myxococcales bacterium	MCA9650222.1	75/86
orf4	104	Polyhydroxyalkanoic acid system family protein	Deltaproteobacteria bacterium	MCH9682166.1	73/86
orf5	1020	Spermidine synthase	Deltaproteobacteria bacterium	MCH9682165.1	81/88
miuD	461	Cytochrome P450	Myxococcales bacterium	MCB9753755.1	67/77
orf6	493	Peptidase M4 family protein	Deltaproteobacteria bacterium	RME25565.1	51/65
orf7	171	Hypothetical protein	*Balneola sp.*	MBE78502.1	27/49
orf8	138	DUF4398 domain-containing protein	Bacterium	MCR9159996.1	46/67
orf9	302	OmpA family protein	Deltaproteobacteria bacterium	MBC8068113.1	47/63
orf10	182	Hypothetical protein	Deltaproteobacteria bacterium	MCH9682164.1	69/80
orf11	497	OmpA family protein	Myxococcales bacterium	MCA9650212.1	69/84
orf12	274	FHA domain-containing protein	Myxococcales bacterium	MCA9652678.1	58/68
miuE	257	O-methyltransferase	*Stigmatella erecta*	SEU19554.1	35/54
orf13	288	Hypothetical protein DHS20C18_22780	Saprospiraceae bacterium	GJM33277.1	32/49
miuA	4105	Type I polyketide synthase	*Pyxidicoccus fallax*	WP_169347329.1	60/72
miuB	3926	Amino acid adenylation domain-containing protein	*Pyxidicoccus fallax*	NPC81269.1	51/64
orf14	554	Mechanosensitive ion channel family protein	*Vitiosangium sp.* GDMCC 1.1324	WP_108076111.1	40/62
orf15	545	Hypothetical protein	Myxococcales bacterium	MBL8973146.1	78/89
orf16	686	Heavy metal translocating P-type ATPase	Proteobacteria bacterium	MBU0970734.1	41/63
orf17	94	Hypothetical protein	Myxococcales bacterium	MBL8970963.1	60/76
orf18	125	Hypothetical protein	Myxococcales bacterium	MBL8970963.1	70/83
miuC	5546	Non-ribosomal peptide synthetase	*Chondromyces crocatus*	WP_169796632.1	40/55
orf19	730	Bifunctional metallophosphatase/5'-nucleotidase	*Chondromyces crocatus*	WP_050432501.1	59/74
orf20	164	DUF697 domain-containing protein	Myxococcales bacterium	MCB9755747.1	59/80
miuF	241	Thioesterase	Myxococcales bacterium	MCA9716988.1	62/75
orf21	95	Hypothetical protein	Myxococcales bacterium	MBL8970963.1	67/81
orf22	233	Kinase/phosphodiesterase	*Nannocystis sp.* MB1016	ALD82529.1	64/73
orf23	728	Heavy metal translocating P-type ATPase	*Nannocystis sp.* MB1016	ALD82534.1	61/79
miuG	621	FAD-dependent oxidoreductase;	*Symploca sp.* SIO1A3;	NER47269.1	39/54
		Bmp5, Flavin-dependent single-component p-hydroxybenzoate brominase/decarboxylase (MIBiG database)	*Pseudoalteromonas phenolica* O-BC30	KF540211.1	35/52
orf24	58	No significant homology			
orf25	235	OmpA family protein	Myxococcales bacterium	MCA9650211.1	61/79
orf26	771	LysM peptidoglycan-binding domain-containing protein	Myxococcales bacterium	MCA9705957.1	66/78
orf27	441	Protein kinase	Deltaproteobacteria bacterium	MCH9682160.1	69/80
orf28	599	HAMP domain-containing protein	Myxococcales bacterium	MCA9650207.1	76/86
orf29	594	PAS domain S-box protein	Myxococcales bacterium	MCA9650206.1	66/76

The biosynthetic mechanism was proposed based on the organization of the *miu* cluster (3-2B). The first PKS (MiuA) exhibits an unusual starter module arrangement, ACP-KS-AT-AT-KR-ACP, in which the loading domain acyltransferase (the first AT) is ripped away from the starter domain acyl carrier protein (the first ACP) by the interruption of the ketosynthase (KS) domain in the first elongation module (Module 1). This particular loading type has been reported several times in the biosynthesis of other myxobacterial compounds, such as soraphen from *Sorangium cellulosum* So ce26 [22], myxothiazol from *Stigmatella aurantiaca* DW4/3-1 [23], myxalamide from *S. aurantiaca* Sga15 [24], chondramide from *Chondromyces crocatus* Cm c5 [25], etc. The first AT domain in MiuA loaded the starter molecule acetyl-CoA, and then the four polyketide elongation modules (Modules 1–4) in MiuA and MiuB added three malonyl-CoA (mal) and one methylmalonyl-CoA (mmal) in the sequence of mal-mmal-mal-mal. The resulting polyketide intermediate tethered to Module 4 in MiuB was transferred to the peptidyl carrier protein (PCP) domain carrying L-alanine by the first condensation domain (LCL) of Module 5 in MiuC. The second condensation domain (LCL) in Module 6 recruits 3-bromo-L-tyrosine (or L-tyrosine) to the alanine residue. The epimerization (E) domain of Module 6 converted the incorporated L-tyrosine to the D configuration. MiuG was predicted to be the halogenase that catalyzes the bromination of tyrosine (or the tyrosine residue) since the closest homolog to MiuG in the MiBIG database is a marine bacterial brominase, Bmp5, which catalyzes the biosynthesis of bromophenols [26]. The DCL domain of Module 7 recruits L-phenylalanine to the C-terminus of the peptidyl unit. The incorporated L-phenylalanine is possibly converted to the D form by the epimerization domain (E) of Module 7, although the stereogenic center at C-13 will eventually be lost. MiuC, besides the three regular NRPS modules (Modules 5– 7), possesses two extra domains, DCL* and phosphoenolpyruvate synthase (PEP*), which functions are unknown. The release and cyclization of the linear polyketide/peptide from MiuC could be catalyzed by the thioesterase (TE) MiuF, yielding the tentative early

intermediate **2**. The β-carbon (C-14) of phenylalanine of **2** may be oxidized by MiuD (cytochrome P450) to produce the known ketone congener miuraenamide E (**3**), which was previously isolated from the original strain SMH-27-4 as a natural congener [27]. As the final step, MiuE (*O*-methyltransferase) catalyzes *O*-methylation accompanied by enolization of the C-14 ketone group of **3** to generate **1**.

3.2.3. Verification of modification enzyme genes

To verify the proposed biosynthetic mechanism, the four estimated modification enzyme genes, *miuD–miuG*, were disrupted separately. The gene disruptions were conducted on the BAC vector though the Red/ET recombination technology. The gene-disrupted BAC vectors were then integrated into the *M. xanthus* genome via single crossover homologous recombination at the same position as that of the initially constructed transformant *M. xanthus*::*miu* to construct the four mutants *M. xanthus*::*miu* Δ*miuD–*Δ*miuG*. The production of **1** and its congeners were detected by liquid chromatography-mass spectroscopy (LC-MS) (Figure 3-5) and the yields were recorded in Table 3-2. The mass spectra for the products are listed in Figure 3-6.

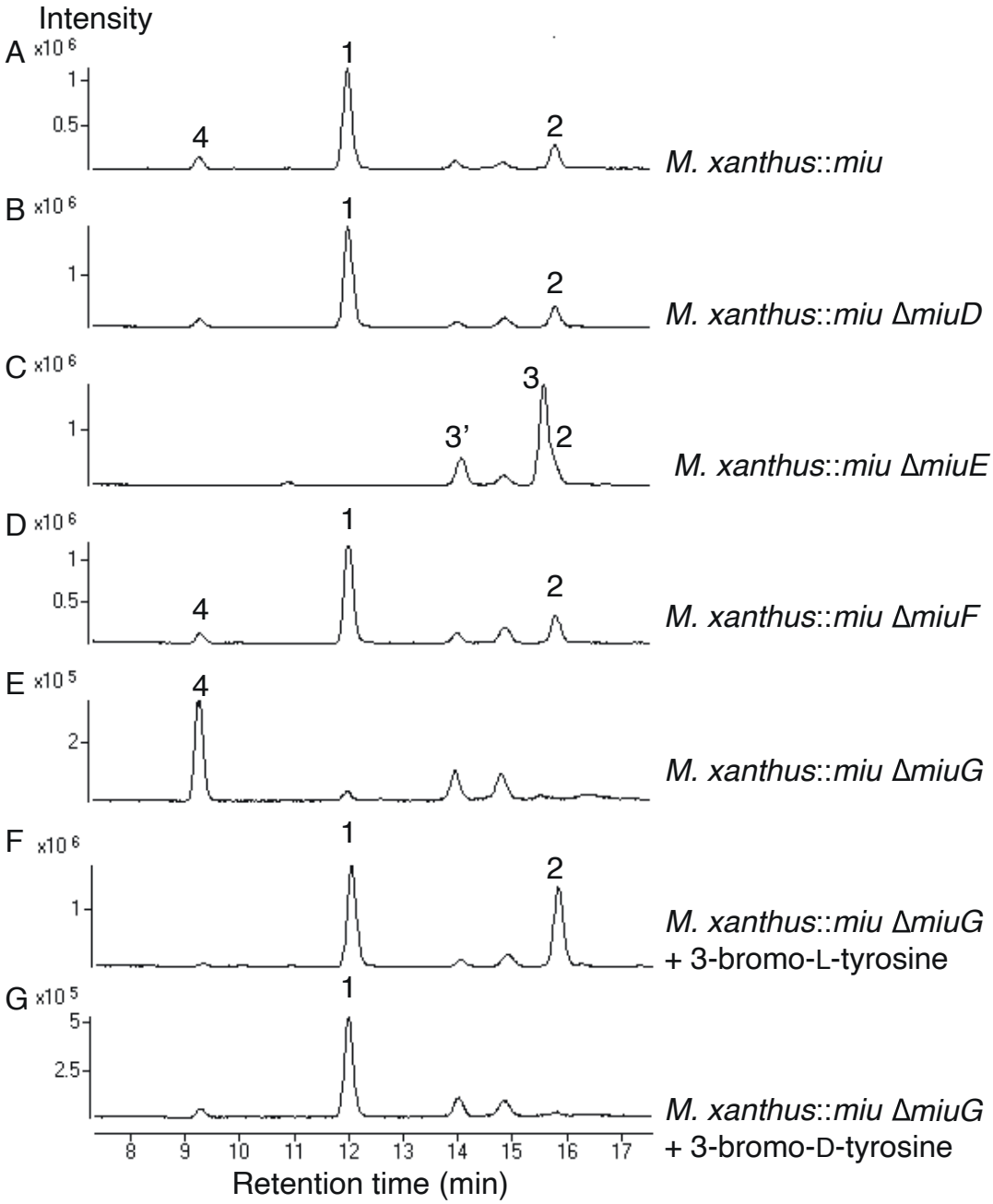

Figure 3-5. Production of miuraenamide A (**1**) and its congeners by four heterologous mutants lacking *miuD–G*. Extracted ion chromatographs (merged from *m/z* 684.2216, 606.3125, 656.2285, 670.2068, and 672.2217) of the extracts of the heterologous producer without gene disruption *M. xanthus*::*miu* (A), *miuD* (cytochrome P450 gene)-disrupted mutant *M. xanthus*::*miu* Δ*miuD* (B), *miuE* (*O*-methyltransferase gene)-disrupted mutant *M. xanthus*::*miu* Δ*miuE* (C), *miuF* (thioesterase gene)-disrupted mutant *M. xanthus*::*miu* Δ*miuF* (D), *miuG* (halogenase gene)-disrupted mutant *M. xanthus*::*miu* Δ*miuG* (E), *M. xanthus*::*miu* Δ*miuG* fed on 3-bromo-L-tyrosine (F), *M. xanthus*::*miu* Δ*miuG* fed on 3-bromo-D-tyrosine (G).

Table 3-2. Production of miuraenamide A (**1**) and its congeners in heterologous mutants lacking *miuD–G*.

Heterologous host	Yield of **1** (mg/L)	Produced congeners
M. xanthus::*miu*	0.06	**2**, **4**
M. xanthus::*miu* Δ*miuD*	0.13	**2**, **4**
M. xanthus::*miu* Δ*miuE*	-	**2**, **3**, **3'**
M. xanthus::*miu* Δ*miuF*	0.08	**2**, **4**
M. xanthus::*miu* Δ*miuG*	-	**4**
M. xanthus::*miu* Δ*miuG* + 3-bromo-L-tyrosine	0.09	**2**
M. xanthus::*miu* Δ*miuG* + 3-bromo-D-tyrosine	0.02	**4**

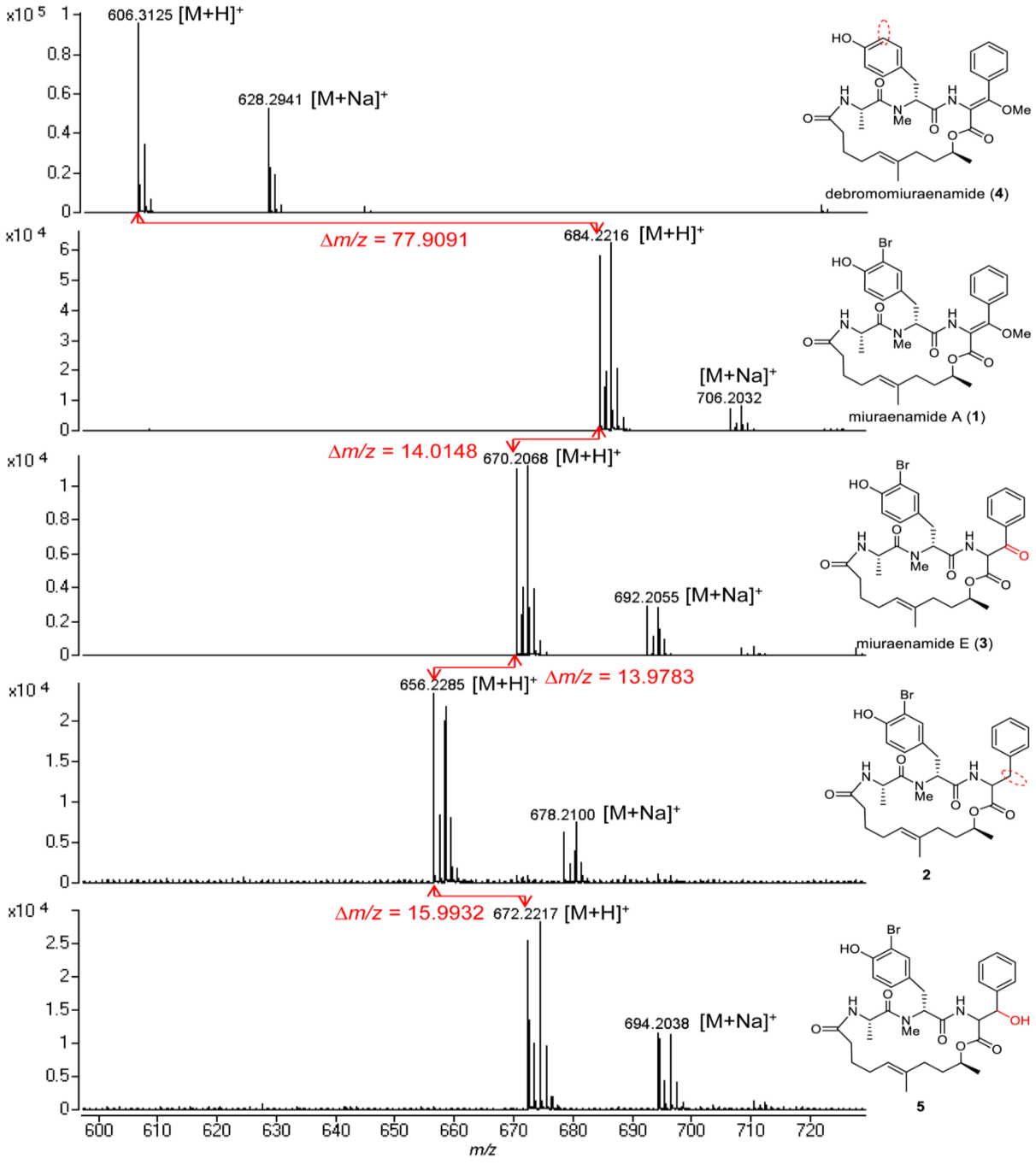

Figure 3-6. Mass spectra of miuraenamide A and its congeners. The structures of **2**, **4**, **5** are estimated by the molecular formulae compared with those of **1** and **3** and not verified by NMR.

3.2.3.1. Congeners produced by the heterologous transformant *M. xanthus::miu*

First of all, by LC-MS analysis that can cover the range of the molecular weights of all expected congeners, the heterologous transformant *M. xanthus::miu* without gene disruption was demonstrated to produce not only **1** but also several related congeners **2** and **4** (Figure 3-5A). The congener ***2*** was deduced to be an early biosynthetic precursor lacking the enol ether at C-14 (Figure 3-2B) based on the molecular formula smaller than **1** by CO (observed difference 27.9931, calcd. 27.9949, Figure 3-6). The intermediate **2** was the second most abundant product, indicating that the following oxidation did not completely proceed in the heterologous host, whereas **2** had never been detected in the original producer SMH-27-4. The congener **4** had the molecular formula smaller than **1** by ^{79}Br–H (observed difference 77.9091, calcd. 77.9105, Figure 3-6), indicating that **4** was debromomiuraenamide A. These congeners **2** and **4** could be produced due to incomplete reactions by the predicted enzymes oxidase (MiuD) and halogenase (MiuG), respectively. The heterologous expression may affect the activity or expression level of some modification enzymes.

3.2.3.2. Disruption of the Cytochrome P450 Gene (*miuD*)

The *M. xanthus*::*miu ΔmiuD* was constructed in the scheme showed in Figure 3-7A and verified by PCR (Figure 3-7B). Although MiuD (cytochrome P450) was estimated to oxidize the phenylalanine residue of **2** to form **3**, the disruption of *miuD* did not affect the production of **1** (0.13 mg/L, Figure 3-5B, Table 3-2). Therefore, it was concluded that MiuD was not involved in the biosynthesis of **1** and unidentified gene(s) in the host genome could be responsible for the oxidation.

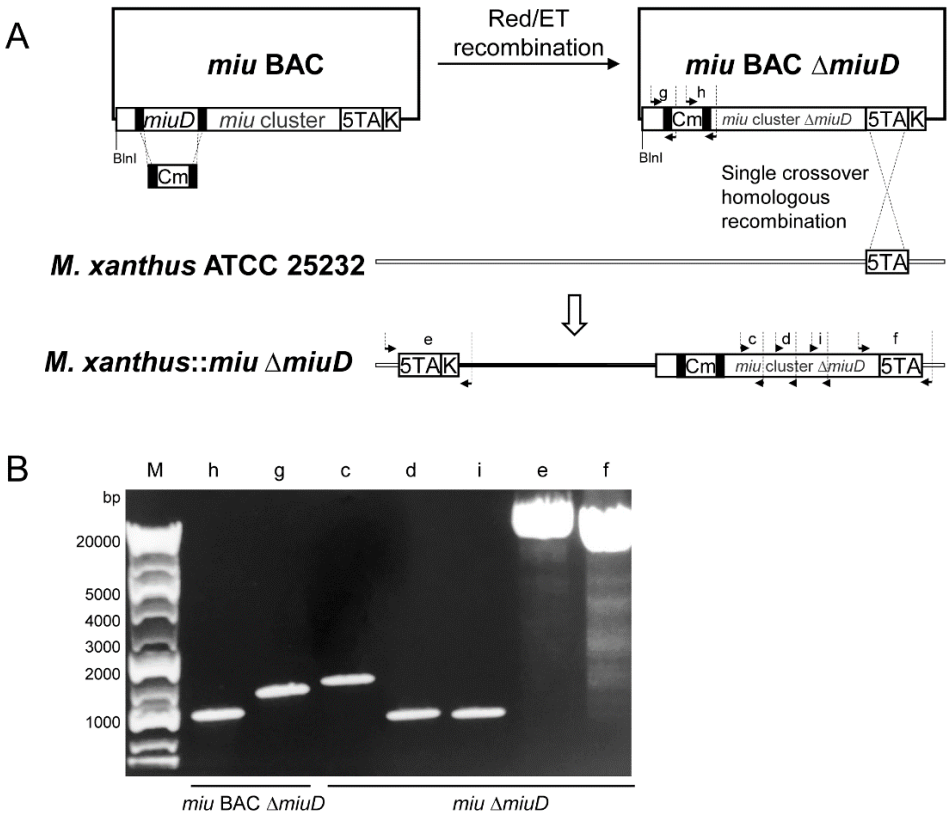

Figure 3-7. Construction of *M. xanthus*::*miu* Δ*miuD*. (A) The gene *miuD* in *miu* BAC was replaced with the chloramphenicol resistance gene (Cm, amplified from pCCIBAC with primer pair Cm-miuD-F/R) by Red/ET recombination. The generated *miu* BAC Δ*miuD* was integrated into the genome of *M. xanthus* ATCC 25232 by homologous recombination via the 5TA region. (B) PCR verification of the constructed mutants by the following primer pairs: g (dmiuD cF/Cm cR, 1186 bp), h (Cm cF/dmiuD cR, 949 bp), c (T1PKS1 cF/T1PKS1 cR, 1274 bp), d (T1PKS2 cF/T1PKS2 cR, 783 bp), I (NRPS cF/NRPS cR, 756 bp), e (loupF/loupR, 7957 bp), and f (0lodownF/2lodownR, 7488 bp). M: DNA marker.

3.2.3.3. Disruption of the *O*-methyltransferase Gene (*miuE*)

The *M. xanthus*::*miu ΔmiuE* was constructed in the scheme showed in Figure 3-8A, and verified by PCR (Figure 3-8B). The MiuE (*O*-methyltransferase) was expected to be responsible for the methylation of **3** to produce **1**. Actually, the disruption of *miuE* (mutant *M. xanthus::miu* Δ*miuE*) resulted in the abolition of the production of **1** and the accumulation of **3** instead (Figure 3-5C, Table 3-2), which verified the role of MiuE. The structure of **3** was determined by comparing of LC-MS data as the known product miuraenamide E, which was previously isolated from the original producer SMH-27-4 [27]. The compound **3'** was

estimated as 13-*epi*-**3**, based on the same molecular formula and susceptibility of the position 13 of **3** for racemization. Another related product **2** was also observed at a similar retention time to **3**. The accumulation of **2** was also observed in other heterologous mutants (Figure 3-5A, B, D). The absence of **4** is probably due to the lack of *O*-methylation of the corresponding debromo-precursor.

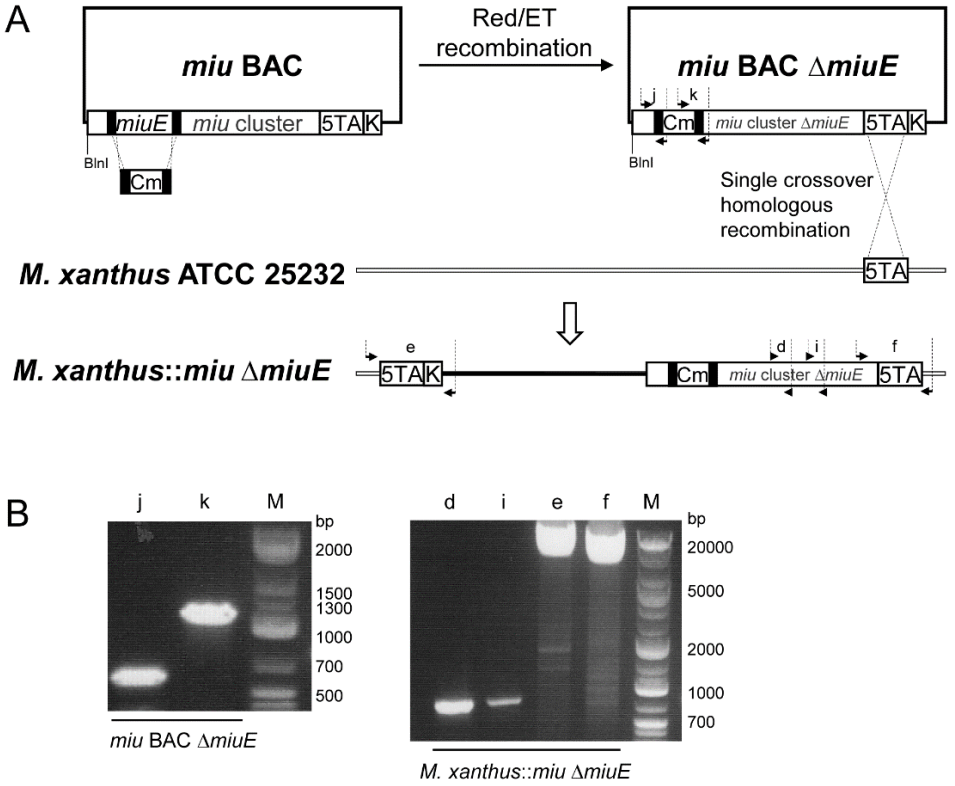

Figure 3-8. Construction of *M. xanthus*::*miu* Δ*miuE*. (A) The gene *miuE* in *miu* BAC was replaced with the chloramphenicol resistance gene (Cm, amplified from pCCIBAC with primer pair Cm-miuE-F/R) by Red/ET recombination. The generated *miu* BAC Δ*miuE* was integrated into the genome of *M. xanthus* ATCC 25232 by homologous recombination via the 5TA region. (B) PCR verification of the constructed mutants by the following primer pairs: j (miuEF/Cm cR, 599 bp), k (Cm cF/dmiuE cR, 1037 bp), d (T1PKS2 cF/T1PKS2 cR, 783 bp), i (NRPS cF/NRPS cR, 756 bp), e (loupF/loupR, 7957 bp), and f (0lodownF/2lodownR, 7488 bp). M: DNA marker.

3.2.3.4. Disruption of the Thioesterase Gene (*miuF*)

The *M. xanthus*::*miu ΔmiuF* was constructed in the scheme showed in Figure 3-9A, and verified by PCR (Figure 3-9B). MiuF (thioesterase) was proposed to release and cyclize the precursor polyketide/peptide chain. However, the disruption of this gene did not affect the

production of 1 (0.08 mg/L, Figure 3-5D, Table 3-2). This fact suggests that there is another responsible protein, which could be the extra DCL* (biosynthetic function unassigned domain in the proposed pathway) in MiuC because this domain contains the $HHXXXDX_{14}Y$ motif, the conserved motif possessed by a ester-bond formation condensation enzyme SgcC5 [28].

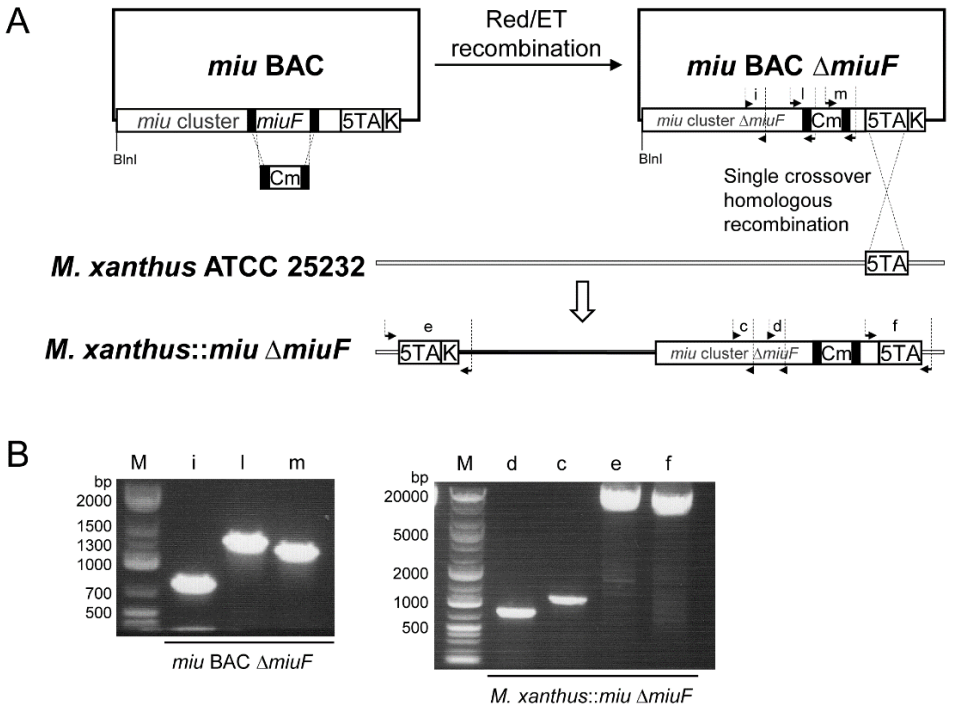

Figure 3-9. Construction of *M. xanthus*::*miu* Δ*miuF*. (A) The gene *miuF* in *miu* BAC was replaced with the chloramphenicol resistance gene (Cm, amplified from pCCIBAC with primer pair Cm-miuF-F/R) by Red/ET recombination. The generated *miu* BAC Δ*miuF* was integrated into the genome of *M. xanthus* ATCC 25232 by homologous recombination via the 5TA region. (B) PCR verification of the constructed mutants by the following primer pairs: i (NRPS cF/NRPS cR, 756 bp), l (dmiuF cF/Cm cR, 1201 bp), m (Cm cF/dmiuF cR, 1121 bp), c (T1PKS1 cF/T1PKS1 cR, 1274 bp), d (T1PKS2 cF/T1PKS2 cR, 783 bp), e (loupF/loupR, 7957 bp), and f (0lodownF/2lodownR, 7488 bp). M: DNA marker.

3.2.3.5. Disruption of the Halogenase Gene (*miuG*)

The *M. xanthus*::*miu* Δ*miuG* was constructed in the scheme showed in Figure 3-10A and verified by PCR (Figure 3-10B). MiuG (Halogenase) was suggested to be responsible for the bromination of tyrosine. The disruption of *miuG* resulted in the abolition of the production of **1** and the accumulation of **4** instead (Figure 3-5E, Figure 3-6), verifying that MiuG is the

bromination enzyme for tyrosine. Since this disruption mutant fed on 3-bromo-L-tyrosine entirely restored the production of 1 (0.09 mg/L, Figure 3-5F, Table 3-2), the condensation domain LCL in Module 6 highly preferred bromotyrosine over tyrosine and MiuG may preferred free tyrosine over the tyrosine residue on the peptide chain. Feeding the mutant on 3-bromo-D-tyrosine also restored the production of **1**, although the yield was lower (0.02 mg/L, Figure 3-5G, Table 3-2) than that for the L-form. Similar results were observed for the original transformant *M. xanthus*::*miu* (0.16 mg/L for L-form and 0.07 mg/L for D-form, Figure 3-11), supporting the preference of the LCL domain in Module 6 for L-amino acid.

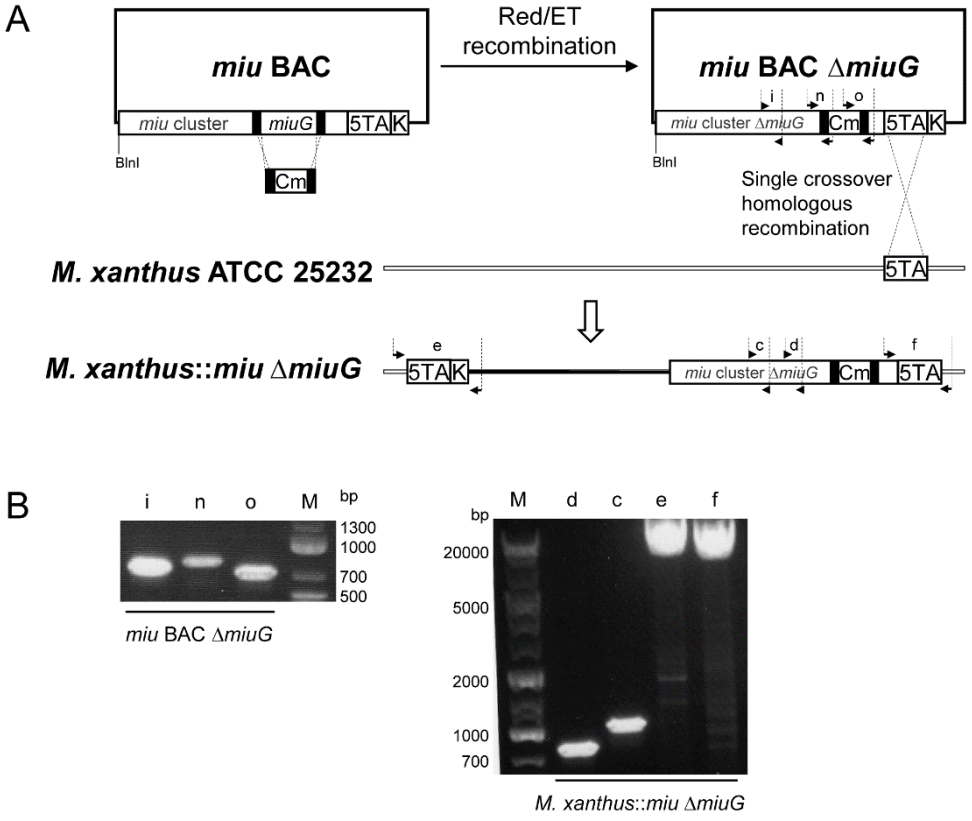

Figure 3-10. Construction of *M. xanthus*::*miu* Δ*miuG*. (A) The gene miuG in miu BAC was replaced with the chloramphenicol resistance gene (Cm, amplified from pCCIBAC with primer pair Cm-miuG-F/R) by Red/ET recombination. The generated miu BAC ΔmiuG was integrated into the genome of M. xanthus ATCC 25232 by homologous recombination via the 5TA region. (B) PCR verification of the constructed mutants by the following primer pairs: i (NRPS cF/NRPS cR, 756 bp), n (dmiuG cF/Cm cR, 778 bp), o (Cm cF/miuGR, 701 bp), c (T1PKS1 cF/T1PKS1 cR, 1274 bp), d (T1PKS2 cF/T1PKS2 cR, 783 bp), e (loupF/loupR, 7957 bp), and f (0lodownF/2lodownR, 7488 bp). M: DNA marker.

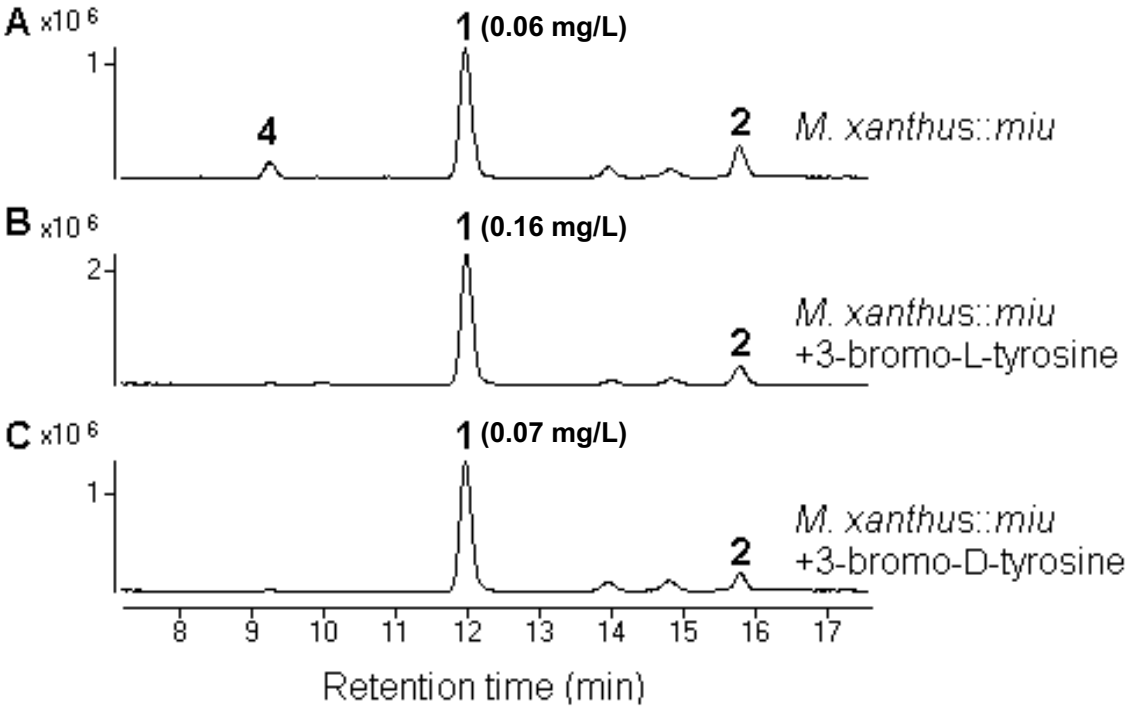

Figure 3-11. Production of miuraenamide A (1) and its congeners by *M.xanthus*::*miu* mutant fed on bromotyrosine. Extracted ion chromatographs (merged from m/z 684.2216, 606.3125, 656.2285, 670.2068, and 672.2217) of the extracts of the heterologous producer *M. xanthus*::*miu* not feeding on bromotyrosine (A), *M. xanthus*::*miu* fed on 3-bromo-L-tyrosine (B), *M. xanthus*::*miu* fed on 3-bromo-D-tyrosine (C).

3.2.4. Verification of unknown genes by multi-gene disruption

The gene disruption experiments revealed that two modification enzyme genes (*miuE* and *miuG*) were involved in the biosynthesis of **1** in addition to the core genes *miuA–C*. The other function-unknown genes were clustered into the four regions, *orf1–10*, orf*14–16*, *orf19–23*, and *orf25–29* (Figure 3-2A). These regions were next removed to explore whether they were related to the biosynthesis of **1** (Figures 3-12). The production of **1** and its congeners were detected by LC-MS (Figure 3-13) and the yields were recorded in Table 3-3.

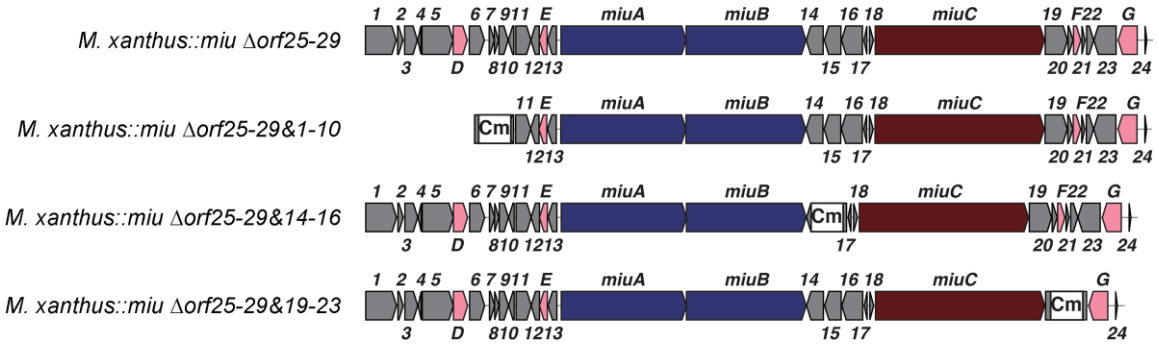

Figure 3-12. Gene organizations of *miu* clusters lacking multi-gene regions. Cm represents the chloramphenicol resistance gene that was used as a selection marker.

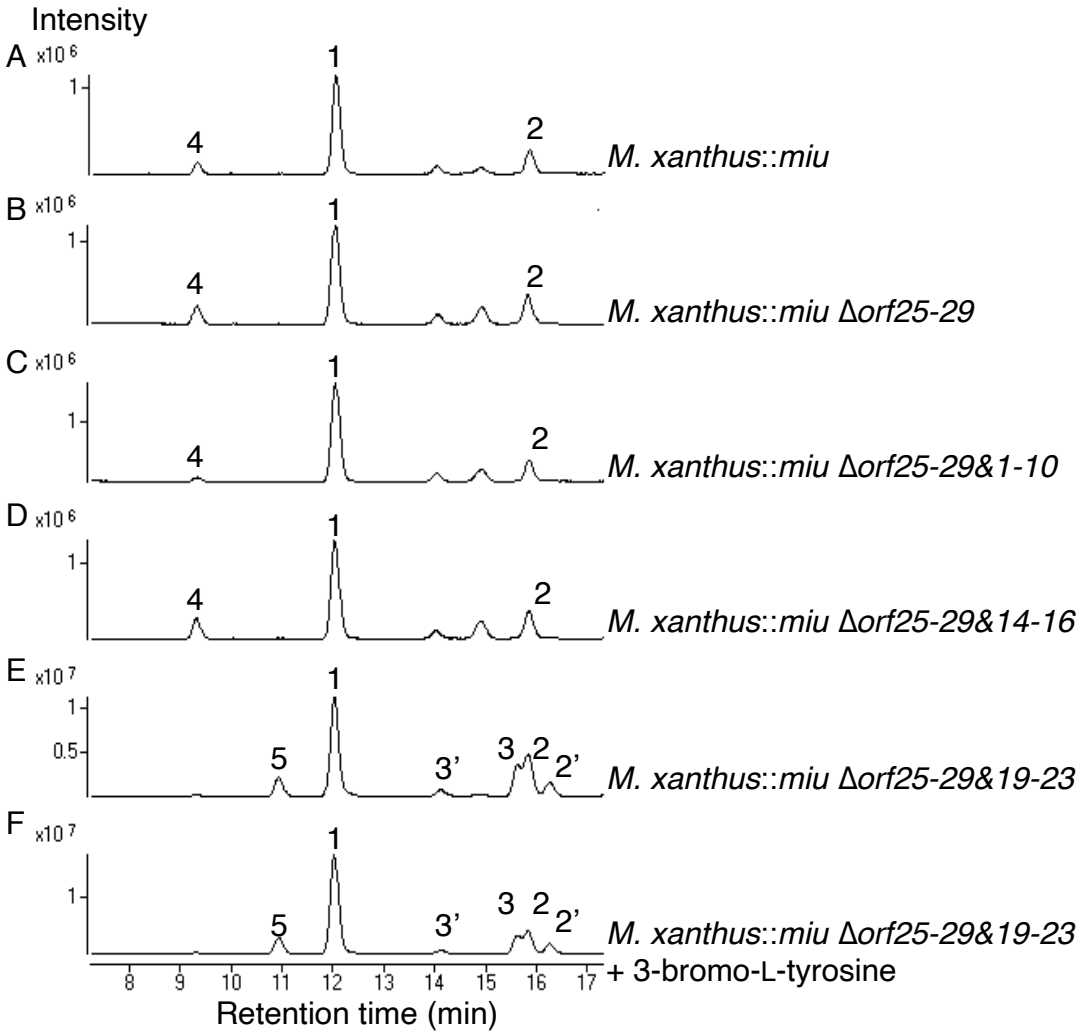

Figure 3-13. Production of miuraenamide A (1) and its congeners by multi-gene-disrupted heterologous hosts. Extracted ion chromatogram (merged from *m/z* 684.2216, 606.3125, 656.2285, 670.2068, and 672.2217) of the extracts of *M. xanthus*::*miu* (A), *M. xanthus*::*miu* Δ*orf25-29* (B), *M. xanthus*::*miu* Δ*orf25-29&1-10* (C), *M. xanthus*::*miu* Δ*orf25-29&14-16* (D), and *M. xanthus*::*miu* Δ*orf25-29&19-23* (E and F).

Table 3-3. Production of miuraenamide A (**1**) and its congeners in multi-gene disrupted heterologous mutants

Heterologous host	Yield of **1** (mg/L)	Produced congeners
M. xanthus::*miu* Δ*orf25-29* (31 orfs, 77.0 kbp)	0.07	**2**, **4**
M. xanthus::*miu* Δ*orf25-29&1-10* (20 orfs, 62.1 kbp)	0.10	**2**, **4**
M. xanthus::*miu* Δ*orf25-29&14-16* (28 orfs, 72.6 kbp)	0.07	**2**, **4**
M. xanthus::*miu* Δ*orf25-29&19-23* (25 orfs, 70.9 kbp)	0.70	**2**, **2'**, **3**, **3'**, **5**
M. xanthus::*miu* Δ*orf25-29&19-23* + 3-bromo-L-tyrosine	1.21	**2**, **2'**, **3**, **3'**, **5**

Since there are apparent non-coding regions between *miuG* and *orf25* (Figure 3-2A), it is likely that the region *orf25–29* is not involved in the biosynthesis of **1**. The removal of the region *orf25–29* was conducted on the above-mentioned BAC vector p17-9A through the Red/ET recombination technology since the region *orf25–29* is located at the end of the *miu* cluster (Figure 3-2A). The recombinant BAC *miu* BAC Δ*orf25–29* was then integrated into the *M. xanthus* genome via single crossover homologous recombination (Figure 3-14). Actually, the mutant *M. xanthus*::*miu* Δ*orf25–29* produced **1** in the yield of 0.07 mg/L like *M. xanthus*::*miu* did (Figure 3-13B, Tables 3-2 and 3-3), indicating that the real BGC ranged between *orf1* and *orf24* (Figure 3-12).

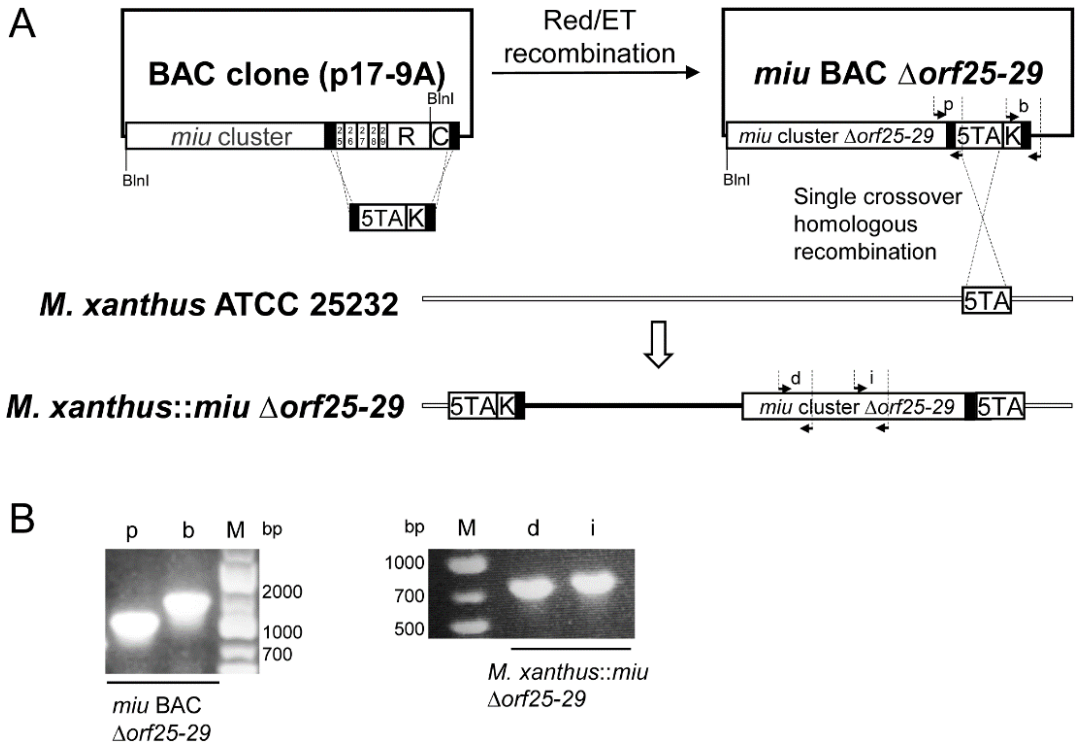

Figure 3-14. Construction of *M. xanthus*::*miu* Δ*orf25-29*. (A) The gene region *orf25-29,* the redundant fragment and chloramphenicol resistance gene (*25*|*26*|*27*|*28*|*29*|R|C), in the BAC clone p17-9A was replaced with the cassette 5TA-Kan^R (5TA|K, amplified from p5TA-Kan^R with primer pair 5TA-orf25-F/ploTA-Kan red R) by Red/ET recombination. The generated *miu* BAC Δ*orf25-29* was integrated into the genome of *M. xanthus* ATCC 25232 by homologous recombination via the 5TA region. (B) PCR verification of the constructed mutants by the following primer pairs: p (orf24 cF/loTA cR, 1020 bp), b (kanf/pCC1BAC R, 1299 bp), d (T1PKS2 cF/T1PKS2 cR, 783 bp), and i (NPRS cF/NRPS cR, 756 bp). M: DNA marker.

The subsequent disruptions of the other regions were, therefore, performed on this mutant *M. xanthus*::*miu* Δ*orf25–29*. The construction scheme of the *M. xanthus*::*miu* Δ*orf25–29&1-10*, *M. xanthus*::*miu* Δ*orf25–29&14–16* and *M. xanthus*::*miu* Δ*orf25–29&19–23* were shown in Figures 3-15, 3-16 and 3-17.

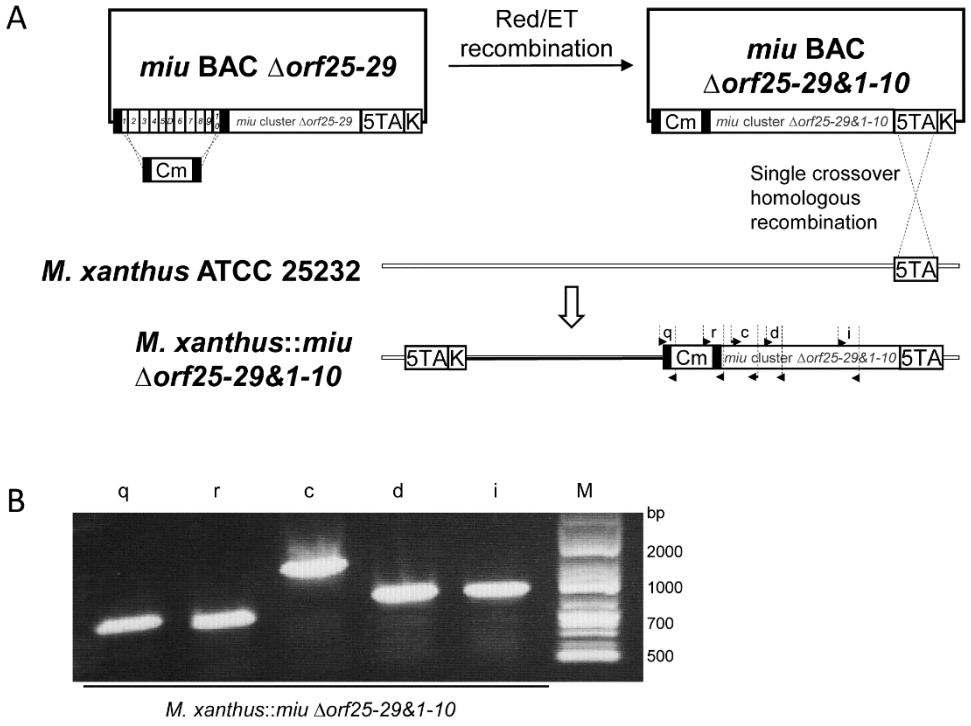

Figure 3-15. Construction of *M. xanthus*::*miu* Δ*orf25-29&1-10*. (A) The gene region *orf1-10* (*1*|*2*|*3*|*4*|*5*|*D*|*6*|*7*|*8*|*9*|*10*) in *miu* BAC Δ*orf25-29* was replaced with the chloramphenicol resistance gene (Cm, amplified from pCCIBAC with primer pair Cm-orf1-F/ Cm-orf10-R) by Red/ET recombination. The generated *miu* BAC Δ*orf25-29&1-10* was integrated into the genome of *M. xanthus* ATCC 25232 by homologous recombination via the 5TA region. (B) PCR verification of *M. xanthus*::*miu* Δ *orf25-29&1-10* by the following primer pairs: q (dorf1 cF/Cm cR, 694 bp), r (Cm cF/dorf10 cR, 621 bp), c (T1PKS1 cF/T1PKS2 cR, 1274 bp), d (T1PKS2 cF/T1PKS2 cR, 783 bp), and i (NPRS cF/NRPS cR, 756 bp). M: DNA marker.

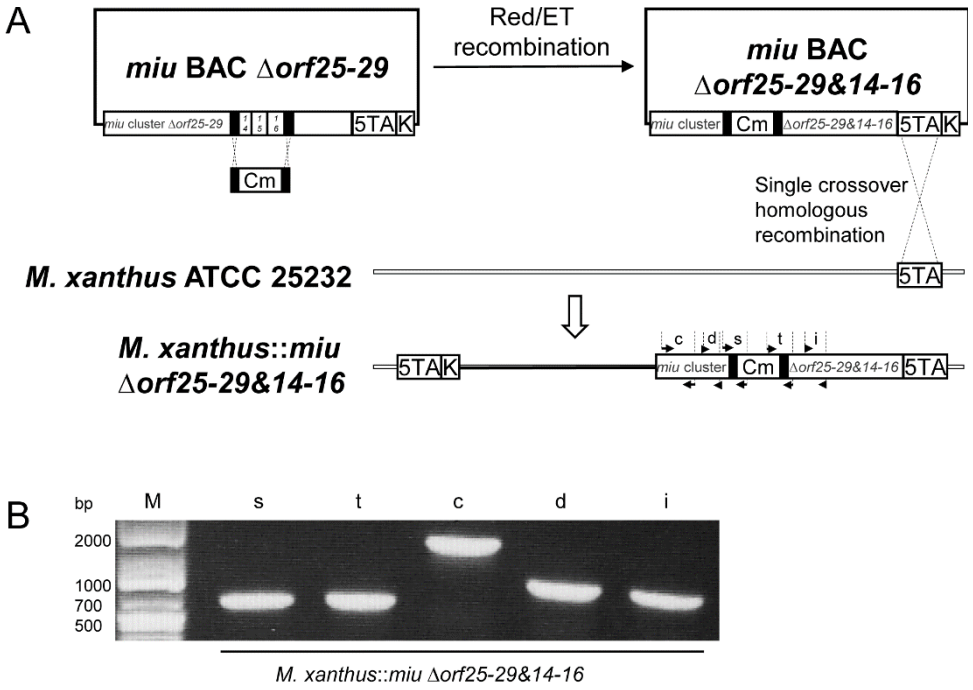

Figure 3-16. Construction of *M. xanthus*::*miu* Δ*orf25-29&14-16*. (A) The gene region *orf14-16* (*14*|*15*|*16*) in *miu* BAC Δ*orf25-29* was replaced with the chloramphenicol resistance gene (Cm, amplified from pCCIBAC with primer pair Cm-orf14-F/ Cm-orf16-R) by Red/ET recombination. The generated *miu* BAC Δ*orf25-29&14-16* was integrated into the genome of *M. xanthus* ATCC 25232 by homologous recombination via the 5TA region. (B) PCR verification of *M. xanthus*::*miu* Δ *orf25-29&14-16* by the following primer pairs: s (dorf14 cF/Cm cR, 577 bp), t (Cm cF/dorf16 cR, 591 bp), c (T1PKS1 cF/T1PKS2 cR, 1274 bp), d (T1PKS2 cF/T1PKS2 cR, 783 bp), and i (NPRS cF/NRPS cR, 756 bp). M: DNA marker.

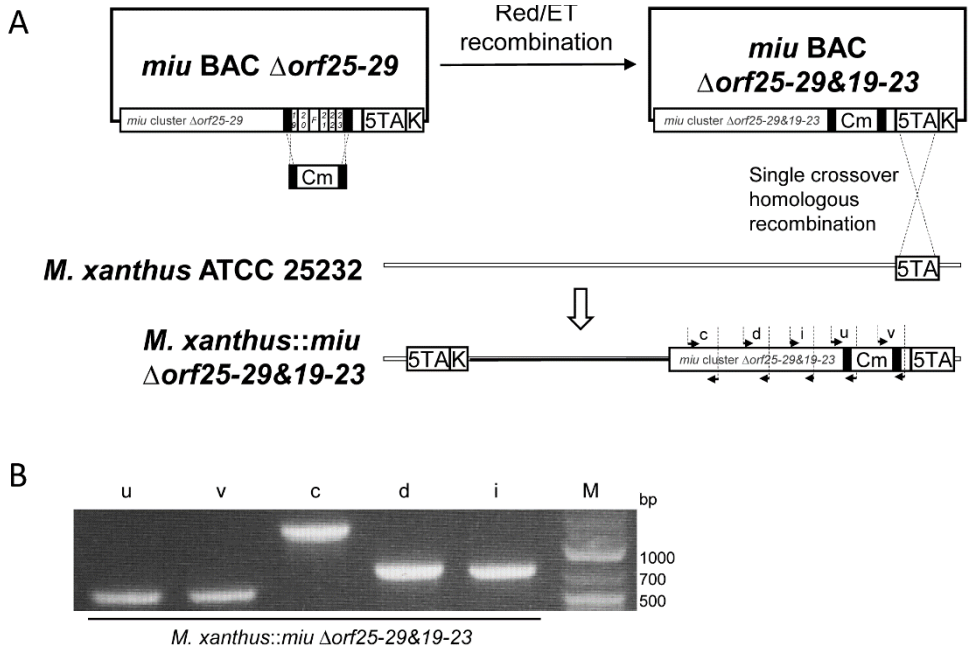

Figure 3-17. Construction of *M. xanthus*::*miu* Δ*orf25-29&19-23*. (A) The gene region *orf19-23* (*19*|*20*|*F*|*21*|*22*|*23*) in *miu* BAC Δ*orf25-29* was replaced with the chloramphenicol resistance gene (Cm, amplified from pCCIBAC with primer pair Cm-orf19-F/ Cm-orf23-R) by Red/ET recombination. The generated *miu* BAC Δ*orf25-29&19-23* was integrated into the genome of *M. xanthus* ATCC 25232 by homologous recombination via the 5TA region. (B) PCR verification of *M. xanthus*::*miu* Δ *orf25-29&19-23* by the following primer pairs: u (dorf19 cF/Cm cR, 582 bp), v (Cm cF/dorf23 cR, 576 bp), c (T1PKS1 cF/T1PKS2 cR, 1274 bp), d (T1PKS2 cF/T1PKS2 cR, 783 bp), and i (NPRS cF/NRPS cR, 756 bp). M: DNA marker.

The two double disruption mutants *M. xanthus::miu* Δ*orf25–29&1-10* and *M. xanthus::miu* Δ*orf25–29&14–16* also normally produced **1** in the yields of 0.07–0.10 mg/L (Figures 3-13C and D, Table 3-3). The result of the former mutant indicates the minimal range of the BGC is *orf11–orf24* (62.1 kbp) or narrower. On the other hand, after removing the region *orf19–23*, the resulting mutant *M. xanthus::miu* Δ*orf25–29&19–23* produced **1** in the highest yield of 0.70 mg/L (Figure 3-13E, Table 3-3). In addition, the metabolic profile of this mutant was somewhat complicated, namely the production of several related metabolites **3**, **2'**, **3'**, and **5**. The products **2'** and **3'** were estimated as the C-13 epimers of **2** and **3**, respectively, because of the same molecular formulae and similar retention times (Figure 3-13E). The compound **5** possessed the molecular formula larger than 2 by an oxygen (observed difference 15.9932, calcd. 15.9949; Figure 3-6), which corresponds to a hydroxylated **2**. We tentatively proposed a plausible structure for **5** as shown later (Figure 3-18), in which the phenylalanine residue is hydroxylated at C-14. The region *orf19–23* may contain factor(s) affecting the transcription of some genes constituting *miu* cluster. Interestingly, the feeding of the mutant *M. xanthus::miu* Δ*orf25–29&19–23* on 3-bromo-L-tyrosine boosted the yield of 1 to 1.21 mg/L (Table 3-3), which corresponded to a 20-fold increase compared to the original transformant *M. xanthus::miu* (Table 3-2) and a little higher than that of the original producer SMH-27-4.

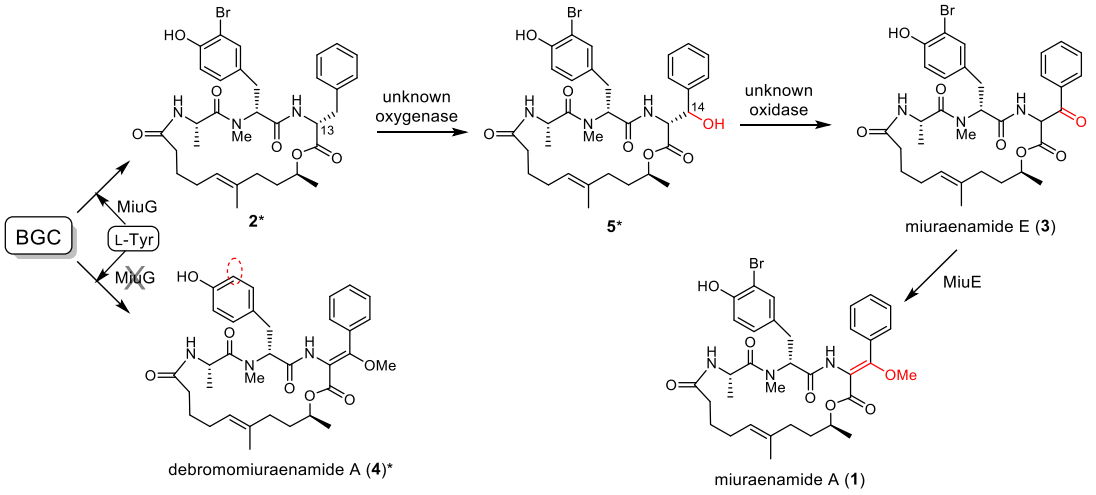

Figure 3-18. Plausible biosynthetic route for miuraenamide A (**1**) and related congeners. The compounds with an asterisk were estimated by the molecular formulae obtained by HRMS.

3.3. Materials and methods

3.3.1. Bacterial strains and culture conditions

All bacterial strains, plasmids, and primers (Eurofin Genomics, Tokyo) used in this study are listed in Table 3-4, 3-5, and 3-6, respectively. The myxobacterium *P. miuraensis* SMH-27-4 was cultivated as previously described [11]. CTT medium [29] was used for the preculture of *M. xanthus* ATCC25232 (wild type) and its mutants at 30 °C. PM1 medium (see below) supplemented with 2% (w/v) Sepabeads SP207 resin (Mitsubishi Chemical Co., Tokyo) was used for the heterologous production of **1**.

PM1 medium: 1% (w/v) Bacto™ casitone (Thermo Fisher Scientific, Waltham, MA, USA), 1% (w/v) HEPES, 0.2% (w/v) Bacto™ malt extract (Thermo Fisher Scientific), 0.1% (w/v) Bacto™ yeast extract (Thermo Fisher Scientific) and 0.18% (w/v) $MgSO_4 \cdot 7H_2O$. pH was adjusted to 7.0 with 1 M NaOH before autoclave. A vitamin B_{12} solution was sterilized by filtration and added to the autoclaved broths at the final concentration of 0.1 mg/L.

Table 3-4. Bacterial strains used in this study.

Strain	Description
"P. miuraensis" SMH-27-4	Original miuraenamide A producer (Ajinomoto)
E.coli HST08 premium	Cloning host for constructing genomic library (Takara bio)

Strain	Description
E.coli DH5α	General cloning host (Toyobo)
E.coli SW105	Red/ET recombineering host (NCI)
M. xanthus ATCC 25232	Wild type, heterologous expression host (Ajinomoto)
M. xanthus::*miu*	Heterologous transformant expressing *miu* cluster
M. xanthus::*miu* Δ*miuD*	*miu*D gene-disrupted *M. xanthus*::*miu*
M. xanthus::*miu* Δ*miuE*	*miuE* gene-disrupted *M. xanthus*::*miu*
M. xanthus::*miu* Δ*miuF*	*miu*F gene-disrupted *M. xanthus*::*miu*
M. xanthus::*miu* Δ*miuG*	*miu*G gene-disrupted *M. xanthus*::*miu*
M. xanthus::*miu* Δ *orf25-29*	*orf25-29* genes-disrupted *M. xanthus*::*miu*
M. xanthus::*miu* Δ*orf25-29&1-10*	*orf25-29* and *orf1-10* genes-disrupted *M. xanthus*::*miu*
M. xanthus::*miu* Δ*orf25-29&14-16*	*orf25-29* and *orf14-16* genes-disrupted *M. xanthus*::*miu*
M. xanthus::*miu* Δ*orf25-29&19-23*	*orf25-29* and *orf19-23* genes-disrupted *M. xanthus*::*miu*

Table 3-5. Plasmids used in this study.

Plasmid	Description
pCCIBAC	BAC cloning vector, Chl^R (Epicentre)
p17-9A	pCCIBAC-derived, harbouring *miu* cluster, Chl^R
pTA-Kan^R	pGEM-T easy vector-derived, harbouring 1.8 kb *M. xanthus* homologous fragment, Amp^R, Kan^R [31]
p5TA-Kan^R	pTA-Kan^R-derived, harbouring 5 kb *M. xanthus* homologous fragment, Amp^R, Kan^R
miu BAC	p17-9A-derived, harbouring *miu* cluster, 5TA, Kan^R
miu BAC Δ*miuD*	*miu* BAC-derived, *miuD* gene was disrupted, Chl^R, Kan^R
miu BAC Δ*miuE*	*miu* BAC-derived, *miuE* gene was disrupted, Chl^R, Kan^R
miu BAC Δ*miuF*	*miu* BAC-derived, *miuF* gene was disrupted, Chl^R, Kan^R
miu BAC Δ*miuG*	*miu* BAC-derived, *miuG* gene was disrupted, Chl^R, Kan^R
miu BAC Δ*orf25-29*	p17-9A-derived, harbouring *orf25-29* genes-disrupted *miu* cluster, 5TA, Kan^R
miu BAC Δ*orf25-29&1-10*	*miu* BAC Δ*orf25-29*-derived, *orf1-10* genes were disrupted, Chl^R, Kan^R
miu BAC Δ*orf25-29&14-16*	*miu* BAC Δ*orf25-29*-derived, *orf14-16* genes were disrupted, Chl^R, Kan^R
miu BAC Δ*orf25-29&19-23*	*miu* BAC Δ*orf25-29*-derived, *orf19-23* genes were disrupted, Chl^R, Kan^R

Table 3-6. Primers used in this study.

Primer	Sequence
pCC-BlnI 2 F	atgcctaggatcctctagagtcgacctg
pCC-BlnI 2 R	atgcctaggatccccgggtaccgagctc
miuBGC p F	caaccaagacggtcagagca
miuBGC p R	ctgaacccgaacgaactcac
loTA Gib F	aacagtgagaggttcgggtgg
loTA Gib R	cacggcgaacatccggaagaac
ploTA F	ccacccgaacctctcactgtt
ploTA R	tcttccggatgttcgccgtgccttttttcaattcagaagaactcgtcaag
ploTA check F	ttctccgccgagtagacgaa
ploTA check R	cattaggcaccccaggcttt
ploTA-Kan red F	agcagtgacaggccgtagaggcttccgatcgccgagatcggaatgagcataacagtgagag gttcgggtg

Primer	Sequence
ploTA-Kan red R	cctgttgataccgggaagccctgggccaacttttggcgaaaatgagacgtggcgcaagggctgctaaagg
T1PKS1 cF	ggcgaaggcgtggaggaatt
T1PKS1 cR	cagttggcggcggcatagtt
T1PKS2 cF	gacttcttcgtgctgttctcctctt
T1PKS2 cR	gaagcgacaaccgataccgatgat
NRPS cF	gctggctgttcgttctggtcatc
NRPS cR	tggcggtggtgaatcggaagt
kanf	cgtcaagaaggcgatagaagg
pCC1BAC R	accgttctgtccgtcacttc
loTA cF	agccgaagcgataggtgag
loTA cR	cactgccgttgttgaggag
loupF	aagtgctggttcggctcggagtagttc
loupR	ttcagcatcgcaaccgcatcagactcc
0lodownF	gcatcgagctggtggaatttctggaacagc
2lodownR	agcagcaccacaccttcttcaccatcc
Cm-miuD-F	ccacctgcggcgaatcctccggaccaacgtgcgcaactatccaaaggcggtattcaggcgtagcaaccaggcg
Cm-miuD-R	ggtcacgaacggcaccacgttcgtgttctcgcccgctcgcacccggactcgttgatcggcacgtaagaggttccaa
Cm-miuE-F	cctgataggagacgatctcgaagccggatgtctcgaccgcattgcggtagtattcaggcgtagcaaccaggcg
Cm-miuE-R	gggattccaccccgtgcatcggtacagcgtcgcgttcatcgaattcctctgttgatcggcacgtaagaggttccaa
Cm-miuF-F	agacgaggctgcgcgagcccccactcaccgagatgagcgcgctcgtgagttattcaggcgtagcaaccaggcg
Cm-miuF-R	catggtgccgaaccacgcggcgatcggtacttcgagcggtgcctcggcaagttgatcggcacgtaagaggttccaa
Cm-miuG-F	gttcgaggctctgctcggcgagttcgggcgcggagtctggaccggtgaggtattcaggcgtagcaaccaggcg
Cm-miuG-R	atccgcagccggatccacctagagcatcgggtcgagcaggcgcacttcgagttgatcggcacgtaagaggttccaa
5TA-orf25-F	agtagatcttcacgcccgcacccaggtgcatcgcggcatcgacgtcgttgaacagtgagaggttcgggtggt
Cm-orf1-F	tcgaggacgaggtactgcatgcgctcttcgaacagttcgtggtcgagcattattcaggcgtagcaaccaggcg
Cm-orf10-R	acgaccgaccacacgtttggccacacgtttggcccgcccactggccaaatgttgatcggcacgtaagaggttccaa
Cm-orf14-F	gacgaatgcctcgagcagcaggcggttgagcgcattcttgatctcgaagttattcaggcgtagcaaccaggcg
Cm-orf16-R	gccgagatcgaccagcagttcgatctgtcgctcgtgtgcctgggcatcaagttgatcggcacgtaagaggttccaa
Cm-orf19-F	atcactcttgtcgtcgctcaatcggtccaagaggtcaccggtgaagggcctattcaggcgtagcaaccaggcg
Cm-orf23-R	tgagctggtggaccgagctgcgggattttggactcgagctcatccaggatgttgatcggcacgtaagaggttccaa
Cm cF	ggtattcactccagagcgat
Cm cR	agacggtgagctggtgatatgg
dmiuD cF	cgtgaagatgccgctgtggaa
dmiuD cR	cctgccacgattctcatcg
dmiuE cR	accagacgacaccgacaa

Primer	Sequence
miuEF	gctcttcaagtacgcctcca
dmiuF cF	cagacacaacgaacgacgaac
dmiuF cR	agcaagccgagcgagatt
dmiuG cF	atggtgacgagtggcggtag
miuGR	cgctcaaggagttcactgc
orf24 cF	cgaactatgccgatgaggaga
dorf1 cF	agtggtgaggtgcttccga
dorf10 cR	ggctggcaacctacactt
dorf14 cF	cctcgaactcgatgcccttc
dorf16 cR	cgcagggaatccaaggtt
dorf19 cF	tcggcttgtagtcaacggatg
dorf23 cR	accatgacggcgatgaac

3.3.2. Chemicals

The antibiotics chloramphenicol and kanamycin were purchased from FUJIFILM Wako Pure Chemical Co. (Osaka, Japan). They were added to mediums at the final concentrations of 35 μg/mL and 50 μg/mL, respectively.

Bromotyrosines were synthesized according to a published protocol [30] using 0.9 g L-tyrosine (FUJIFILM Wako Pure Chemical Co.) or D-tyrosine (FUJIFILM Wako Pure Chemical Co.). The 3-bromo-L-tyrosine and 3-bromo-D-tyrosine was purified by reversed-phase HPLC under the following conditions: ODS-HG-5 column (i. d, 20 × 250 mm, Nomura Chemical, Aichi, Japan), solvent program of 15–50% (35 min) 0.1% tri-fluoroacetic acid (TFA)–acetonitrile in 0.1% TFA–water. The yield of 3-bromo-L-tyrosine and 3-bromo-D-tyrosine are 362.3 mg and 345.4 mg, respectively. 3-bromo-L-tyrosine: $[\alpha]^{15}_{D}$ –3.0 (*c* 0.50, 1.0 M HCl), 3-bromo-D-tyrosine: $[\alpha]^{15}_{D}$ +3.7 (*c* 0.46, 1.0 M HCl). Filter-sterilized bromotyrosine solutions were added to autoclaved broths at the final concentration of 0.5 mM.

3.3.3. PCR and products purification

The prepared transformants were verified by PCR experiments by using GoTaq® Green Master Mix (Promega, Madison, WI, USA) with primer pairs listed in Table 3-6 under the following conditions: predenature at 94 °C for 5 min; 40 cycles of denature at 94 °C for 30 s, annealing st 53 °C for 30 s, and extension at 72 °C for 1 min/kbp; and final extension at 72 °C for 7 min. The DNA fragments used for cloning were amplified by PCR using the

enzyme KOD FX Neo (TOYOBO, Osaka, Japan) under the following conditions: predenature (94 °C, 2 min); 45 cycles of denature (98 °C, 10 s) and extension (68 °C, 60 s/kbp).

3.3.4. Construction and screening of a genomic BAC library

The *miu* cluster was identified by antiSMASH analysis of the draft genome of *P. miuraensis* SMH-27-4 (Genbank accession number: JAOVZF000000000.1) [20]. The genomic DNA was isolated following the protocols described previously [20]. 7 μg of genomic DNA was completely digested with 40 U BlnI (Takara Bio, Kusatsu, Shiga, Japan) overnight at 37°C, and then separated on 0.5% Certified™ Low Melt Agarose gel (Bio-Rad Laboratories, Hercules, CA, USA) by gel electrophoresis. DNA fragments around 50–165 kb in size were extracted from the agarose gel using Thermostable β-Agarase (NIPPON GENE Co., Toyama, Japan). The DNA was purified from the digested solution by ethanol precipitation [31]. The bacterial artificial chromosome (BAC) vector pCC1BAC-BlnI was derived from the commercial pCC1BAC (Epicentre Biotechnologies, WI, USA). The pCC1BAC was linearized by PCR using the primer pair pCC-BlnI 2 F/R and introducing BlnI cutting sites at both ends. Following electrophoresis, the PCR product was putified from agarose gel using Wizard SV Gel and PCR Clean-Up System (Promega). The purified DNA was digested with BlnI for 2 h, and then washed with an equivalent amount of PCI solution (phenol:chloroform:isoamyl alcohol, 25:24:1). Following ethanol precipitation and redissolved in Milli-Q water, the BlnI digested pCC1BAC-BlnI was treated with alkaline phosphatase CIAP (Takara Bio) and ligated with the purified 50–165 kb genomic DNA fragments using Takara DNA Ligation Kit Long (Takara Bio). The ligation product was transformed into *E. coli* HST08 premium Electro-Cells (Takara Bio) to generate a genomic BAC library consisting of 1920 clones. The primer pair miuBGC p F/R located at the second KS domain of *miuB* was used for screening the genomic library. The recombinant BAC p17-9A clone harboring the complete *miu* cluster was verified by PCR experiments using the primer pairs T1PKS1 cF/R, NPRS cF/R, FMO cF/R located in *miuA*, *miuC*, and *miuG*, respectively.

3.3.5. Construction of the Red/ET recombination modification cassette 5TA-Kan^R

The *M. xanthus* genomic DNA isolation was performed with the QIAamp DNA Mini Kit (Qiagen, Hilden, Germany). The 5TA fragment was amplified from myxovirescin A biosynthetic gene *ta-1* of *M. xanthus* with primer pair loTA Gib F/R. The vector pTA-Kan^R [32] was linearized using the primer pair ploTA F /R. The PCR products were purified by electrophoresis on 1% agarose gel followed by extraction from the gel using FavorPrep GEL/PCR Purification Mini Kit (Favorgen Biotech Corp., Taiwan, China). The concentrations of the DNA solutions were measured on a V-730BIO UV/visible spectrophotometer (JASCO, Tokyo, Japan). The DNA fragment “5TA” was assembled to the linearized vector using NEBuilder® HiFi DNA Assembly Master Mix (NEW ENGLAND BioLabs Inc., Ipswich, MA, USA) at a DNA molar ratio of 3:1 (in total 0.2 pmol) to generate the plasmid p5TA-Kan^R following the manufacturer’s manual. 2 μL of the assembled product were transformed into Competent high DH5α (TOYOBO) following the manufacturer’s manual. The resulting colonies were verified by PCR using primer pair ploTA check F/R located at one end of the assembly site. The Red/ET recombination modification cassette 5TA-Kan^R was amplified by PCR using the assembled plasmid p5TA-Kan^R as template.

3.3.6. Modification of BAC vector to *miu* BAC via Red/ET recombination

The BAC vector p17-9A containing *miu* cluster was purified using QIAGEN Plasmid Midi Kit (Qiagen). Approximately 200 ng of the BAC p17-9A was transformed into 70 μL electrocompetent *E. coli* SW105 cells [33] in a 1-mm cuvette (NEPAGENE, Ichikawa, Chiba, Japan) at 1,800 V, one pulse. *E. coli* transformants were recovered at 30 °C for 1 h in 1 mL of SOC medium (Takara Bio) and then plated onto LB medium (Thermo Fisher Scientific) containing chloramphenicol at 30 °C for 24–36 h. Individual colonies were picked up and verified by colony PCR.

The Red/ET recombination modification cassette 5TA-Kan^R was amplified using the primer pair ploTA-Kan red F/R from the vector p5TA-Kan^R. The PCR products were purified

following above-mentioned method. Approximately 200 ng of the modification cassette "5TA-Kan^R" was transformed into electrocompetent *E. coli* SW105 cells harboring the BAC vector p17-9A via electroporation followed by recovery and cultivation under the above-mentioned conditions to obtain the recombinant *miu* BAC harboring the complete *miu* cluster and 5.0 kbp *M. xanthus* homologous fragment (5TA). The resulting colonies were verified by PCR using the two primer pairs loTA cF/R and kanf/pCC1BAC R (Figure 3-3).

3.3.7. Gene disruption

The disruption of the modification genes *miuD–miuG* was performed on the *miu* BAC (Figures 3-7 – 3-10). The chloramphenicol gene fragment "Cm" was amplified using the template pCC1BAC and the primer pairs Cm-miuD-F/R, Cm-miuE-F/R, Cm-miuF-F/R, and Cm-miuG-F/R for the disruption of *miuD–miuG*, respectively. The PCR products were purified following above-mentioned method. Approximately 200 ng of "Cm" was transformed into electrocompetent *E. coli* SW105 cells harboring *miu* BAC via electroporation followed by recovery and cultivation under the above-mentioned conditions to obtain the four gene-disrupted BAC vectors.

The removal of a terminal region (*orf25-29*) of the *miu* cluster was performed on the BAC vector p17-9A (Figure 3-14). The gene cassette 5TA-Kan^R was amplified using the primer pair 5TA-orf25-F/ploTA-Kan red R from the vector p5TA-Kan^R. The PCR product was purified following the above-mentioned method. Approximately 200 ng of "5TA-Kan" was transformed into electrocompetent *E. coli* SW105 cells harboring p17-9A via electroporation followed by recovery and cultivation under the above-mentioned conditions to obtain the *orf25-29* region-disrupted BAC vectors, *miu* BAC Δ*orf25-29*.

The removals of the other three gene regions (*orf1-10, orf14-16, orf19-23*) were performed on the *miu* BAC Δ*orf25-29* (Figures 3-15 – 3-17). The chloramphenicol gene fragment "Cm" was amplified using the template pCC1BAC and the primer pairs Cm-orf1-F/ Cm-orf10-R, Cm-orf14-F/ Cm-orf16-R, and Cm-orf19-F/ Cm-orf23-R for the disruption of gene regions

orf1-10, orf14-16, orf19-23, respectively. The PCR products were purified following the above-mentioned method. Approximately 200 ng of “Cm” was transformed into electrocompetent *E. coli* SW105 cells harboring *miu* BAC Δ*orf25-29* via electroporation followed by recovery and cultivation under the above-mentioned conditions to obtain the three gene regions disrupted BAC vectors.

3.3.8. Construction of *M. xanthus* transformants

Approximately 10 μg of the recombinant *miu* BAC harboring the complete *miu* cluster and the 5.0 kbp *M. xanthus* homologous fragment was transformed into 240 μL electrocompetent *M. xanthus* cells in a 2-mm cuvette (NEPAGENE) at 1,500 V, 5 ms, two pulses. For the preparation of the electrocompetent cells, *M. xanthus* were harvested when OD_{600} reached 0.2–0.6 in the CTT medium. After precooling on ice for 20 min, the cells were washed with ice-cold Milli-Q water three times and dissolved in Milli-Q water of 1/100 volume of the culture medium. *M. xanthus* transformants were recovered at 30 °C for 10–12 h in 3 mL of CTT medium and then plated onto CTT medium containing kanamycin. The resulting colonies that appeared after 5–7 days were verified by PCR experiments using the four primer pairs T1PKS1 cF/R, T1PKS2 cF/R, loupF/R, 0lodownF/2lodownR located at *miuA*, *miuB*, and two integration sites (Figure 3-3). Other *M. xanthus* transformants were constructed by the same method.

3.3.9. Production of miuraenamide A (**1**) by *M. xanthus* heterologous mutants

The *M. xanthus* mutants were cultivated in 50 mL of the PM1 medium supplemented with 2% (w/v) Sepabeads SP207 absorber resin. The cells and resin were harvested after 4 days of culture by centrifugation and extracted twice with acetone (30 mL) by shaking at 30 °C for 30 min. After filtration, the combined filtrates were concentrated in vacuo and dried to afford a yellow oil. The extract was dissolved in 70% MeOH (5 mL) and a portion (5 μL) equivalent to 0.05 mL broth was subjected to LC-MS analysis.

3.3.10. LC-MS analysis of miuraenamide A (**1**) and congeners (**2**–**5**)

HPLC was performed by an Agilent 1100 HPLC system (Agilent Technologies, Santa Clara, CA) under the following conditions: Cadenza CD-C18 column (i. d. 3 × 50 mm, Imtakt, Kyoto, Japan), solvent program of 40–75% (20 min) acetonitrile in water, and flow rate of 0.2 mL/min. MS coupled to the HPLC system was performed on an Agilent 6520 Accurate-Mass Q-TOF spectrometer in the mass range of *m/z* 50–1700 in the positive ion mode. For the quantitative analysis of 1, 0.1 and 0.5 μM solutions of the standard **1** were used. The congeners **2**–**5** were not quantified due to the lack of their standard samples. **1** (t_R = 12.0 min): *m/z* 684.2216 (calcd for $C_{34}H_{43}BrN_3O_7$ 684.2279) and 706.2032 (calcd for $C_{34}H_{42}BrN_3O_7Na$ 706.2098); **2** (t_R = 15.8 and 16.2 min): *m/z* 656.2285 (calcd for $C_{33}H_{43}BrN_3O_6$ 656.2330) and 678.2100 (calcd for $C_{33}H_{42}BrN_3O_6Na$ 678.2149); **3** (t_R = 15.6 and 14.1 min): *m/z* 670.2068 (calcd for $C_{33}H_{41}BrN_3O_7$ 670.2122) and 692.2055 (calcd for $C_{33}H_{40}BrN_3O_7Na$ 692.1942); **4** (t_R = 9.3 min): *m/z* 606.3125 (calcd for $C_{34}H_{44}N_3O_7$ 606.3174) and 628.2941 (calcd for $C_{34}H_{43}N_3O_7Na$ 628.2993); **5** (t_R = 10.9 min): 672.2217 (calcd for $C_{33}H_{43}BrN_3O_7$ 627.2279) and 694.2038 (calcd for $C_{33}H_{42}BrN_3O_7Na$ 694.2098).

3.4. Summary

The antifungal and antitumor antibiotic miuraenamide A (**1**) is produced by the slightly halophilic myxobacterium *P. miuraensis* SMH-27-4. Since the strain is a rare marine myxobacteria and hard-to-culture, the genetic engineering of the biosynthetic machinery is essential to perform effective production of the valuable antibiotic **1**. The BGC for **1** (*miu* cluster) was successfully cloned and heterologously expressed in the well-known terrestrial myxobacterium *M. xanthus*. Although the obtained heterologous transformant *M. xanthus::miu* was much easier to treat and more quickly grew than the original strain SMH-27-4, the productivity of **1** was quite low (6% of that of the original strain). The proposed biosynthetic mechanism of the *miu* cluster was partially verified by gene disruption experiments using the transformant *M. xanthus::miu*. The type I PKSs (MiuA and MiuB) and

NRPS (MiuC) recruit and sequentially couple C_2/C_3 carboxylic acid and amino acid units to generate the early intermediate **2** (Figure 3-18). The thioesterase gene *miuF*, although regarded as a candidate gene responsible for the release and cyclization of the enzyme-bound linear precursor, was found not to be involved in the biosynthesis of **1**. This reaction may, instead, be catalyzed by the extra DCL* domain in MiuC because it possess the conserved motif of a ester-bond formation condensation enzyme SgcC5 [28]. In the biosynthesis of **1**, the DCL* domain may catalyze the formation of the ester bond between the hydroxy group of C-9 and the carbonyl group of D-phenylalanine, leading to releasing and cyclization of the polyketide/peptide chain. Since this domain is D-specific for the peptidyl donor, the configuration at C-13 of the phenylalanine residue in **2** is possibly *R* (D) as indicated in Figure 3-18. The detection of **2**, **3**, and **5** in this study suggested the presence of an oxidation enzyme gene that catalyzes oxygen transfer to the β-carbon (C-14) of phenylalanine. Although *miuD* encoding cytochrome P450 seemed to be the exclusive candidate for this reaction within the *miu* cluster, the *miuD*-disrupted mutant still produced **1**. The fact that no other orfs in the *miu* cluster were annotated as oxidation enzymes suggested the presence of a responsible oxygenase outside the cluster. The *O*-methyltransferase MiuE was readily confirmed responsible for the methylation of **3** to the final product **1** by gene disruption. The halogenase MiuG was found to be the tyrosine bromination enzyme that utilized free L-tyrosine as the substrate because the inactivation of MiuG led to the generation of the unnatural congener debromomiuraenamide A (**4**) and the production of **1** was restored by feeding on bromotyrosine. The A domain of Module 6 seems to prefer 3-bromo-L-tyrosine over tyrosine itself. Feeding with 3-bromo-L-tyrosine increased the productivity of miuraenamide A. However, the multi-gene deletion experiments created a breakthrough leading to a dramatic increase in the yield of **1** and the construction of more compact *miu* clusters. The deletion of 15 orfs in total (*orf25–29* and *orf1–10*) didn't affect the production of **1**, indicating that the remaining 20 orfs extending over 62.1 kbp (corresponding

to 72% of the original *miu* cluster) were enough for the biosynthesis of **1** (Figure 3-12). On the other hand, the removal of the *orf25–29* and *orf19–23* regions resulted in a substantial increase in the yield of **1** and the complicated metabolic profile (Figure 3-13E), suggesting the presence of unknown gene(s) in the *orf19–23* region that affects transcriptional regulation of some of the functionally defined *miu* genes. Interestingly, feeding this mutant *M. xanthus::miu* Δ*orf25–29&19–23* on 3-bromo-L-tyrosine promoted the production of **1** at a little higher level (1.2 mg/L) than the original SMH-27-4 strain (1 mg/L). Considering the growth rate of this mutant (4 days), the efficiency of the production is five times as high as that of SMH-27-4 (18 days of culture time). Further studies will be needed to unveil the function of unidentified genes in the *miu* cluster for a much more effective heterologous production of **1**.

References

1. Velicer, G.J.; Vos, M. Sociobiology of the myxobacteria. *Annu. Rev. Microbiol.* **2009**, *63*, 599–623.
2. Kaiser, D.; Robinson, M.; Kroos, L. Myxobacteria, polarity, and multicellular morphogenesis. *Cold Spring Harb. Perspect. Biol.* **2010**, *2*, 1–27.
3. Muñoz-dorado, J.; Marcos-torres, F.J.; García-bravo, E.; Moraleda-muñoz, A.; Pérez, J. Myxobacteria: moving , killing , feeding , and surviving together. *Front. Microbiol.* **2016**, *7*, 781.
4. Wenzel, S.C.; Müller, R. Myxobacteria —'microbial factories' for the production of bioactive secondary metabolites. *Mol. BioSyst.* **2009**, *5*, 567–574.
5. Diez, J.; Martinez, J.P.; Mestres, J.; Sasse, F.; Frank, R.; Meyerhans, A. Myxobacteria: natural pharmaceutical factories. *Microb. Cell Fact.* **2012**, *11*, 2–4.
6. Hug, J.J.; Müller, R. Host development for heterologous expression and biosynthetic studies of myxobacterial natural products. In *Comprehensive Natural Products III,* 3rd ed.; Liu, H., Begley, T.P., Eds.; Elsevier: San Diego, California, USA, 2020; Vol. 6, pp. 149–216.
7. Dávila-Céspedes, A.; Hufendiek, P.; Crüsemann, M.; Schäberle, T.F.; König, G.M. Marine-derived myxobacteria of the suborder Nannocystineae: an underexplored source of structurally intriguing and biologically active metabolites. *Beilstein J. Org. Chem.* **2016**, *12*, 969–984.
8. Albataineh, H.; Stevens, D.C. Marine myxobacteria: a few good halophiles. *Mar. Drugs* **2018**, *16*, 209.
9. Gemperlein, K.; Zaburannyi, N.; Garcia, R.; La Clair, J.J.; Müller, R. Metabolic and biosynthetic diversity in marine myxobacteria. *Mar. Drugs* **2018**, *16*, 314.
10. Moghaddam, J.A.; Crüsemann, M.; Alanjary, M.; Harms, H.; Dávila-Céspedes, A.; Blom, J.; Poehlein, A.; Ziemert, N.; König, G.M.; Schäberle, T.F. Analysis of the genome and metabolome of marine myxobacteria reveals high potential for biosynthesis of novel specialized metabolites. *Sci. Rep.* **2018**, *8*, 16600.
11. Iizuka, T.; Fudou, R.; Jojima, Y.; Ogawa, S.; Yamanaka, S.; Inukai, Y.; Ojika, M. Miuraenamides A and B, novel antimicrobial cyclic depsipeptides from a new slightly halophilic myxobacterium: taxonomy, production, and biological properties. *J. Antibiot.* **2006**, *59*, 385–391.
12. Sumiya, E.; Shimogawa, H.; Sasaki, H.; Tsutsumi, M.; Yoshita, K.; Ojika, M.; Suenaga, K.; Uesugi, M. Cell-morphology profiling of a natural product library identifies bisebromoamide and miuraenamide A as actin filament stabilizers. *ACS Chem. Biol.* **2011**, *6*, 425–431.

13. Moser, C.; Rüdiger, D.; Förster, F.; Blume, J. Von; Yu, P.; Kazmaier, U.; Vollmar, A.M.; Zahler, S. Persistent inhibition of pore-based cell migration by sub-toxic doses of miuraenamide, an actin filament stabilizer. *Sci. Rep.* **2017**, *7*, 16407.
14. Gegenfurtner, F.A.; Zisis, T.; Al Danaf, N.; Schrimpf, W.; Kliesmete, Z.; Ziegenhain, C.; Enard, W.; Kazmaier, U.; Lamb, D.C.; Vollmar, A.M.; et al. Transcriptional effects of actin-binding compounds: the cytoplasm sets the tone. *Cell. Mol. Life Sci.* **2018**, *75*, 4539–4555.
15. Wang, S.; Crevenna, A.H.; Ugur, I.; Marion, A.; Antes, I.; Kazmaier, U.; Hoyer, M.; Lamb, D.C.; Gegenfurtner, F.; Kliesmete, Z.; et al. Actin stabilizing compounds show specific biological effects due to their binding mode. *Sci. Rep.* **2019**, *9*, 9731.
16. Baltes, C.; Thalla, D.G.; Kazmaier, U.; Lautenschläger, F. Actin stabilization in cell migration. *Front. Cell Dev. Biol.* **2022**, *10*, 931880.
17. Karmann, L.; Schultz, K.; Herrmann, J.; Müller, R.; Kazmaier, U. Total syntheses and biological evaluation of miuraenamides. *Angew. Chem. Int. Ed.* **2015**, *54*, 4502–4507.
18. Ojima, D.; Yasui, A.; Tohyama, K.; Tokuzumi, K.; Toriihara, E.; Ito, K.; Iwasaki, A.; Tomura, T.; Ojika, M.; Suenaga, K. Total synthesis of miuraenamides A and D. *J. Org. Chem.* **2016**, *81*, 9886–9894.
19. Kappler, S.; Karmann, L.; Prudel, C.; Herrmann, J.; Caddeu, G.; Müller, R.; Vollmar, A.M.; Zahler, S.; Kazmaier, U. Synthesis and biological evaluation of modified miuraenamides. *Eur. J. Org. Chem.* **2018**, 6952–6965.
20. Liu, Y.; Ojika, M. Genomic analysis of the rare slightly halophilic myxobacterium "*Paraliomyxa miuraensis*" SMH-27-4, the producer of the antibiotic miuraenamide A, *Microorganisms*, **2023**, *11,* 371.
21. Simunovic, V.; Zapp, J.; Rachid, S.; Krug, D.; Meiser, P.; Müller, R. Myxovirescin A biosynthesis is directed by hybrid polyketide synthases/nonribosomal peptide synthetase, 3-hydroxy-3-methylglutaryl-CoA synthases, and trans-acting acyltransferases. *Chembiochem* **2006**, *7*, 1206–1220.
22. Ligon, J.; Hill, S.; Beck, J.; Zirkle, R.; Molnár, I.; Zawodny, J.; Money, S.; Schupp, T. Characterization of the biosynthetic gene cluster for the antifungal polyketide soraphen A from *Sorangium cellulosum* So Ce26. *Gene* **2002**, *285*, 257–267.
23. Silakowski, B.; Schairer, H.U.; Ehret, H.; Kunze, B.; Weinig, S.; Nordsiek, G.; Brandt, P.; Blöcker, H.; Höfle, G.; Beyer, S.; et al. New lessons for combinatorial biosynthesis from myxobacteria. the myxothiazol biosynthetic gene cluster of *Stigmatella aurantiaca* DW4/3-1. *J. Biol. Chem.* **1999**, *274*, 37391–37399.
24. Silakowski, B.; Nordsiek, G.; Kunze, B.; Blöcker, H.; Müller, R. Novel features in a combined polyketide synthase/non-ribosomal peptide synthetase: the myxalamid biosynthetic gene cluster of the myxobacterium *Stigmatella aurantiaca* Sga15. *Chem. Biol.* **2001**, *8*, 59–69.

25. Rachid, S.; Krug, D.; Kunze, B.; Kochems, I.; Scharfe, M.; Zabriskie, T.M.; Blöcker, H.; Müller, R. Molecular and biochemical studies of chondramide formation-highly cytotoxic natural products from *Chondromyces crocatus* Cm c5. *Chem. Biol.* **2006**, 13, 667–681.
26. Agarwal, V.; EL Gamal, A.A.; Yamanaka, K.; Poth, D.; Kersten, R.D.; Schorn, M.; Allen, E.E.; Moore, B.S. Biosynthesis of polybrominated aromatic organic compounds by marine bacteria. *Nat. Chem. Biol.* **2014**, *10*, 640–647.
27. Ojika, M.; Inukai, Y.; Kito, Y.; Hirata, M.; Iizuka, T.; Fudou, R. Miuraenamides: antimicrobial cyclic depsipeptides isolated from a rare and slightly halophilic myxobacterium, *Chem. Asian J.* **2008,** *3*, 126–133.
28. Chang, C.Y.; Lohman, J.R.; Huang, T.; Michalska, K.; Bigelow, L.; Rudolf, J.D.; Jedrzejczak, R.; Yan, X.; Ma, M.; Babnigg, G.; et al. Structural insights into the free-standing condensation enzyme SgcC5 catalyzing ester-bond formation in the biosynthesis of the enediyne antitumor antibiotic C-1027. *ACS Biochem*. **2018**, *57*, 3278–3288.
29. Hodgkin, J.; Kaiser, D. Cell-to-cell stimulation of movement in nonmotile mutants of *Myxococcus*. *Proc. Natl. Acad. Sci. U. S. A.* **1977**, 74, 2938–2942.
30. McCord, T.J.; Smith, D.R.; Winters, D.W.; Grimes, J.F.; Hulme, K.L.; Robinson, L.Q.; Gage, L.D.; Davis, A.L. Synthesis and microbiological activities of some monohalogenated analogs of tyrosine. *J. Med. Chem.* **1975**, *18*, 26–29.
31. Green, M.R; Sambrook, J. *Molecular Cloning: A Laboratory Manual*, 4th ed; Cold Spring Harbor Laboratory Press: Cold Spring Harbor, NY, USA, 2012; pp. 21-25.
32. Sun, Y.; Feng, Z.; Tomura, T.; Suzuki, A.; Miyano, S.; Tsuge, T.; Mori, H.; Suh, J.W.; Iizuka, T.; Fudou, R.; et al. Heterologous production of the marine myxobacterial antibiotic haliangicin and its unnatural analogues generated by engineering of the biochemical pathway. *Sci. Rep.* **2016**, *6*, 220911.
33. Warming, S.; Costantino, N.; Court, D.L.; Jenkins, N.A.; Copeland, N.G. Simple and highly efficient BAC recombineering using *galK* selection. *Nucleic Acids Res.* **2005**, *33*, 1–12.

Chapter 4. Conclusion

In this thesis, the potential of the secondary metabolite production of *P. miuraensis* SMH-27-4 and the biosynthetic machinery for miuraenamide A were illustrated.

4.1. Genomic analysis of *P. miuraensis* SMH-27-4

Myxobacteria are common in terrestrial habitats and known for their potential to produce novel natural products, whereas marine-derived (or halophilic) ones are quite rare and only seven species (five genera) have been identified since the isolation of the first marine myxobacteria *H. ochraceum* and *P. pacifica* in 1998. Although these marine myxobacteria are regarded as a good factory of valuable secondary metabolites beyond the terrestrial ones, their cultivation is generally difficult and takes a long period for enough growth. Their genomic information is therefore important to elucidate their great potential to produce novel leads with unique molecular scaffolds and bioactivities. *P. miuraensis* SMH-27-4 produces a series of PKS/NRPS hybrid molecules named miuraenamides, but its metabolic profile indicated a scarcity of metabolite diversity; no other distinct metabolites were detected in the extracts. The genomic analysis of this strain was therefore performed in this study and revealed the presence of 17 BGCs for producing metabolites, one of which was estimated to encode the biosynthesis of miuraenamides. The complete genome sequence was not available in this study due to the extremely difficult cultivation and DNA extraction from aggregated mucous cells. Nevertheless, because of the high-quality sequence data, 93% coverage of the complete genome (the rest could be repetition), and no overlooking of other possible BGCs, the present draft genome information could contribute to improving the inadequate expertise in the marine myxobacterial genomic functions, especially for hidden biosynthetic machineries leading to brand-new natural products. Further studies will be needed to reveal the mechanism of the miuraenamide biosynthesis as well as more precise genomic analysis.

4.2. Heterologous biosynthesis of miuraenamide A

Due to the difficulty in cultivation and the lack of genetic manipulation tools, the biochemical studies on the native producer *P. miuraensis* SMH-27-4 are hard to process. The heterologous biosynthesis became a promising methodology for the biosynthesis mechanism elucidation and efficient production of miuraenamide A (**1**, Figure 4-1B). The antiSMASH predicted the biosynthetic gene cluster of miuraenamide A (*miu* cluster, Figure 4-1A) was successfully cloned and heterologously expressed in the well-known terrestrial myxobacterium *Myxococcus xanthus* with a productivity miuraenamide A of 6% of the original strain. The proposed biosynthetic mechanism of the *miu* cluster was partially verified by gene disruption experiments using the transformant. The type I PKSs (MiuA and MiuB), one NRPS (MiuC), one *O*-methyltransferase (MiuE), and one tyrosine halogenase (MiuG) were verified to be responsible for the biosynthesis. Besides miuraenamide A, four congeners (**2**–**5**, Figure 4-1B) were identified based on their mass spectra. The antifungal activities of the miuraenamide E (**3**) or **4** were confirmed to be lower than the **1** due to the lack of β-methoxyacrylate group or halogenation. Although the activities of **2** and **5** had not been measures, they were estimated to be weaker than **1** due to the lack of the β-methoxyacrylate group. The BGC for **1** was narrowed to 20 orfs (*orf11–orf24* region) extending over 62.1 kbp (corresponding to 72% of the original *miu* cluster). The removal of the *orf25–29* and *orf19–23* regions resulted in a substantial increase of the yields of **1**, suggesting the presence of unknown gene(s) in the *orf19–23* region that are related to the expression regulation or even affecting the substrate supply of the biosynthetic pathway. The detailed mechanism is well worth exploring and may provide a new strategy for secondary metabolite production boosting. Based on the results of in vivo experiments, it is likely that the halogenase (MiuG) is tyrosine specific. It is also worthwhile to explore the potential

industrial applications and development of this enzyme.

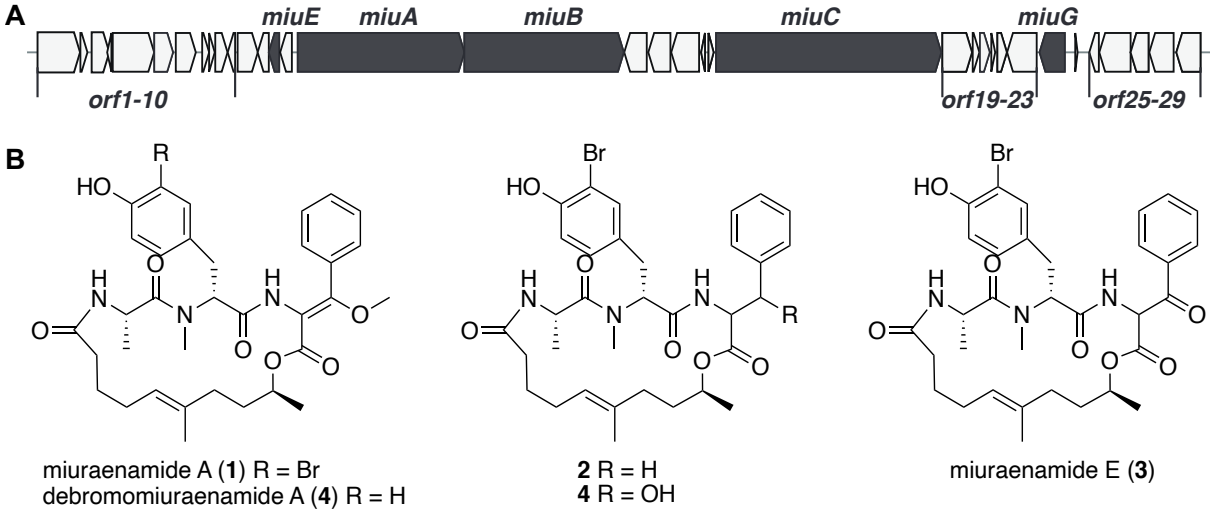

Figure 4-1. Organization of *miu* cluster (A) and strctures of miuraenamide A (**1**) and related congeners (B).

Acknowledgements

The work for this thesis was carried out in the Bioactive Molecules Laboratory of the Department of Applied Molecular Biosciences, Graduate School of Bioagricultural Sciences, Nagoya University, Japan. First, I would like to thank my supervisor, Professor Ojika, for leading me into myxobacteria's wonderful and exciting world. Thank you for all your support and patience. With your careful guidance, I made it to the end. My procrastination has caused you a lot of trouble for the past four years. I always handed you the content that needed to be revised just before the deadline was about to come. You never gave up on me, which was the biggest motivation to support me in completing my coursework. Besides the content presented in the thesis, many exploratory studies yielded no positive results. Whenever I had ideas, Professor Ojika actively supported me in exploring and practicing. This unwavering support has been a memorable experience for me. It will be a source of motivation for my future life. If I had the opportunity to be a teacher for someone else, I would give my students the diligence, trust, and patience I learned from Professor Ojika to help them become better people.

I also want to thank Prof. Kita, Prof. Nishikawa, Prof. Tsunematsu, and Dr. Kondo for reviewing my thesis and providing practical advice on my research. Also, thank all my lab mates who had helped me with many things over the years.

I particularly thank Dr. Fudou and Dr. Iizuka from Ajinomoto Co. Inc. for their supply of myxobacterium. Mr. Yamazaki, for his excellent previous work on genome library construction and screening, made a solid foundation for my research.

I am deeply thankful to the Interdisciplinary Frontier Next-Generation Researcher Program of the Tokai Higher Education and Research System, the Toyo Suisan Foundation Scholarship, and the Hattori International Student Education Association for their financial support and kind care. Without your support, I would not have been able to complete my

thesis, so I am genuinely grateful. I will remember the help and warmth I received in Japan, work hard, and live well in the future, and try to be a bridge of friendship between China and Japan.

Then again, I would like to thank my parents for their constant and unconditional trust and support.

Finally, dearly cherish the memory of my grandmother Wang Xianhua, my grandfather Liu Xuemin, and Shimajiri Shouta.

2023

LIU Ying